BIBLIOGRAPHIC DATA SHEET

1. CONTROL NUMBER
PN-AAI-934

2. SUBJECT CLASSIFICATION (695)
TA00- -G232

3. TITLE AND SUBTITLE (240)
Chemistry workshop, Cairo, 28 Nov.-8 Dec. 1977, part 2: corrosion and metallurgical analyses.

4. PERSONAL AUTHORS (100)
Ammar, I.A.; Leidheiser, Henry; Gouda, V.K.; Shawki, Saher; El-Raghy, S.M.; Shams el Din, A.M.; Abdul Azim, A.A.

5. CORPORATE AUTHORS (101)

6. DOCUMENT DATE (110)	7. NUMBER OF PAGES (120)	8. ARC NUMBER (170)
1977	80p.	

9. REFERENCE ORGANIZATION (130)
USAID/Egypt

10. SUPPLEMENTARY NOTES (500)
Pt. 1: Pesticide analyses and syntheses.
Pt. 3: Chemical modification of cotton.
Pt. 4: Utilization of fibrous raw materials.
(Sponsored by National Research Centre, Arab Rep. of Egypt; and American Chemical Society)

11. ABSTRACT (950)

12. DESCRIPTORS (920)
Egypt
Chemistry
Corrosion
Metallurgy

13. PROJECT NUMBER (150)
263-0005(local costs support funds)

14. CONTRACT NO.(140)
None

15. CONTRACT TYPE (140)
-----

16. TYPE OF DOCUMENT (160)

AID 590-7 (10-79)

TA00-G252
PN-AAI-934

Chemistry Workshop

Corrosion and Metallurgical Analyses
Part 2

Sponsored by

National Research Centre

and

American Chemical Society

USAID/CAIRO
DEVELOPMENT
INFORMATION
CENTER

Cairo
Arab Republic of Egypt
November 28-December 8, 1977

PART 2

CONTENTS

Contribution to the Theory of Galvanostatic Anodization / I. A. Ammar 3

Surface Chemistry and Crystallographic Factors Affecting Adherence of Paint to Galvanized Steel / Henry Leidheiser, Jr. 30

Some Aspects of the Corrosion of Reinforcing Steel in Concrete / V. K. Gouda 32

Chemical Aspects of Fireside Corrosion in Oil-Fired Boilers / Saher Shawki 46

Effect of Cations on the Corrosion of Stainless Alloys in Saline Water at Elevated Temperatures / S. M. El-Raghy, S. M. Morsy, A. A. Elsayed, and A. E. El-Mehairy 49

A Review of the Thermometric Method of Corrosion Testing / A. M. Shams El Din 62

Hot Corrosion of the Sinter Grates by a Chloride-Containing Iron Ore / A. A. Abdul Azim 75

Contribution to the Theory of Galvanostatic Anodization

Dr. I. A. Ammar
Professor of Physical and Electrochemistry
Department of Chemistry, Faculty of Science
Cairo University

INTRODUCTION

The theory of galvanostatic anodization dates to the early work of Güntherschulze and Betz (1-2) on valve metals in the period between 1931 and 1937. Later in the period between 1955 and 1964, it was extended by Adams and co-workers (3-6) who first defined the oxide formation rate as the rate of potential rise at constant current density. The same authors were able to calculate another important parameter; namely, the reciprocal capacity which was used to differentiate between the two modes of ionic conduction in the oxide film known as the low and high field approximations. Among other contributions to the theory, one may mention the significant work of Vermilyea (7-9) and of Young (10).

My co-workers at Cairo University and I became interested in galvanostatic anodization in 1970 simply because the experimental technique is very simple and does not require elaborate instruments which are still lacking. The group at Cairo University was able to rationalize the theory in order to enable it to predict some new information concerning the parameters of oxide growth. Theoretical deductions were tested by experiments on the anodization of Ta and Zr (11), Ti (12, 13), Nb (14, 15), W (16, 17), Al (18-20), Te (21), Sb (22, 23), and Bi (24-26). The present paper summarizes the important results of these publications and indicates some new applications of the theory of galvanostatic anodization.

EXPERIMENTAL TECHNIQUE

Anodization does not require extensive purification of solution, e.g., by pre-electrolysis, a procedure which is necessary for other fields of electrochemical kinetics. "AR" grade reagents are sufficient for this purpose. Furthermore, there is no need to guard the solution against air, since experiments in aerated and deaerated solutions give practically the same results. The electrolytic cell simply consists of a beaker containing the working anode, the auxiliary Pt cathode, and the probe of the reference half cell. The electrical circuit is composed of a galvanostat or a stabilized constant current unit and a potentiometer. Since recording potentiometers are not available, the potential/time relation is recorded manually.

Below the region of dielectric breakdown, the possible anodic processes are anodic dissolution, gas (O_2) evolution, and oxide film growth. The contribution of each of the three processes has been found to depend markedly on the state of the metal surface. While a heterogeneous surface favors anodic dissolution and O_2 evolution, a homogeneous surface favors oxide film growth.

The composition of solution undoubtedly plays an important role. Therefore, successful anodization can only be achieved if the surface is free from scratches and other defects. In this case the efficiency of oxide growth approaches 100%.

Various methods of pretreatment have been used, including chemical and mechanical, with the latter preferred since chemical methods invariably leave a film on the metal surface whose composition depends on the chemical used. Mechanical pretreatment involves the use of metallurgical papers of various grades, but the essential step is to subject the surface finally to thorough rubbing with fine tissue paper, and to examining the surface now and then until all scratches disappear and edges become smooth. The surface at the metal to glass seal should be properly covered with a resin.

Another source of error is the presence of halides, particularly chloride ions, which hinder oxide growth. Therefore, when sat.calomel is used as a reference, the reference electrode probe should lead to a small beaker. The probe and this beaker are filled with the solution used for the test. The calomel is connected to this beaker via a conventional salt bridge. This arrangement retards the diffusion of chloride ions to the test anode.

All potentials are referred to nhe, and current densities are calculated on the basis of geometric areas. Stirring of the test solution is recommended, particularly at current densities which release heat in the anolyte.

BASIC PRINCIPLES

An oxide film grows anodically onto an existing prepolarization film formed either by tarnishing reactions in air or by interaction with the solution prior to polarization or by chemical pretreatment. The composition of the prepolarization film is not necessarily similar to that of the growing oxide. Two partial reactions are associated with the beginning of oxide growth. The first is the forward i_f related to ions moving in the direction of the field, and the second, i_r, is the backward due to ions moving against the field. The net ionic current density becomes:

$$i = i_f - i_r \quad (1)$$

Expressing both rates in the exponential form of Güntherschulze and Betz (1, 2) one gets:

$$i = A \exp (BH) - A' \exp (-B'H) \quad (2)$$

where A, A' and B, B' are constants, H is the field, and the negative sign is for the cathodic process. At sufficiently low fields, one gets by expanding the exponentials:

$$i = (A - A') + (AB + A'B') H \quad (3)$$

indicating a direct proportionality between i and H in accordance with Ohm's law of conductivity. This situation is known as the low field approximation. However, at high fields the cathodic rate becomes negligibly small and can be neglected, and Equation 2 reduces to the familiar law of Güntherschulze which describes the high field approximation:

$$i = A \exp (BH) \quad (4)$$

The ionic and the measured anodic current densities (cds) are equal when the anode process is exclusively oxide formation. This situation is approached in most of the work to be presented here by the proper choice of solution and by careful pretreatment of the surface. In some cases, such as W in acid, neutral, and alkaline solutions, anodic dissolution cannot be suppressed completely at the beginning of polarization, particularly at low cds, but as polarization proceeds the efficiency of oxide growth rises to about 90%. The oxide film grows at the phase boundary oxide/solution if the mobile ion is the cation, at the phase boundary metal/oxide if the mobile ion is the anion, and at both boundaries when both cation and anion are mobile. Therefore, the potential E of a working anode as measured against nhe may be replaced by the sum $\emptyset$ of the pds at the two phase boundaries and the pd E_f across the oxide film.

The simplest case occurs when the phase boundary potentials remain constant during oxide growth and the whole change in E is manifested across the oxide phase. Hence:

$$E = E_f + \emptyset \quad (5)$$

If δ represents the oxide thickness:

$$H = \left(\frac{dE}{d\delta}\right)_i = \left(\frac{dE_f}{d\delta}\right)_i \quad (6)$$

and in practice H is calculated from ($\Delta E/\Delta \delta$). This gives the effective overall field, which is a useful parameter insofar as it does not depend on the nature of the rate-determining step whether it is: (i) the entry of metal ion from metal to oxide, as in the Caberera-Mott theory (27), (ii) the transfer of cation within the oxide phase, as in the Verwey theory (28), or (iii) both interfacial and bulk control, as in the Dewald theory (29).

The amount of electricity (Q = i t) which passes per cm.^{2} at constant i increases the oxide thickness by $\Delta \delta$ such that at any time:

$$\delta = \delta_o + \Delta\delta \qquad (7)$$

where δ_o is the prepolarization film thickness. It follows that:

$$\Delta\delta = \left(\frac{M}{\sigma\ sn\ F}\right) i\ t = \left(\frac{r}{\sigma}\right) i\ t \qquad (8)$$

where M is the molecular weight of oxide, s its density, n the number of Faradays required for the formation of one mole oxide, σ is a roughness factor, r is the volume of oxide in cm.^{3} formed per coulomb, and t is reckoned from the beginning of polarization. If at stationary states the oxide suffers from dissolution with a rate i_s then:

$$\Delta\delta = \left(\frac{M}{sn\ F}\right) (i - i_s)\ t \qquad (9)$$

and i_s can be neglected when $i \gg i_s$. In general one may write:

$$i = \beta i_a \qquad (10)$$

where as previously mentioned i is the ionic cd, i_a is the total anodic cd, and β is the efficiency of oxide growth. Except for W, the efficiency is 100% for all other metals studied here. For W, however, β is 90%.

FORMATION RATE

Representative anodic charging curves are given in Figure 1 for Ti in 0.1M ammonium borate at 40° C., in Figure 2 for W in 0.05M Na_2SO_4 at 30° C., in Figure 3 for Bi in H_2SO_4 at 30° C., and in Figure 4 for Al in 0.1M H_3PO_4 at 30° C. In general, the shape of the charging curve depends on the metal, the composition of solution, the temperature, and the polarizing cd. In the region where anodic dissolution is significant, the potential does not rise at all, e.g., W at low cds, or rises nonlinearly with time at the beginning of polarization. This is followed in most cases by a linear E/t relation characteristic of galvanostatic oxide growth, a process which occurs under constant field since at constant i the potential across the growing oxide increases with increase of the time of polarization, i.e., with increase of oxide thickness thus maintaining a constant effective field. In this manner, the linear part of the charging curve is associated with a steady rate of oxide growth. Therefore, it follows from Equations 4, 7, and 8 that:

$$i = A \exp \frac{B\ E_f}{\delta_o + (rit/\sigma)} \qquad (11)$$

from which

$$E_f = \frac{\delta_o + rit/\sigma}{B} \ln\left(\frac{i}{A}\right) \qquad (12)$$

and the experimentally measured potential becomes:

$$E = \phi + \frac{\delta_o + rit/\sigma}{B} \ln\left(\frac{i}{A}\right) \qquad (13)$$

Therefore, the oxide formation rate is given by:

$$\left(\frac{dE}{dt}\right)_i = \left(\frac{d\ E_f}{dt}\right)_i = \left(\frac{ri}{\sigma\beta}\right) \ln\left(\frac{i}{A}\right) \qquad (14)$$

which is a constant at constant i.

The formation rate can be expressed in terms of the field by introducing the relation:

$$H = \frac{1}{B} \ln \left(\frac{i}{A}\right) \quad (15)$$

in Equation 14. Thus:

$$\left(\frac{dE}{dt}\right)_i = \left(\frac{ri}{\sigma}\right) H \quad (16)$$

and this relation can be used to calculate H from the experimental formation rate with the knowledge of r and σ

In almost all the literature on the anodization of value metals, the formation rate is related to i by the empirical relation:

$$\left(\frac{dE}{dt}\right)_i = a\,(i)^b \quad (17)$$

where a and b are constants characteristic of the system. Consequently, log $(dE/dt)_i$ is linearly related to log i as shown in Figure 5 for Ti in 0.1M ammonium borate at several temperatures between 20 and 70° C. The formation rate is expressed here in V/sec. The empirical relation does not follow directly from the theory (Equation 14) unless

$$a = \left(\frac{2.303\ r}{\sigma\ B}\right) \log \left(\frac{i}{A}\right) \text{ and } b = 1 \quad (18)$$

in which case a should be a linear function of log i. However, the experimental results show that a is practically constant in a certain solution over a range of cds. Furthermore, b is not exactly one. It is possible that a varies with log i according to Equation 18, but the variation is of the order of the experimental error, particularly in a limited range of cds. Regardless of this difficulty, the constants a and b are useful to predict the oxide formation rates at cds within the range in which a and b are determined from experimental results. Table 1 gives some values of a and b.

RECIPROCAL CAPACITY

The reciprocal capacity is derived from Equation 14 by dividing both sides by i:

$$\frac{1}{C} = \frac{1}{i}\left(\frac{dE}{dt}\right)_i = \left(\frac{dE}{dQ}\right)_i = \left(\frac{r}{\sigma\ B}\right) \ln \left(\frac{i}{A}\right) \quad (19)$$

and 1/C is given in $cm.^2$/farad. The linear relation between reciprocal capacity and log i gives a slope of $(2.303\ r/\sigma\ B)$ and an intercept on the 1/C axis of $-\left(\frac{2.303\ r}{\sigma\ B}\right) \log A$. This enables us to calculate both A and B which are known as "electrolytic parameters." Examples of 1/C vs. log i plots are given in Figure 6 for Al and in Figures 7 and 8 for W. Since Equation 19 is based on the exponential law of Güntherschulze, straight lines as shown in Figures 6-8 are taken as positive criteria for the applicability of the high field approximation, i.e., high field ionic conduction. In all cases studied here, the linearity between 1/C and log i is established for all cds at which oxide growth occurs even at low cds between 1 and 10 $\mu A/cm.^2$, and no indication of the low field approximation has been obtained here. It is possible that Ohm's law of conduction may operate at cds below 1 $\mu A/cm.^2$ and also for tarnishing reactions. Again, the effective field H can be calculated from reciprocal capacity by introducing Equation 15 in 19:

$$\frac{H}{\sigma} = \frac{1}{r\ C} \quad (20)$$

It is better to express the field as H/σ in order to eliminate the uncertainty in σ. Alternatively, one may take a value of 2-3 for σ which has been experimentally found for fine mechanical pretreatment. The value of r depends on the nature of the oxide species which is predominantly formed during anodization. This species can be indicated after consulting thermodynamics concerning the stability of the various oxides.

EFFECTIVE FIELD

Some representative values of H are given in Table 2. These are calculated on the basis of $\sigma = 2$. While most of the results lie around 10^6 V/cm., W is associated with values higher than 10^6 and both Sb and Bi give slightly lower values. The effect of cd is evident from the data given in Table 2, and direct proportionality between i and H is established in accordance with the requirements of the theory. Moreover, information regarding the effect of solution composition on the film can be obtained by comparing the values of H calculated for a certain metal at constant cd and constant temperature in different solutions. Thus for Bi, the effective field at 100 μA/cm.^{2} decreases in the order Na_2SO_4, Na_2CO_3, and NaOH (all 0.05M). This behavior may be related to the pH of solution.

PREPOLARIZATION THICKNESS

The potential/log i relation, i.e., the usual Tafel relation of electrode kinetics, can be constructed from the anodic charging curves at various cds but at the same value of t. Assuming careful work, the same procedure of pretreatment leads to the same prepolarization oxide thickness δ_o. Therefore, one gets from Equation 13:

$$\left(\frac{dE}{d \ln i}\right)_t = \left(\frac{\delta_o}{B}\right) + \left(\frac{rit}{\sigma B}\right) \left[1 + \ln \frac{i}{A}\right] \qquad (21)$$

which shows that the Tafel slope increases with increase of cd.

One may also construct Tafel lines at constant Q. Thus, replacing it by Q in Equation 13 one gets:

$$\left(\frac{dE}{d \ln i}\right)_Q = \left(\frac{\delta_o}{B}\right) + \left(\frac{r\,Q}{\sigma B}\right) \qquad (22)$$

In this case, E/Q relations are first obtained from the experimental E/t curves, and Tafel lines are constructed at some selected values of Q. Examples of the results thus obtained are shown in Figure 9 for W in neutral solutions. It is interesting to note that W is among the few metals which can be anodized in presence of chloride ions. The Tafel slopes in Figure 9 increase with increase of Q in accordance with Equation 22. Thus, with the knowledge of r, σ, B, and Q, the prepolarization oxide thickness δ_o may be estimated from the slope of the Tafel line. Assuming $\sigma = 2$, the values obtained for on W in NaCl and Na_2SO_4 solutions range between 4 and 62 Å. Much lower values of 3-12 Å are obtained for Ti in acid media. One may use these approximate values of δ_o in Equation 13 in order to obtain approximate values for $\emptyset$, the sum of the phase boundary potentials. The results give $\emptyset$ = - 400 to - 600 mV (NHE) for Ti in acid media.

ENERGETICS OF ION TRANSPORT

The exponential law of Güntherschulze (Equation 4) has been derived by Yahalom and Hoar (30) on the basis of the theory of rate processes as:

$$i = z F \left(\frac{k T}{h}\right) \left(\frac{n}{N}\right) \exp\left(-\frac{\Delta G^*_o}{RT}\right) \exp\left(\frac{z F a^*}{RT} H\right) \quad (23)$$

where z is the valency of the mobile ion, n is the number of charge carriers per cm.^{2}, ΔG^*_o is the standard free energy of activation for the ionic jump in absence of field, and a* is the effective activation distance which is related to the width x of energy barrier by:

$$a^* = \alpha \; x \quad (24)$$

where α is the symmetry factor. Therefore, a* is half the barrier width for symmetrical barriers. It follows by comparing Equations 4 and 23 that:

$$A = z F \left(\frac{k T}{h}\right) \left(\frac{n}{N}\right) \exp\left(-\frac{\Delta G^*_o}{RT}\right) = A_o \exp\left(-\frac{W}{R T}\right) \quad (25)$$

where W is the heat of activation in absence of field,

$$B = \frac{z F a^*}{RT} = \frac{z F \alpha x}{RT} = \frac{c a^*}{k T} \quad (26)$$

and q is the charge of the mobile ion. Therefore, the parameters A and B which can be calculated from the reciprocal capacity/log i relations are used to throw some light on the height and width of energy barrier. In this manner, the effect of solution composition on the oxide film can be studied by comparing the height and width of energy barrier for different solution composition and contamination of the oxide film by anions from solution, e.g., phosphate and sulfate can be detected.

Table 3 gives some values of the electrolytic parameters and the activation distance. Since a* is very sensitive to variations in B, both B and a* are reported as σ B and σ a*. Although the data obtained for the activation distance are on the whole very small, some reasonable values of several angstroms are obtained. It must be emphasized here that the nature of the experimental technique does not allow accurate determinations of the activation distance, and the results can only give relative magnitudes for comparison. Thus, for Sb the width of the barrier is maximum in oxalate and minimum in H_2SO_4 solutions.

It is clear from Equation 25 that parameter A is a function of the height of the energy barrier, and values of A can be qualitatively used to study the effect of solution composition, pH, temperature, etc., on the height of the energy barrier.

Quantitative results may be obtained by considering the effect of temperature on A. Thus, if the pre-exponential term A_o is independent of temperature, one expects to get a straight line relation between log A and 1/T according to:

$$\left(d \log A / d \frac{1}{T}\right) = -\frac{W}{2.303 \; R} \quad (27)$$

This linearity is established in many cases, and an example of the results obtained is shown in Figure 10 for thin films on Ti in 0.1M ammonium borate (pH = 7.6) in the temperature range 20-70° C. at cds between 7 and 50 μA/cm.^{2}. Figure 10 gives A_o = 7.9 x 10^{-3} A/cm.^{2} and W = 8.7 Kcal/mole. Similar results have been obtained for Nb.

The effect of temperature on the electric field is derived from:

$$i = A_o \exp\left(-\frac{W}{RT}\right) \exp(BH). \quad (28)$$

When the experimental results indicate constant values of both B and W in a certain temperature range, and since A_o is independent of temperature, one gets at constant i:

$$\left(\frac{d\,H}{d\,1/T}\right)_i = \frac{W}{BR} \cdot \quad (29)$$

The field may be expressed as H/σ in order to eliminate the uncertainty in the roughness factor, and hence Equation 29 may be written as:

$$\left(\frac{d\,H/\sigma}{d\,1/T}\right)_i = \frac{W}{\sigma BR} \quad (30)$$

This relation is shown in Figure 11 for Ti in 0.1M borate for cds between 7 and 30 μA/cm.^{2} Parallel straight lines are obtained in all cases, and these lines are displaced toward higher values of H as the cd increases. It is seen from Equation 28 that at constant A_o, W, B, and H:

$$\left(\frac{d\,\log\,i}{d\,\,1/T}\right)_H = -\frac{W}{2.303\,R} \quad (31)$$

and this is identical to Equation 27. Equation 31 is plotted in Figure 12 for Ti, and three parallel straight lines are obtained at three different values of field. Identical results are obtained for W from the dependence of A, H, and i on the reciprocal of T. This adds another proof for the validity of the high field approximation, even for thin films formed below the oxygen evolution potential.

CURRENT DENSITY/TIME RELATIONS

The dependence of cd on time at constant anode potential (i.e., potentiostatic) can be derived from the experimental galvanostatic charging curves at some selected constant values of potential. Figure 13 shows the results obtained for Ti in 0.1M borate at 40° C. for potentials between 0.5 and 2.5 V (nhe). The cd decreases asymptotically with time at constant E. Figure 14 shows that log i is linearly related to log t at each potential and that the slope of the straight line decreases with increase of E. The straight lines of Figure 14 may be expressed by the relation:

$$i\,(t)^{\gamma} = \text{constant} \quad (32)$$

where γ is the slope of the log/log relation. Figure 14 gives the following values of γ : 1.06, 1.00, 0.95, 0.90, and 0.85 for 0.5, 1.0, 1.5, 2.0, and 2.5 V.

It will be shown below that Equation 32 follows from the theory of galvanostatic anodization under the conditions of high field. Since at constant potential both i and H decrease with time (Figure 13), the oxide thickness must increase with time. In this case, one may write:

$$\Delta\delta = \frac{r}{\sigma}\int_0^t i\,(t)\,dt = \frac{r}{\sigma}\,Q\,(i,t) \quad (33)$$

with the amount of electricity Q as a function of i and t. Therefore, the exponential law (cf. Equation 11) may be written in the general form which applies to galvanostatic and potentiostatic conditions as:

$$i = \left(\frac{dQ}{dt}\right) = A\exp\left[\frac{B\,E_f}{\delta_o + \left(\frac{r}{\sigma}\right)Q}\right] \quad (34)$$

From Equation 34 one gets:

$$\frac{d\,\ln\,i}{dt} = -\frac{B\,E_f\,(r/\sigma)\,(dQ/dt)}{\delta_o + (r/\sigma)\,Q^{\,2}} \quad (35)$$

Multiplying the numerator and denominator by $B\ E_f$ and substituting Equation 34 in the resulting equation, one gets:

$$\frac{d \ln i}{dt} = -\left(\frac{r\ i}{\sigma\ B\ E_f}\right)\left(\ln \frac{i}{A}\right)^2 \quad (36)$$

Putting $dt = t\ d \ln t$, it follows that:

$$\frac{d \ln i}{d \ln t} = -\left(\frac{rit}{\sigma\ B\ E_f}\right)\left(\ln \frac{i}{A}\right)^2 = -\gamma \quad (37)$$

and this reduced to Equation 32 which is based on experimental data. The fact that γ decreases with increase of E is evident from Equation 37.

Equation 37 can be verified in another way. Rearranging (37) and dividing both sides by A, one gets:

$$\left(\frac{i\ t}{A}\right)\left(\ln \frac{i}{A}\right)^2 = \gamma\left(\frac{B\ E_f}{r\ A}\right) = \lambda \quad (38)$$

where λ is a constant at constant potential. Putting $u = (i/A)$, it follows:

$$Y = u\ (\ln u)^2 = \lambda/t \quad (39)$$

and the plot of Y vs 1/t should yield a straight line if Equation 37 is valid. Figure 15 shows that this is true for the results on Ti and that the slope λ increases with increase of potential. The straight lines of Figure 15 do not exactly pass through the origin, and such small deviations are expected since potentiostatic curves are derived from galvanostatic measurements.

DIELECTRIC BREAKDOWN

While measurements at low cds are associated with the development of interference colors on the surface, measurements at relatively higher cds (mA range) produce dull grey films and bring the potential rapidly to high values whereupon dielectric breakdown commences. This is manifested as oscillations in potential, the amplitude of which increases with increase of the time of polarization. In some cases, sparking occurs. The breakdown potential depends on the nature of the metal and the composition of solution. It may reach values as high as 250 V. Visible gas evolution is observed during breakdown. Various mechanisms have been proposed for dielectric breakdown. These include: (i) joule heating, (ii) mechanical flows, (iii) avalanche breakdown, and (iv) internal compressive stress. Wood and Pearson (31) have shown that the breakdown potential does not depend on the rate of electrolyte flow, thus excluding joule heating. Furthermore, this potential does not depend on the distribution of flaws. Therefore, the most likely mechanisms are the avalanche breakdown and the internal compressive stress caused by mechanical changes in the oxide film. Both mechanisms are indicated in the present work, since they depend on the electrolyte by virtue of its conductivity for the avalanche type and due to contamination by anions for the internal compressive stress.

REFERENCES

1. A. Güntherschulze and H. Betz, Z. Phys., 71, 106 (1931).
2. A. Güntherschulze and H. Betz, Elektrolyt-Kondensatoren, Krayn, Berlin (1937).
3. G. B. Adams, P. Van Rysselberghe and M. Maraghini, J. Electrochem. Soc., 102, 502 (1955).

4. H. Johansen, G. B. Adams, and P. Van Rysselberghe, J. Electrochem. Soc., 104, 339 (1957).

5. P. Van Rysselberghe and H. A. Johansen, J. Electrochem. Soc., 106, 335 (1959).

6. G. C. Willis, G. B. Adams, and P. Van Rysselberghe, Electrochim. Acta, 9, 79 (1964).

7. D. A. Vermilyea, Acta Met., 2, 476 (1954).

8. D. A. Vermilyea, J. Electrochem. Soc., 102, 207 (1955).

9. D. A. Vermilyea, J. Electrochem. Soc., 104, 542 (1957).

10. I. Young, Anodic Oxide Films, Academic Press (1961).

11. I. A. Ammar and I. K. Ismail, Werkstoffe und Korrosion, 23, 168 (1972).

12. I. A. Ammar and I. Kamal, Electrochim. Acta, 16, 1539, 1568 (1971).

13. I. A. Ammar and I. K. Ismail, Werkstoffe und Korrosion, 23, 25 (1972).

14. I. A. Ammar and I. K. Ismail, Metalloberfläche, 26, 378 (1972).

15. I. A. Ammar, S. Darwish, and E. A. Ammar, Metalloberfläche, 27, 163 (1973).

16. I. A. Ammar and R. Salim, Corros. Sci., 11, 591 (1971).

17. I. A. Ammar and R. Salim, Werkstoffe und Korrosion, 23, 161 (1972).

18. I. A. Ammar and M. W. Khalil, Metalloberfläche, 26, 337 (1972).

19. I. A. Ammar, S. Darwish, and E. A. Ammar, Werkstoffe und Korrosion, 24, 200 (1973).

20. S. Darwish, Corrosion, 27, 265 (1971).

21. I. A. Ammar, E. A. Ammar, and R. Salim, Metalloberfläche, 26, 427 (1972).

22. I. A. Ammar and A. Saad, J. Electroanal-Chem., 30, 395 (1971); 34, 159 (1972).

23. I. A. Ammar, S. Darwish, and A. Saad, Metalloberfläche, 28, 349 (1974).

24. I. A. Ammar and M. W. Khalil, Electrochim. Acta, 16, 1379, 1601 (1971).

25. I. A. Ammar and M. W. Khalil, J. Electroanal. Chem., 32, 373 (1971).

26. I. A. Ammar, S. Darwish, and M. W. Khalil, Corrosion, 32, 173 (1976).

27. N. Cabrera and N. F. Mott, Repts. Prog. Physics, 12, 163 (1948).

28. F. J. Verwey, Physica, 2, 1059 (1935).

29. J. F. Dewald, J. Electrochem. Soc., 102, 1 (1955).

30. J. Yahalom and T. P. Hoar, Electrochim. Acta, 15, 877 (1970).

31. G. C. Wood and C. Pearson, Corros. Sci., 7, 119 (1967).

Table 1: Constants of Empirical Relation at 30° C.

Metal	Solution	cd Range	a*	b
Ta	0.1M H_3PO_4	1-10 μA/cm.^{2}	2.0×10^3	1.20
Zr	0.1M H_3PO_4	1-10	2.2×10^2	1.06
Nb	0.1M $NH_4H_2PO_4$	500-5000	4.1×10^2	1.10
W	1.0M $HClO_4$	50-250	2.0×10^3	1.27
	1.0M HNO_3	50-250	3.9×10^4	1.57
	0.5M H_2SO_4	50-250	1.2×10^4	1.42
Al	0.1M Borate	5-25	4.7×10^4	1.55
	0.1M $(NH_4)_2HPO_4$	5-25	1.0×10^3	1.26
	0.1M Benzoate	5-25	9.8×10^3	1.38
Te	0.1M Benzoate	1-10 mA/cm.^{2}	5.6×10^3	1.70
	0.1M Na_2SO_4	1-10 mA/cm.^{2}	3.0×10^3	1.70
	0.1M Borate	1-10 mA/cm.^{2}	5.1×10^3	1.82
	0.1M Na_2CO_3	1-10 mA/cm.^{2}	4.0×10^3	1.85
Sb	0.1M K_2CO_3	0.3-1.0 mA/cm.^{2}	2.4×10^3	1.45
	0.1M H_3PO_4	0.3-1.0 mA/cm.^{2}	2.0×10^3	1.43
	0.1M NaOH	0.3-1.0 mA/cm.^{2}	0.8×10^3	1.33
Bi	0.05M Na_2SO_4	10-100 μA/cm.^{2}	2.4×10^2	1.17
	0.05M Na_2CO_3	10-100 μA/cm.^{2}	1.9×10^2	1.16
	0.05M NaOH	10-100 μA/cm.^{2}	2.5×10^2	1.20

*a has the dimensions of reciprocal capacity (cm.^{2}/farad) if b = 1. However, since b $\neq$ 1, a is expressed in (cm.^{2}/farad) x (cm.^{2}/amp)$^{b-1}$.

Table 2: Effective Field at 30° C.

Metal	Solution	cd $\mu A/cm.^2$	$H \times 10^{-6}$ (V/cm)
Ta	0.1M H_3PO_4	5	6.6
		10	7.6
Zr	0.1M Na_3PO_4	5	3.6
		10	3.8
Ti	1.0M Na_2SO_4	10	7.4
		20	8.4
		35	9.2
	1.0M $NaNO_3$	10	6.2
		20	7.0
W	0.5M H_2SO_4	100	9.0
		150	10.8
		200	12.0
Al	0.1M Borate	10	3.6
Sb	0.05M H_2SO_4	60	0.6
		240	2.5
Bi	0.05M H_2SO_4	1000	2.0
	0.05M Na_2SO_4	100	1.0
	0.05M Na_2CO_3	100	0.9
	0.05M NaOH	100	0.7

Table 3: Electrolyte Parameters and Effective Activation Distance at 30° C.*

Metal	Solution	$A \times 10^6$ (A/cm.^{2})	$\sigma B \times 10^6$ (cm./V)	a* (Å)
Nb	0.1M H_3PO_4	13.4	1.00	0.50
	0.1M H_2SO_4	2.3	1.70	0.85
	0.1M HNO_3	14.9	1.58	0.80
	0.1M $NaNO_3$	12.0	2.27	1.13
Ta	0.1M H_3PO_4	0.014	1.80	0.90
	0.1M Na_3PO_4	0.04	1.90	0.90
Al	0.1M Benzoate	0.96	0.98	0.80
	0.1M Borate	1.70	1.00	0.80
	0.1M H_2SO_4	7.4	7.9	6.60
	0.1M $(NH_4)_2HPO_4$	0.12	4.7	3.9
Sb	0.1M Na_2SO_4	53.0	2.5	2.1
	0.05M H_2SO_4	17.0	2.1	1.7
	0.03M H_3PO_4	0.41	3.5	2.9
	0.1M Borate	37.1	3.1	2.6
	0.1M Acetate	3.9	6.5	5.4
	0.1M Oxalate	31.6	14.0	10.5
	0.1M Benzoate	15.5	2.2	1.8
Bi	0.05M Borate	4.1	3.9	3.2
	0.05M Benzoate	1.3	4.7	3.9

* Calculations are made for a mobile cation.

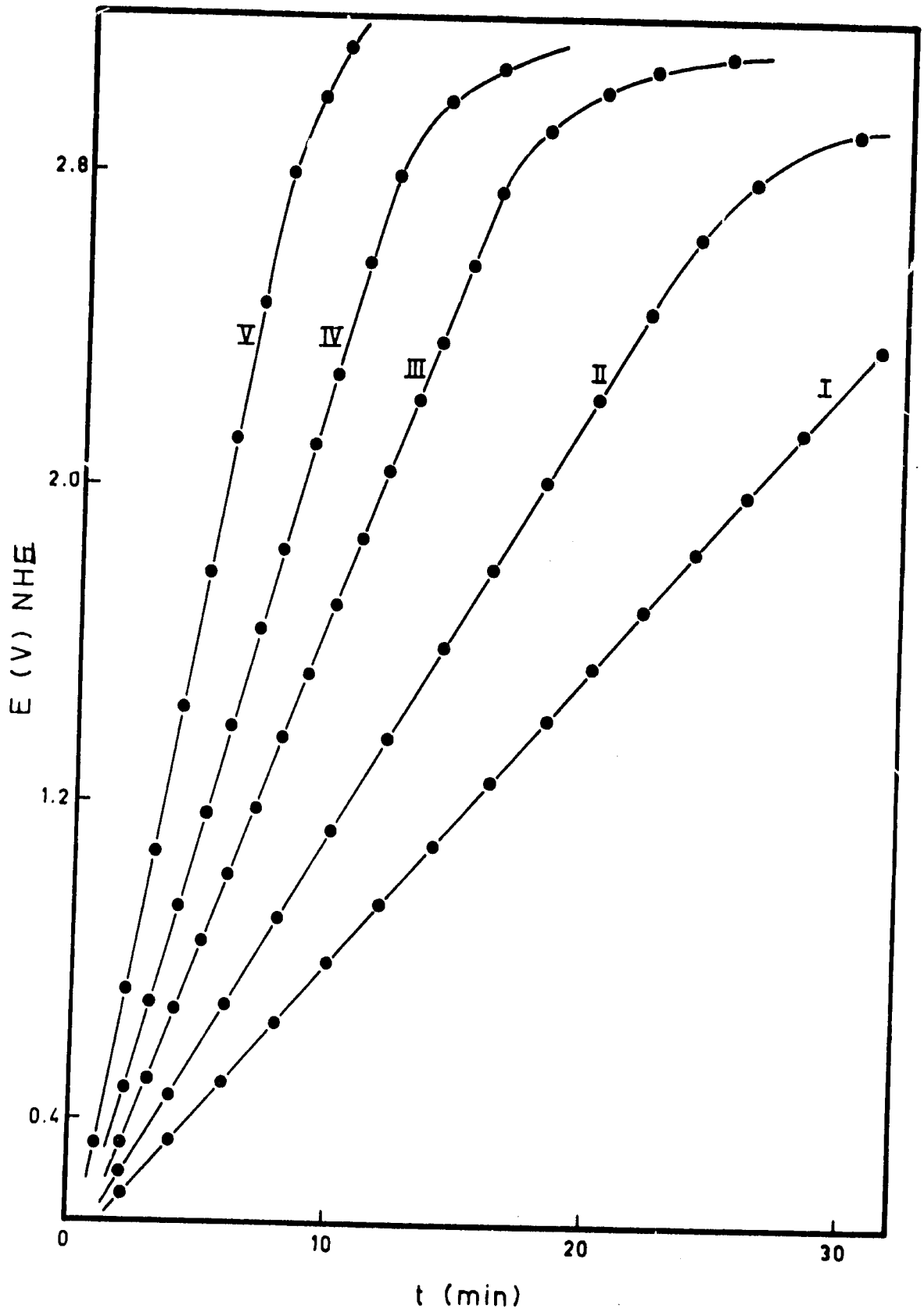

Figure 1

Anodic charging curves on Ti in 0.1M ammonium borate at 40° C. I = 7; II = 10; III = 15; IV = 20; and V = 30 μA/cm.^{2}

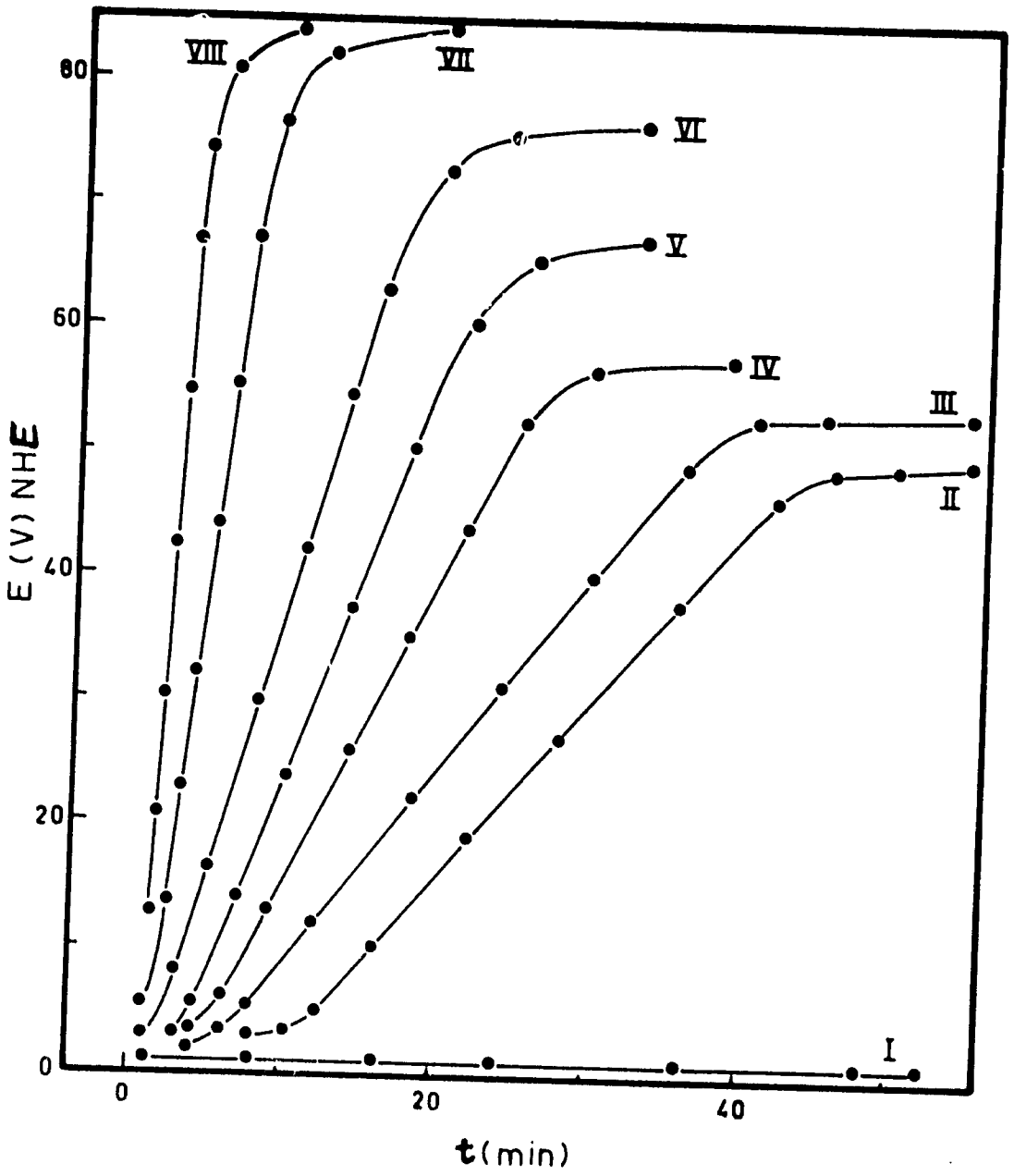

Figure 2

Anodic charging curves on W in 0.05M Na_2SO_4 at 30° C.: I = 150; II = 180; III = 200; IV = 220; V = 250; VI = 300; VII = 500; VIII = 800 $\mu A/cm.^2$

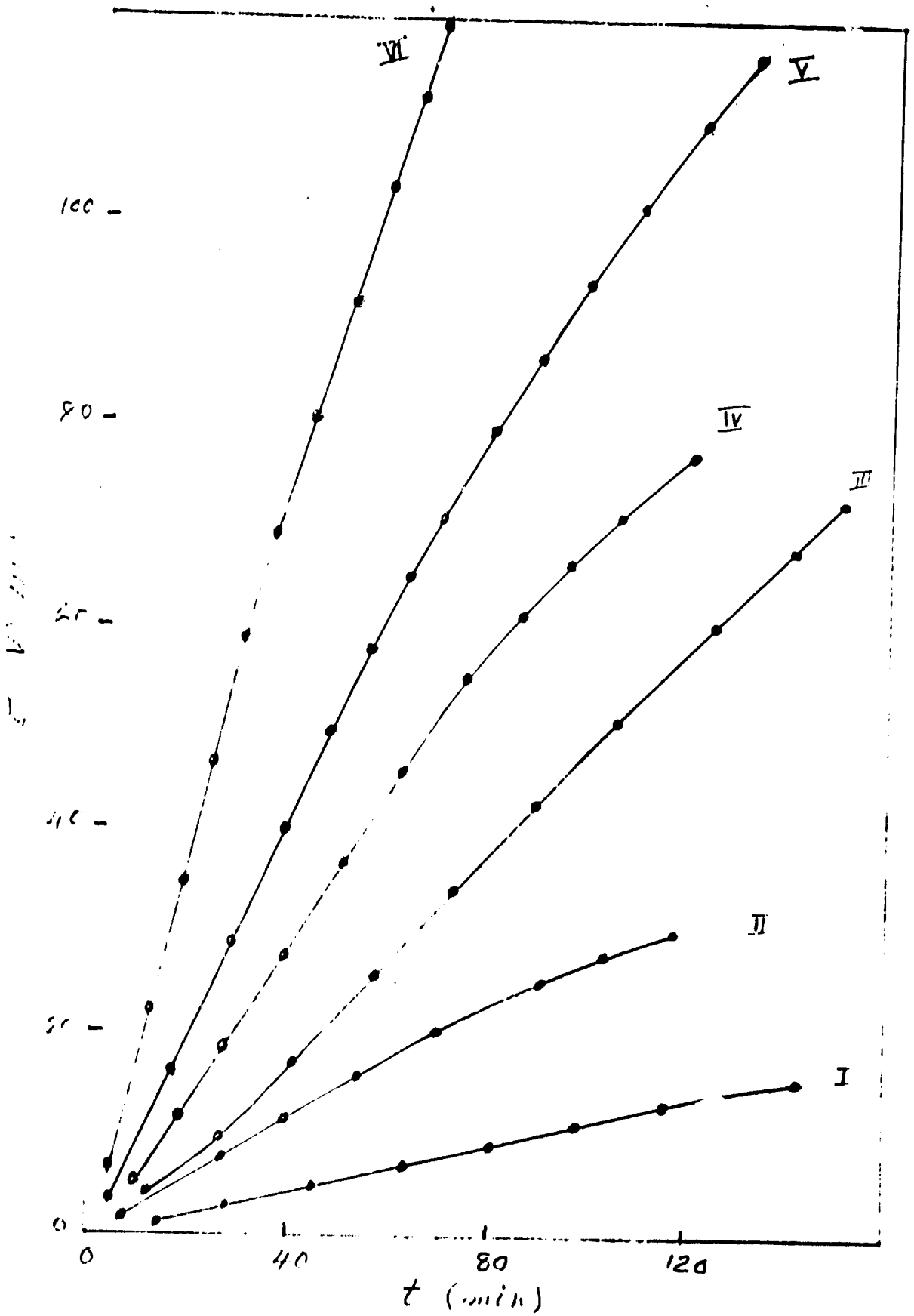

Figure 3

Anodic charging curves on Bi in 0.1N H_2SO_4 at 30° C.: I = 100; II = 150; III = 200; IV = 250; V = 300; VI = 500 $\mu A/cm.^2$

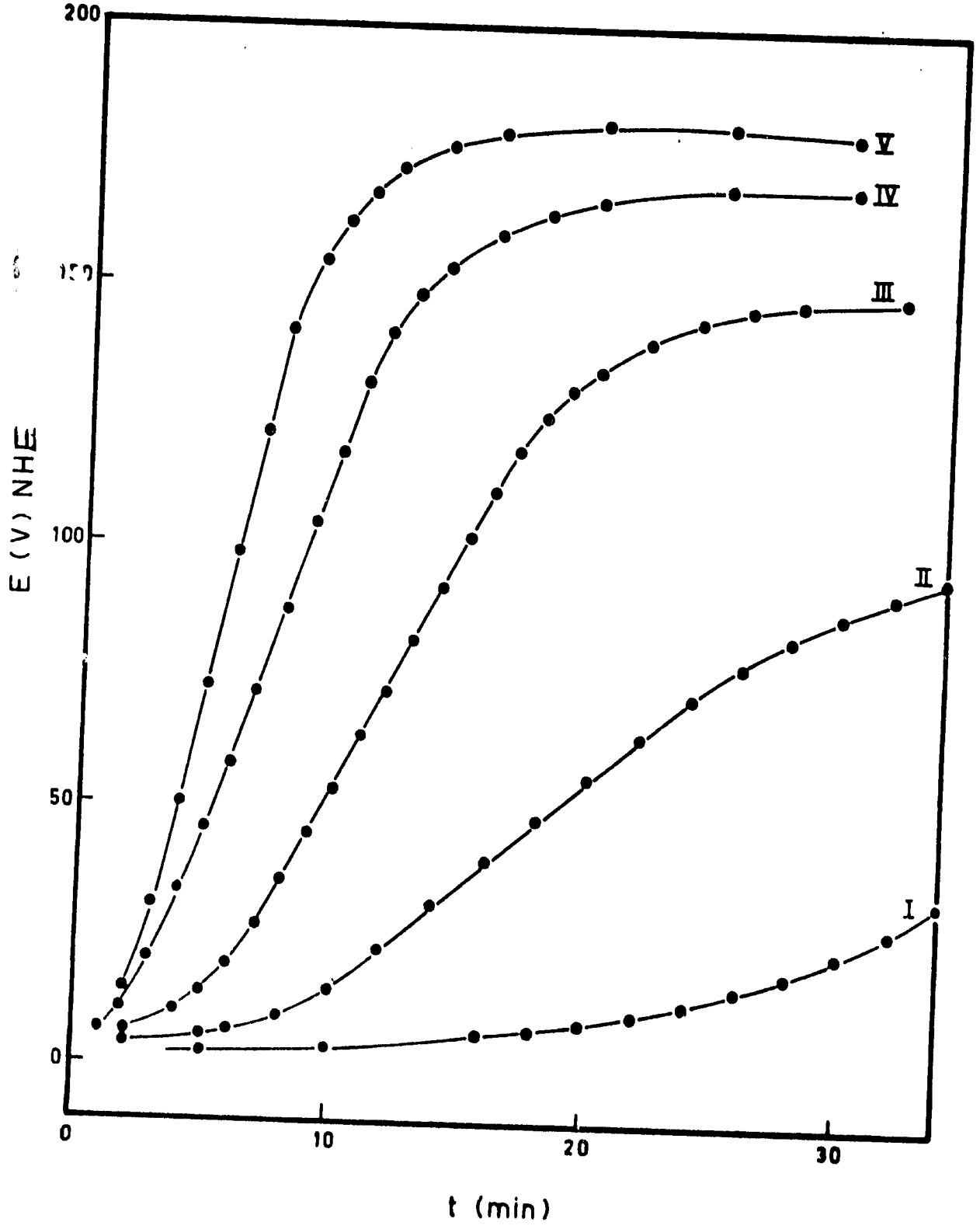

Figure 4

Anodic charging curves on Al in 0.1M H_3PO_4 at 30° C.:
I = 2; II = 3; III = 5; IV = 7; V = 10 mA/cm.^{2}

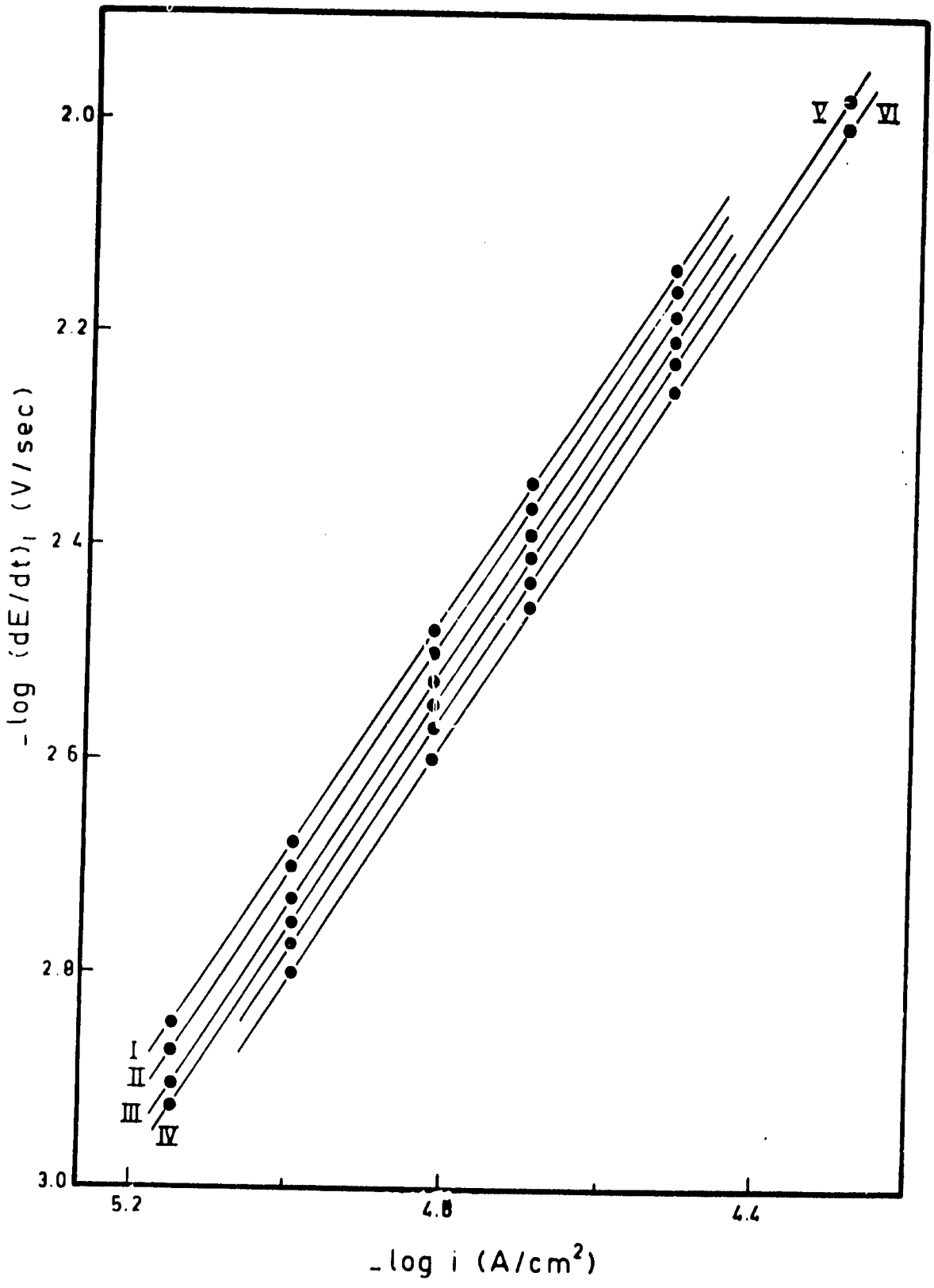

Figure 5

Relation between the logarithm of formation rate and log i for Ti in 0.1M ammonium borate at: I = 20; II = 30; III = 40; IV = 50; V = 60; VI = 70° C.

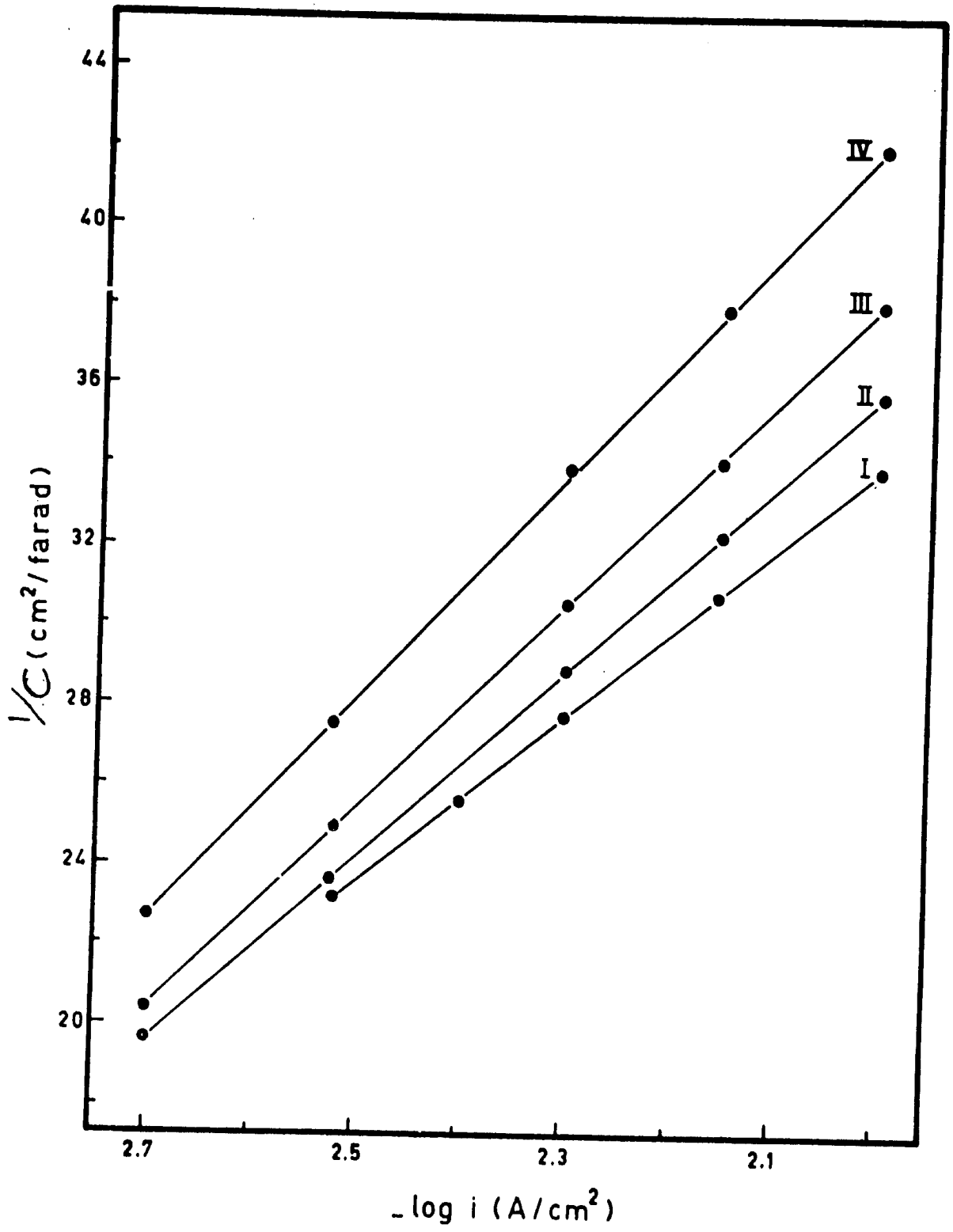

Figure 6

Reciprocal capacity vs. log i plots for Al in 0.1M solutions of Na_3PO_4 (I); Na_2CO_3 (II); H_3PO_4 (III); Na_2HPO_4 (IV) at 300 C.

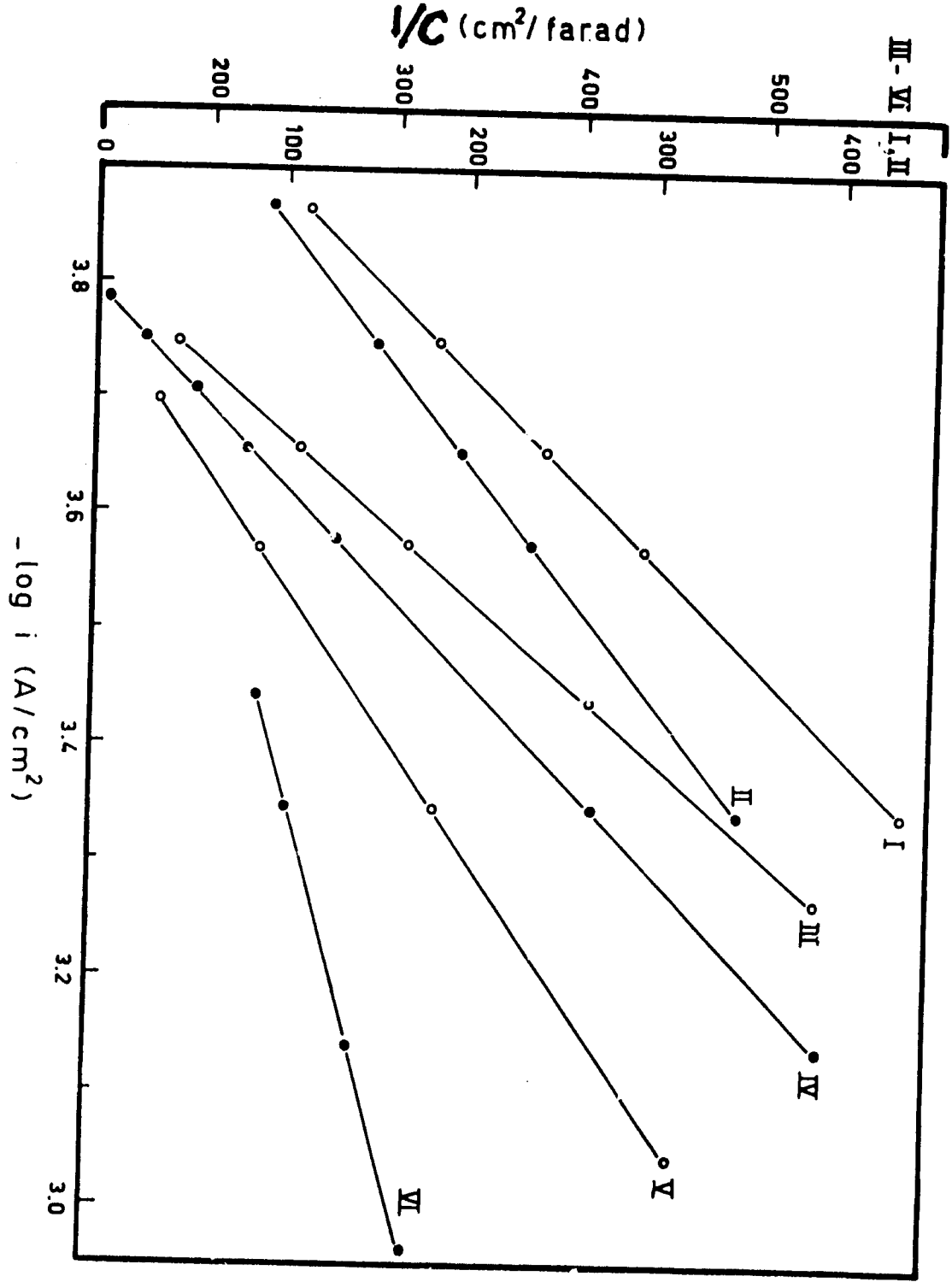

Figure 7

Reciprocal capacity/log i relations for W in chloride and sulfate solutions: NaCl--I = 0.01M, II = 0.05M; Na_2SO_4--III = 0.005M, IV = 0.05M, V = 0.1M, VI = 0.5M

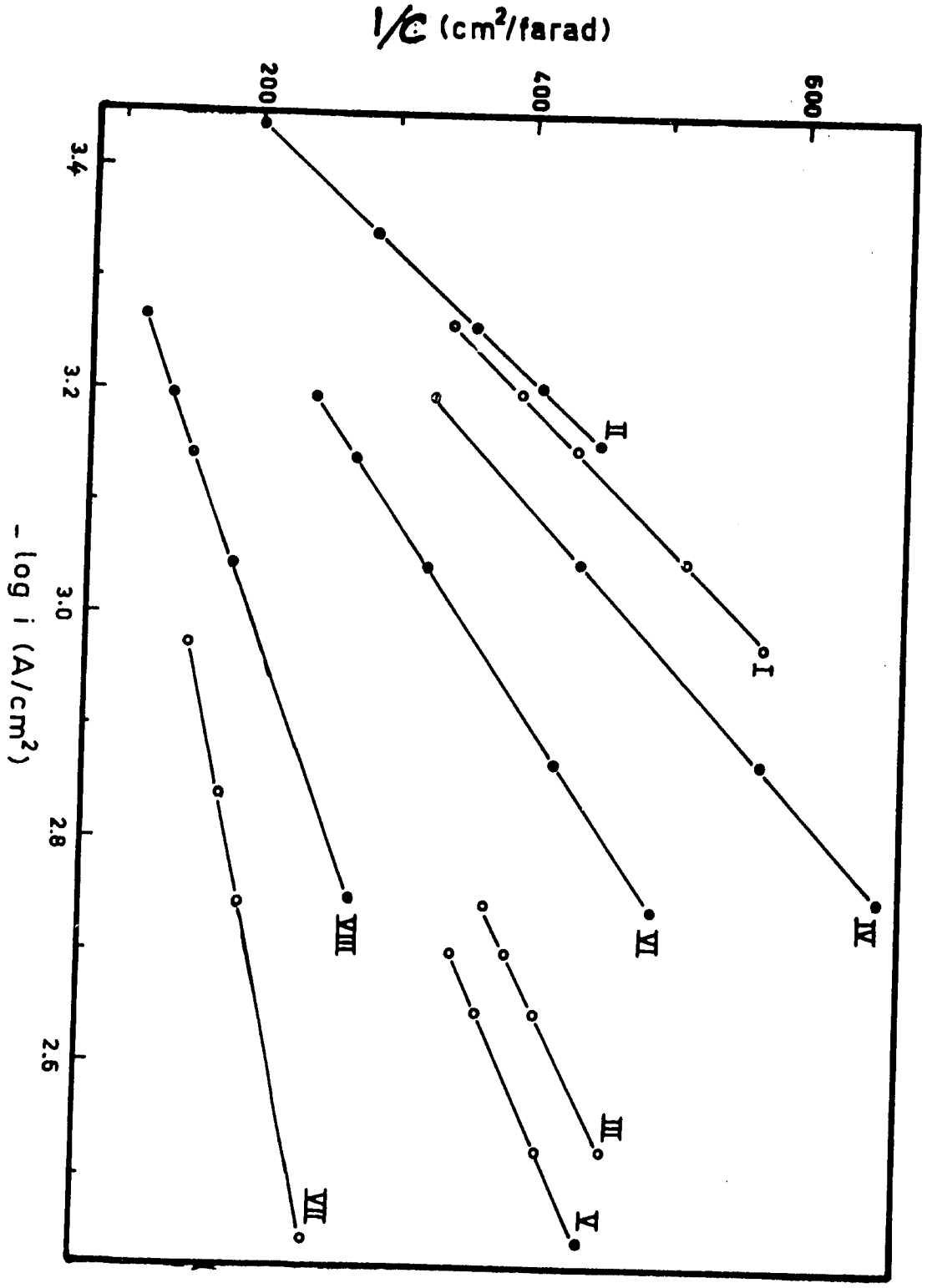

Figure 8

Reciprocal capacity/log i relations for W in alkaline solutions:

- o 0.03M solutions of ammonium borate (I), Na_2CO_3 (III), Na_3PO_4 (V), NaOH (VII).
- • 0.01M solutions of ammonium borate (II), Na_2CO_3 (IV), Na_3PO_4 (VI), NaOH (VIII).

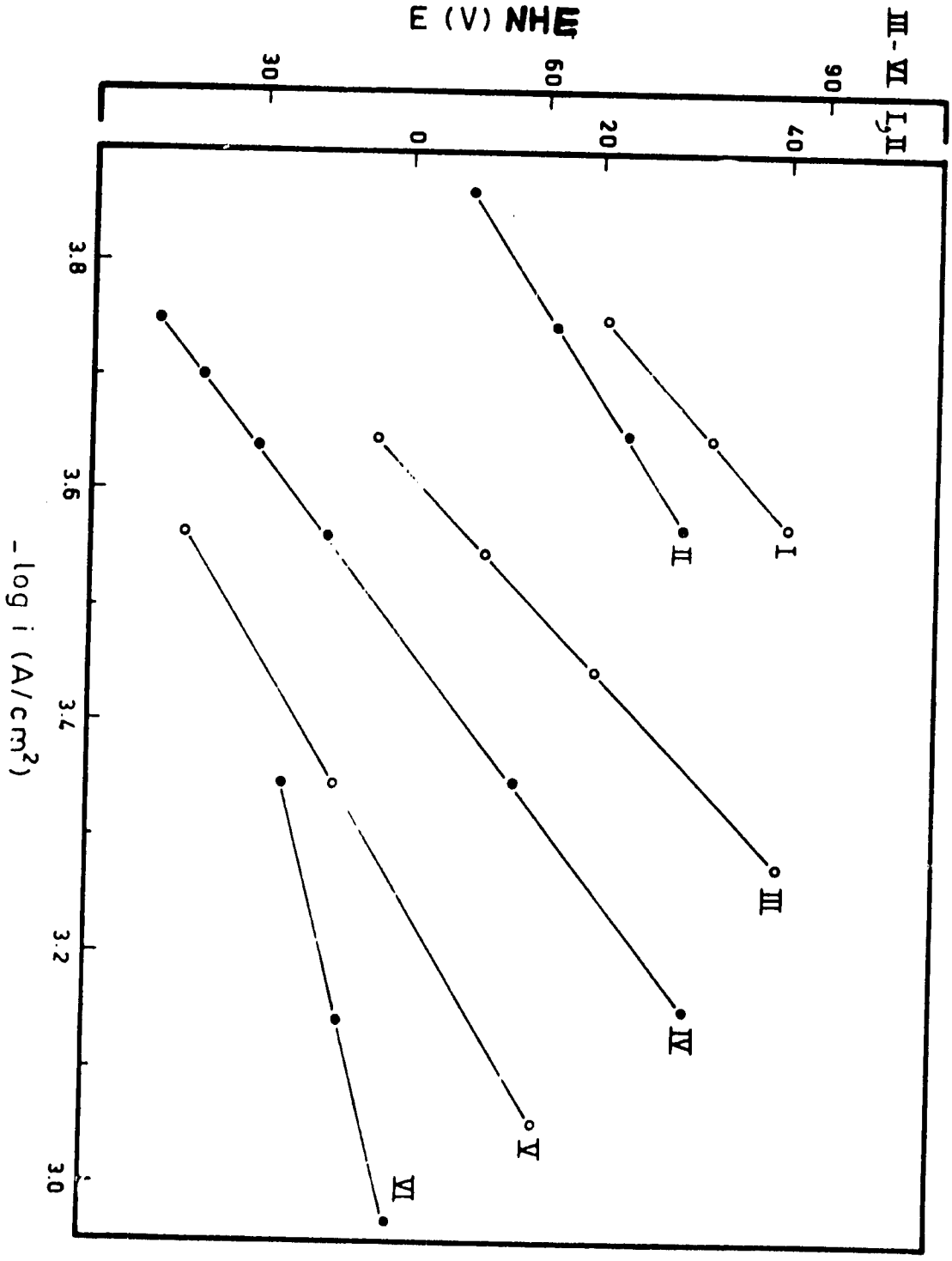

Figure 9

Tafel (E/log i) relations at Q = 162 m C/cm.^{2} for W in 0.01M NaCl (I), 0.05M NaCl (II), 0.005M Na_2SO_4 (III), 0.05M Na_2SO_4 (IV), 0.1M Na_2SO_4 (V), and 0.5M Na_2SO_4 (VI).

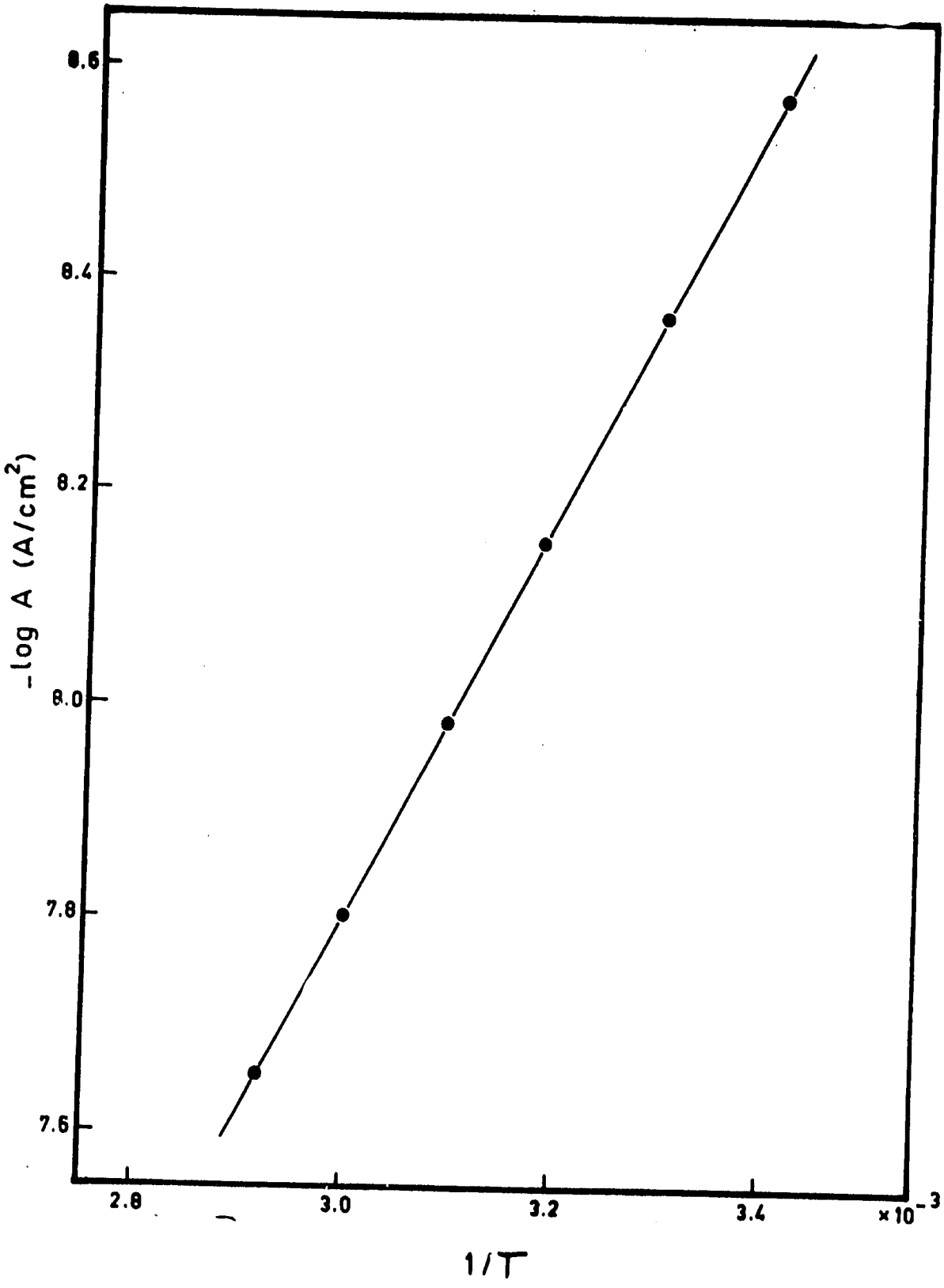

Figure 10

Relation between the logarithm of the electrolytic parameter A and the reciprocal of the absolute temperature for Ti in 0.1M borate.

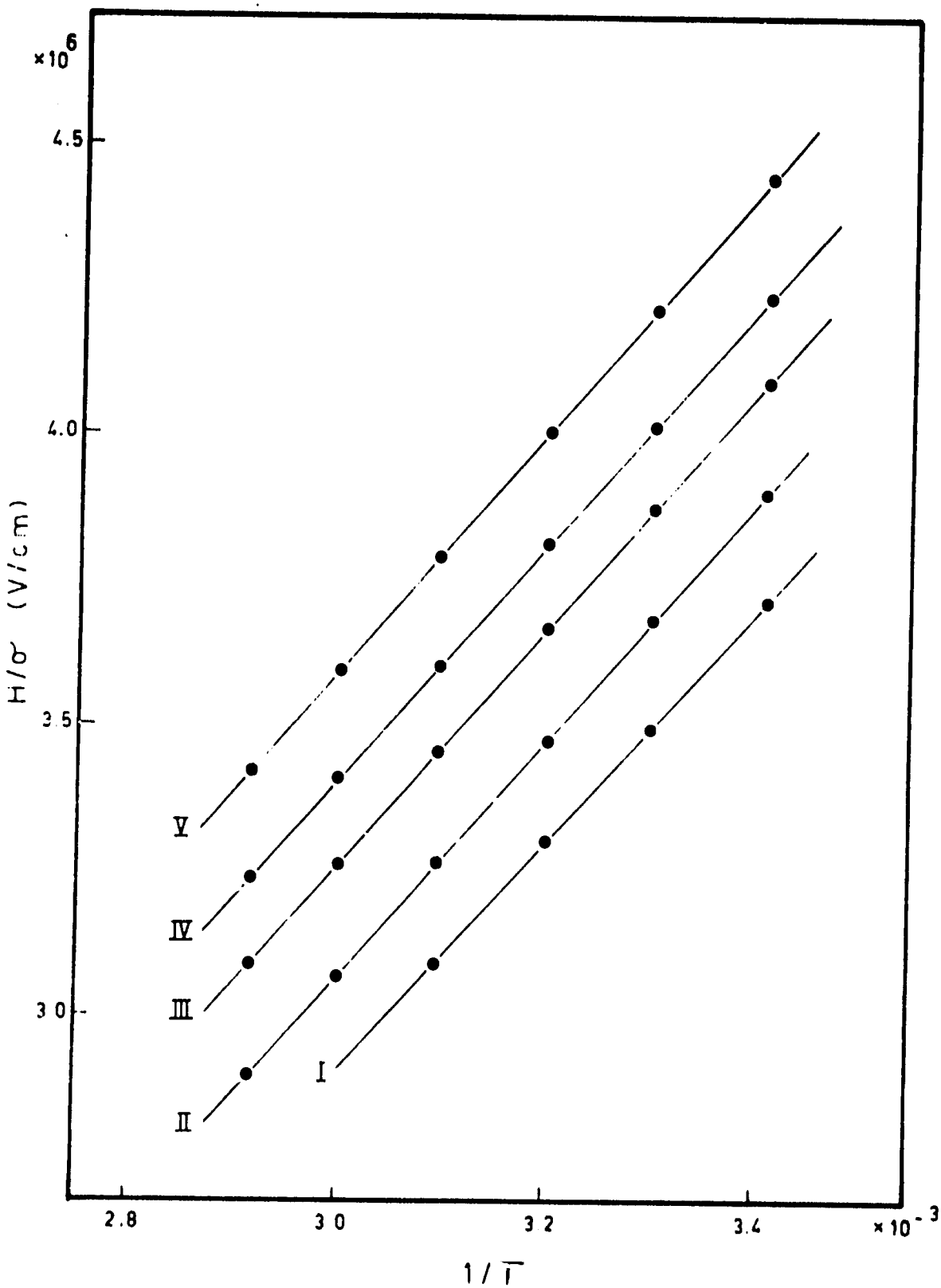

Figure 11

Dependence of the electric field on 1/T for Ti in 0.1M borate: I = 7; II = 10; III = 15; IV = 20; V = 30 $\mu A/cm.^2$

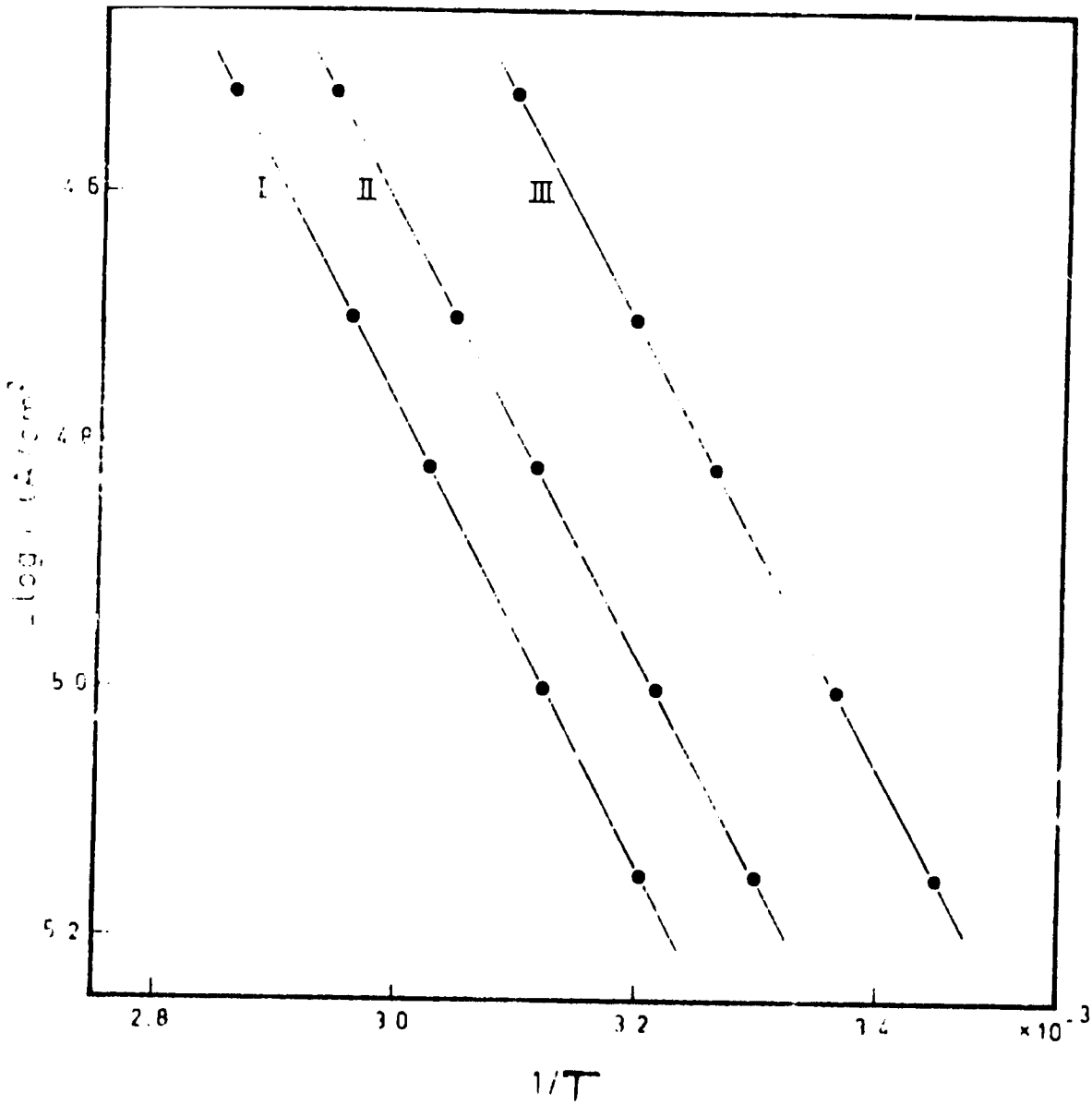

Figure 12

Log $i/\frac{1}{T}$ relations for Ti in 0.1M borate at constant H/σ : I = 3.3; II = 3.5; III = 3.8 x 10^6 V/cm.

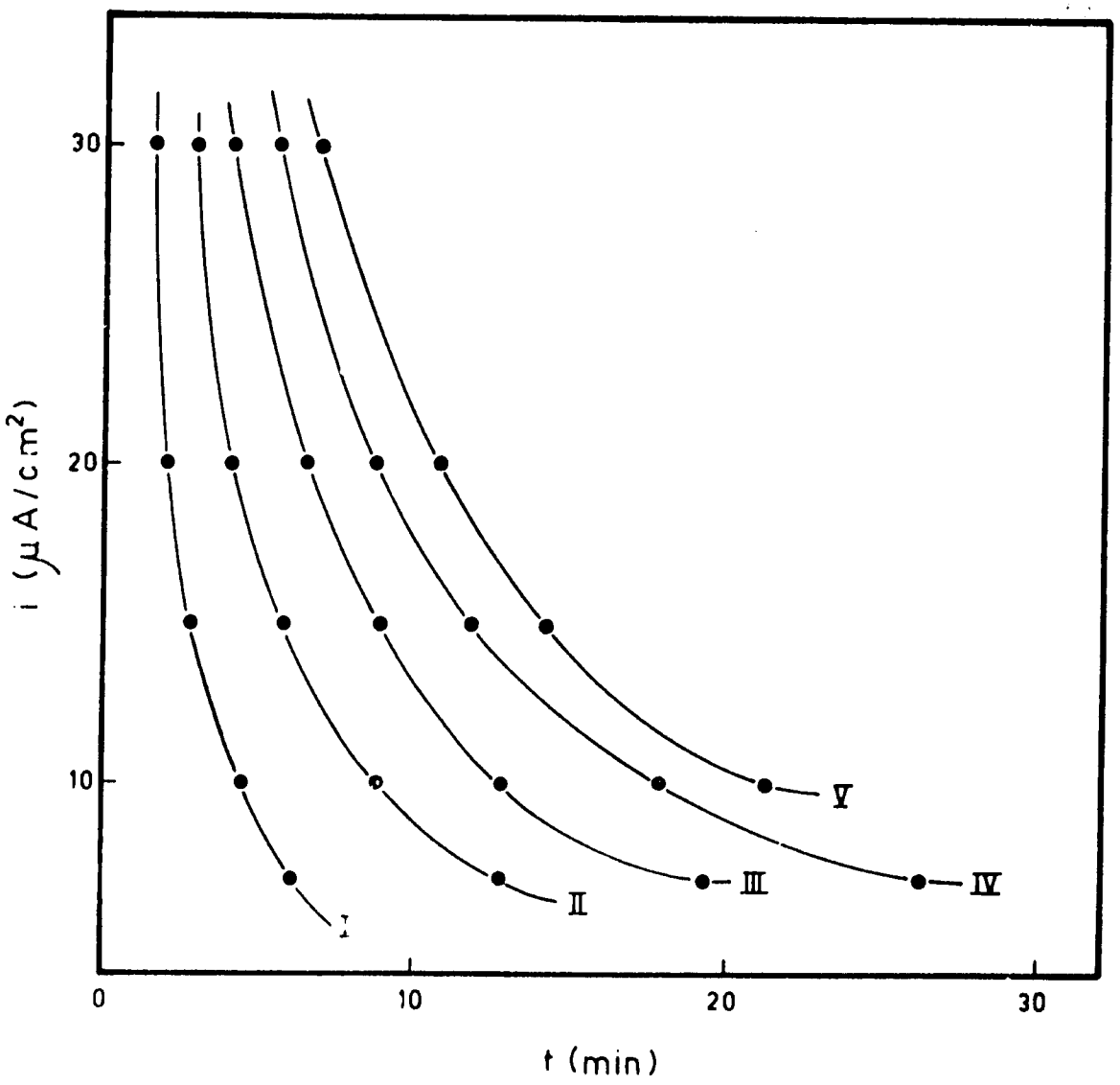

Figure 13

Current density/time relations at constant potential for Ti in borate at 40° C.: I = 0.5; II = 1.0; III = 1.5; IV = 2.0; V = 2.5 V (nhe).

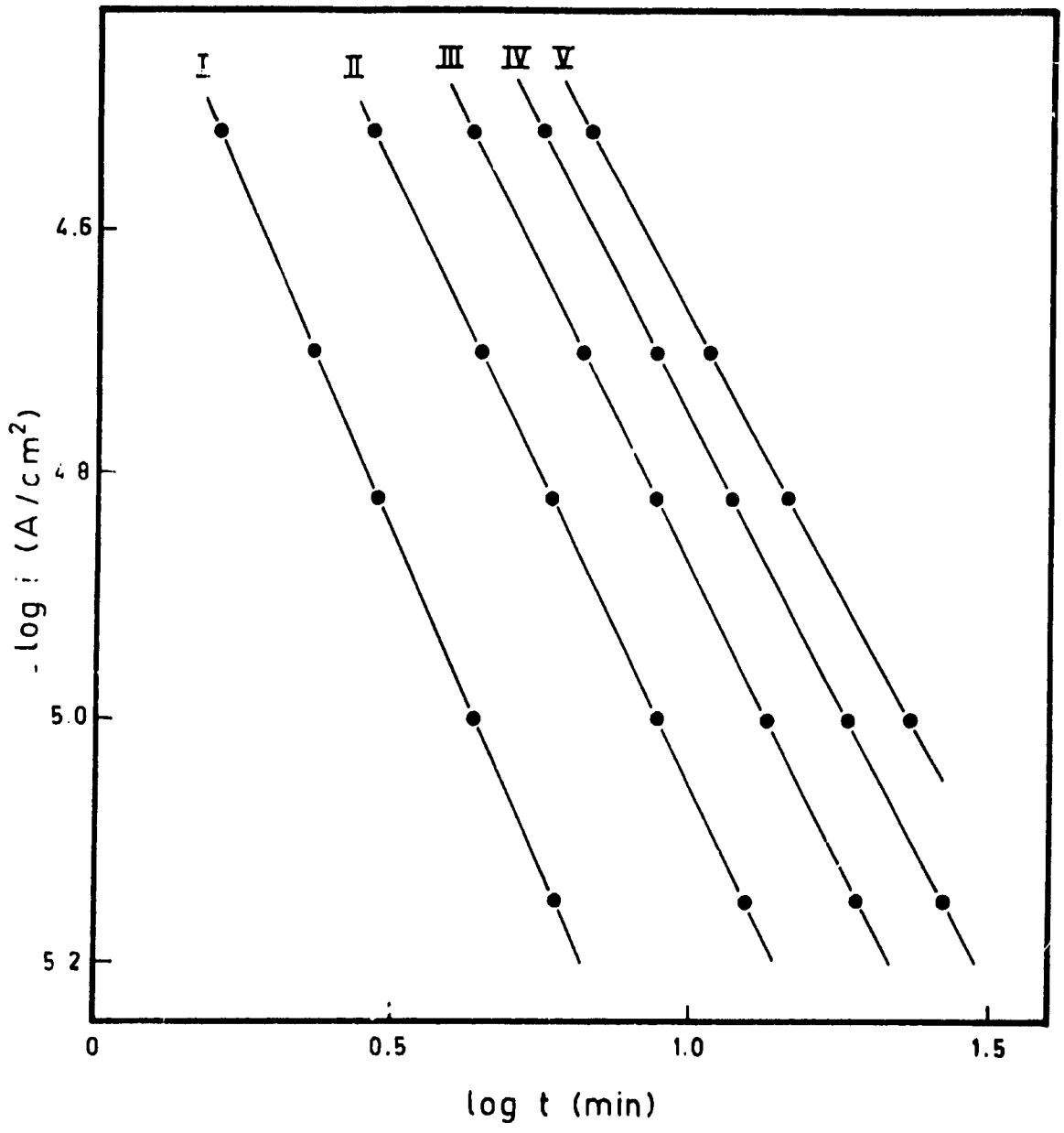

Figure 14

Log i/log t relations for Ti at 40° C.: I = 0.5; II = 1.0; III = 1.5; IV = 2.0; V = 2.5 V.

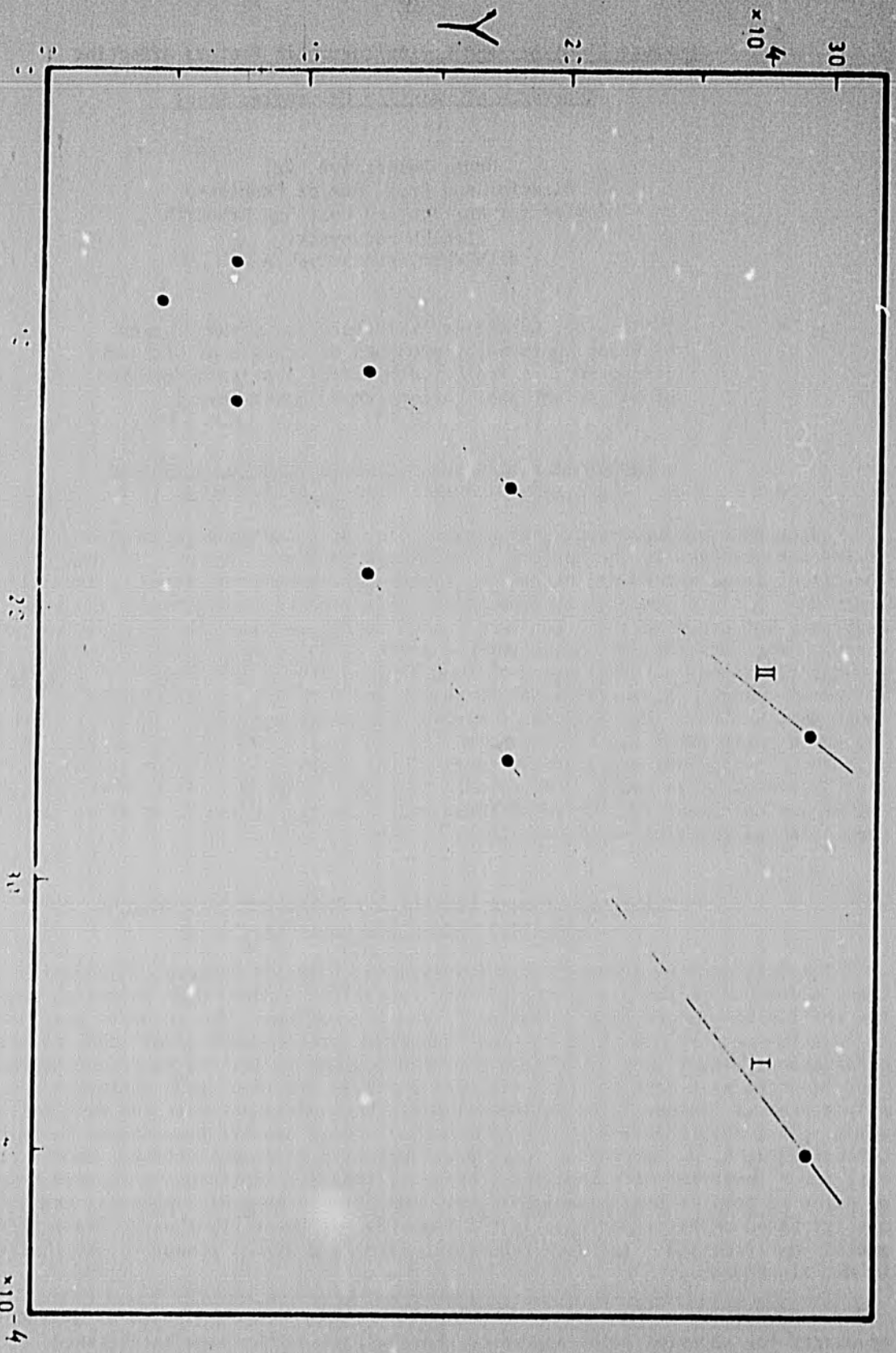

Figure 15

Dependence of Y on 1/t for Ti: I = 1.5; II = 2.5 V (nhe).

Surface Chemistry and Crystallographic Factors Affecting Adherence of Paint to Galvanized Steel

Henry Leidheiser, Jr.
Director and Professor of Chemistry
Center for Surface and Coatings Research
Lehigh University
Bethlehem, Pennsylvania

[Note: Dr. Leidheiser's lecture is in the process of being approved by sponsors of certain of his work. Its content is indicated by brief abstracts from two of his recent publications that appear here.]

Chemistry of the Surface of Hot-Dipped Galvanized Steel and Its Relation to Paint Adherence (1)

"Auger spectroscopy studies of many samples of hot-dipped galvanized steel have revealed the presence in the surface of aluminum, antimony, barium, calcium, carbon, chlorine, iron, lead, magnesium, nitrogen, oxygen, phosphorus, potassium, sulfur, tin and zinc. Auger analysis and electron microprobe analysis yielded approximately the same results for aluminum, but Auger analyses for lead tended to be low under those conditions where carbonaceous matter was present on the surface after cleaning in isopropyl alcohol. The tightly bound carbonaceous material appeared to contain sulfur. The ability of the regular and minimized spangle galvanized steel to retain paint on severe deformation was a maximum on those panels with a low residuum of carbonaceous material after isopropyl alcohol cleaning and was a minimum for those panels with a high residuum of carbonaceous material. This relationship was explained in terms of the degree of (0001) preferred orientation since orientation is known to be related to paint adherence. Organic matter containing sulfur was more readily removed on those panels having crystallites whose (0001) planes were oriented parallel to the substrate."

Crystallographic Factors Affecting the Adherence of Paint to Deformed Galvanized Steel (2)

"The coil coating industry is a fast-growing industry because of economics of production, economies in the use of energy, the capability to deal with polluting solvents, and the ability to provide high standards of quality control. The industry has made great strides in the development of systems (substrate/pretreatment/paint) that permit severe deformation without loss of adherence of the coating or loss of corrosion protection. Galvanized steel as a substrate material has a proven record of good performance but occasionally a product is made in which the paint adherence does not meet the deformation requirements. In a talk delivered before the National Coil Coaters Association in Chicago in October 1972, R. J. Kieckhefer, past president of a major coil coater, made a convincing case for a concerted attack on the problem of sporadic instances of imperfect adhesion of paint to coil-coated galvanized steel. He offered several hypotheses for poor adhesion quality based on his experience in the industry but these hypotheses were lacking in experimental justification. The work reported herein is a direct answer to the challenge made by Mr. Kieckhefer...

• "...It appears clear...that the crystallographic texture of zinc in galvanized steel necessary for superior paint adherence characteristics has been established. The highest quality material is one of small grain size with a high percentage of the grains oriented with the (0001) planes parallel to the surface. Some evidence has been found that rapid cooling of the molten zinc results in superior paint adherence properties. Other work has shown that galvanized steel with a large fraction of the grains oriented parallel to the (0001) plane are more readily cleaned of contaminating organics that might conceivably

interfere with the pretreatment efficiency. Thus, highly (0001)-oriented galvanized steel may be cleaned more efficiently and more economically in production line situations.

"It is obvious that small grain size and (0001) preferred orientation can be obtained under production line conditions as indicated by the fact that such materials were furnished to the study. These two desirable properties must be obtained without deleterious side effects, such as poor adherence at the steel/zinc interface or increased corrosion rate under service conditions. No evidence has come to light so far that reduced grain size and proper crystal orientation lead to any undesirable properties. In fact, it appears from related studies that the (0001) orientation has a low rate of corrosion in an aggressive environment such as sulfuric acid.

The work done to date has focused exclusively on the zinc coating and the directions that production research should take to improve the zinc has been delineated. It is presumed that galvanized zinc of very small grain size and a high degree of (0001) preferred orientation should be capable of deformation more severe than that to which coil coated material can now be subjected. If this presumption is correct, it then becomes the responsibility of the pretreatment industry and the paint industry to develop systems that will allow the full capabilities of such material to be utilized."

REFERENCES

1. Kim, Dong K., and Leidheiser, Henry, Jr., Surface Technology, 5, 379 (1977).

2. Leidheiser, Henry, Jr., and Kim, D. K., J. Metals, 28, (November 1976)

Some Aspects of the Corrosion of Reinforcing Steel in Concrete

Dr. V. K. Gouda
Research Professor
Laboratory of Electrochemistry and Corrosion
National Research Centre

INTRODUCTION

Because of the alkaline nature of concrete, reinforcing steel embedded in good quality, dense concrete with adequate thickness of cover remains unattacked for long periods in the majority of instances. If concrete is carbonated, however, this immunity is lost.

The corrosion of iron and steel in contact with concrete is of much greater importance than all other cases of corrosion of metals. This is not merely because the amount of metal involved is greater, but also because the metal which is corroded is load-bearing and the durability of the structure may depend upon the control of this corrosion. Any corrosion of the reinforcement results in the formation of rust which occupies a volume about 2.2 times that of the iron from which it is formed. This corrosion product has no place to go, so that it produces large internal pressures in the structure, which may be as high as 1 ton/sq. in. (1) and it cracks the concrete.

CORROSION OF REINFORCING STEEL IN DIFFERENT COUNTRIES

A survey (2) made in 1916 of numerous concrete structures along the seaboard of the United States revealed that the majority of the reinforced concrete structures subjected to seawater action showed evidence of deterioration or failure because of the corrosion of the embedded reinforcement above the water line.

The major portions of the San Mateo-Hayward Bridge across San Francisco Bay in California consist of a reinforced concrete two-lane causeway 7 miles long. The structure was built in 1928-29. Starting about seven years after initial construction, an unexpected maintenance problem developed because of excessive spalling of the concrete. Investigations (3) disclosed that the spalling of the concrete was the result of accelerated corrosion of the reinforcing steel. Despite initial preventive measures such as painting, the afflicted areas of corrosion increased progressively and were to be found in the concrete pilings, caps, diaphragms, main deck beams, and occasionally in the underside of the deck.

The major cause of deterioration both in Maine and Florida has been rusting of the reinforcement causing cracking of the concrete (4). In 1959, an investigation (5) by the California Division of Highways showed that 20 out of 66 reinforced concrete bridges in an arid desert had evidence of corrosion of reinforcement within 10 years of service. The investigation indicated high concentration of chlorides (41,000 p.p.m.) in soils to be responsible.

In 1929, a large series of tests was started in the United Kingdom by the Institution of Civil Engineers on the resistance of reinforced concrete to attack by seawater (6). It was found that the reinforced concrete piles suffered less from the direct attack of concrete, and deterioration stemmed primarily from corroding of the reinforcement with consequent cracking and spalling of the concrete.

Within 25 years of the reconstruction of a reinforced concrete bandstand at a seaside resort in the U.K., the concrete cracked badly because of the corrosion of steel reinforcement (7). A reinforced concrete tank 200 ft. in diameter handling magnesium hydroxide slurry was seriously deteriorated (8). Reinforcing rods of 3/4 in. diameter were completely rusted in some areas.

Failures of seawater structures have been observed in Norway and reported to be due to the corrosion of reinforcing steel (9). In Italy, Zingone (10) studied the deformations of the various structural elements in the seacoast area. In general he found a relation between the degree of deterioration of the object and its distance from the seacoast.

In India, a survey by the National Buildings Organization in 1960 revealed premature failure of a large number of constructions caused by reinforcement corrosion (11). The observations made were as follows:

1. The corrosion of reinforcement was generally detected by swelling and spalling of the ceiling plaster.

2. The corrosion of reinforcement was more severe in roofs of latrines, bathrooms, and urinals.

3. Residential buildings located in highly industrialized areas showed heavy rusting of reinforcement in all parts of the structures.

4. In the case of multistoried construction, columns, beams, and staircases were the worst affected portions. The columns facing the sea were more readily affected than those which were protected from the direct sea breeze.

5. Corrosion of reinforcement in buildings within a period of 10 to 15 years after construction was due to inadequate cover thickness.

In the Union of South Africa, it has been observed that reinforced concrete structures exposed to marine atmospheres deteriorate in a relatively short period (12). The conditions are particularly severe on the south coast of Natal. Minor sections such as balusters and handrails of bridges have sometimes disintegrated in four to five years. It has been observed that in marine atmospheres, deterioration because of corrosion has occurred even when the workmanship, design, and general construction practice are apparently sound.

In Egypt, it has frequently been observed that reinforced concrete structures exposed to marine atmospheres deteriorate in a relatively short period. The most important of all is the deterioration which occurred within a few months after completion of the construction of Ashtoom El Gameel, a two-road bridge in Port Said. In 1965 a comparative study of various reported cases of damage because of reinforcement corrosion was carried out by the Ministry of Housing and Public Utilities (13). The observations made can be summarized as follows:

1. Some buildings showed corrosion cracks while still incomplete because of design deficiency.

2. Columns were the structural elements most susceptible to cracking.

3. The susceptibility to ease of cracking in the concrete columns is circular > square > rectangular.

4. The time for cracks to appear differ from a few months to a few years after construction.

A series of studies (14-23) were undertaken at NRC with the aim of elucidating the corrosion behavior of steel reinforcement under various conditions. Another objective was to find out the cause of deterioration of reinforced concrete constructions in different locations in Egypt. Part of these studies were carried out under joint programs between NRC and the Building Research Institute. A summary of what has been done and of the work still in progress follows.

CORROSION BEHAVIOR IN ALKALINE MEDIA

Determination of the Critical pH Value. The pH value above which mild steel becomes passive in pure alkaline solutions has been determined by means of the polarization technique, free corrosion potential measurements, and visual observations. Solutions of NaOH having pH values in the range of 10-13 were tested. Figure 1 shows the change of free corrosion potential of steel vs. time. The results indicated that steel corrodes in all solutions of pH values $<$ 11.5, while in the solutions of pH values $>$ 11.5 the steel remained bright (during the test period of 20 days). It is of interest to mention that in NaOH of pH 11.5 the steel was bright during the first two days and then rusting started to occur exactly at the same time when the potential started to drop toward the active direction.

RELATION BETWEEN pH AND TOLERABLE AMOUNTS OF AGGRESSIVE IONS

The breakdown of steel passivity in alkaline solutions because of the presence of Cl^-, SO_4^{--}, and S^{--} ions was studied in sodium hydroxide solutions of pH values $>$ 11. For each pH value, three series of experiments were conducted in order to find the maximum concentration of each aggressive ions that could be present without disturbing the steel passivity. The results are shown in Figure 2. It is clear that a linear relationship holds between the pH value and log maximum tolerable concentration of each of the aggressive ions tested but only in the range of pH 11.75 to 13.5 (17). This can be represented as follows:

$$pH = a + b \log C_{agg.}$$

CORROSION OF STEEL EMBEDDED IN CONCRETE CONTAINING AGGRESSIVE ANIONS

As corrosion of steel in concrete structures is essentially a long-time process, a rapid method for evaluating the corrosion behavior of embedded reinforcing steel was of great importance. Galvanostatic polarization at a low current density (10-50 μA./cm.^{2}) (14, 15) proved to be a reliable accelerated test for predicting the corrosion or inhibitive character of the medium surrounding the steel reinforcement. Using such a method, three states of metal can be assessed; namely, passive, active, or borderline condition. The effect of the presence of different concentrations of Cl^-, SO_4^{--}, and S^{--} in the mixing water of the concrete on the corrosion behavior of embedded steel was studied. It has been found that steel passivity was impaired when the concrete contains chloride at concentrations $>$ 0.75% (relative to the weight of cement).

It is of interest to find that concrete can tolerate higher concentrations of sulfate and to a lesser extent chloride ions than does a simple saturated lime solution. It should be mentioned that the amounts of Cl^- tolerated by the concrete depend on several factors, the most important of which is the concentration of calcium aluminate and gypsum content of the cement, as calcium sulfoaluminate (being less soluble) forms in preference to the chloroaluminate.

However, when portland blast furnace slag cement was used instead of ordinary portland cement, the corrosion of steel was not inhibited when using concentrations of NaCl $>$ 0.3%. The results indicate that portland blast furnace slag cement has inferior corrosion resistance compared to ordinary portland cement. This may be due to two factors:

1. Slag cement produces less calcium hydroxide than does the equivalent portland cement because of dilution (24).

2. Presence of impurities and namely of sulfide (the concentration of sulfide in the slag cement used was 1.5%).

It may be concluded from these results that the presence of S^{--} ions and to a lesser extent Cl^{--} ions are more dangerous than SO_4^{--} ions for the corrosion of embedded steel reinforcement.

INHIBITION OF EMBEDDED REINFORCING STEEL

In order to simulate the most severe conditions that prevail in our practice, tests were conducted on portland cement concrete and portland blast furnace slag cement concrete admixed with 2% NaCl. The inhibitors used were sodium nitrite, potassium chromate, sodium benzoate, disodium phosphate, and hydrazine. Black liquor (or black lye, which is a commercial by-product from the pulp and paper industry) was also tested as an inhibitor (18). The results are summarized in Table 1.

The effect of coating the steel with portland cement slurry alone or cement slurry containing inhibitors on the inhibition of the corrosion of steel was also tested and the results are shown in Table 2.

IMPROVING THE CORROSION RESISTANCE OF PORTLAND BLAST FURNACE SLAG CEMENT

For economic reasons, portland blast furnace slag cement is nowadays being used frequently in Egypt. Thus, a series of studies (22) were conducted with the aim of improving the corrosion resistance as well as the physical properties of portland blast furnace slag cement concrete by means of controlling the degree of fineness of the dry slag cement, the W/C ratio, and the use of additives. The results indicated that the corrosion resistance of portland blast furnace slag cement is improved with the increase of the blaine area. With pastes produced from high-blaine-area cement (6,535 $cm.^2/g.$), embedded reinforcing steel behaves very closely to steel embedded in normal or Type I portland cement pastes. W/C ratios of 0.25 and 0.4 provided a better passivating medium as compared with W/C ratios of 0.18 and 0.7. However, addition of lime did not appreciably improve the corrosion resistance, while admixing with gypsum had an adverse effect.

DIFFERENTIAL GALVANIC CELLS INVOLVED IN THE CORROSION OF STEEL IN CONCRETE

Galvanic couples simulating those encountered in the corrosion of steel in practice have been investigated extensively in our laboratory. These couples are differential salt concentration, differential pH, differential aeration, passive/active, and rusted/non-rusted cells. A simple technique has been developed for such a study. The corrosion diagrams (Evans diagrams) were determined experimentally for all the cells studied. Thus, a quantitative relationship connecting the principal controlling factors of the corrosion process in each galvanic cell were assessed by studying the kinetics of the anodic and the cathodic reactions. Also, the degree of control for the cathodic and the anodic reactions were calculated. Examples of the corrosion diagrams obtained can be seen in Figures 3 and 4. The parameters obtained from Evans diagrams for the differential cells studied are collected in Table 3.

Interesting conclusions may be drawn from these studies which can be summarized as follows:

1. The increase of aggressiveness of any type of galvanic cell is mainly defined by the kinetic retardation of the corrosion system and not necessarily by cell e.m.f. or mixed potential values.

2. Maximum galvanic current is always produced at pH 10 in the differential salt concentration, in the differential aeration, and in the passive/active cells.

3. Cl^- enhances general attack in near neutral and alkaline media (pH $<$ 11) and induces pitting attack in alkaline media of pH $>$ 11.

4. **The cells can be arranged in order of decreasing aggressiveness as follows: differential aeration > differential sat concentration > passive/active > differential pH cells > rusted/nonrusted cells.**

DIAGNOSIS OF STEEL REINFORCEMENT CORROSION EGYPTIAN CONCRETE CONSTRUCTION

Recently, an investigation has been conducted on some deteriorated construction caused by the corrosion of steel reinforcement (20). Three deteriorated structures exposed to different environments in Egypt were chosen for careful examinations. They are:

1. The rice treatment hall in Alexandria.

2. The filtration building for the domestic water project in Fayoum.

3. The administration building of the Ministry of Housing Public Utility in Cairo.

For comparison, the study included an examination of a nondeteriorated structure in Tanta.

Samples of reinforcing steel, concrete cover, and the surrounding medium were subjected to chemical analysis and microscopic examination. Results are summarized in Tables 4-7 and Figures 5-9. These results indicated that the low concentrations of aggressive ions and high alkalinity met with in Tanta concrete establish ideal conditions in which the passivity of the steel reinforcement is maintained. The relatively low C and S contents of the steel also favor a satisfactory corrosion resistance.

The Alexandria building, which lies directly on the shore, is a typical case where the environmental conditions enhance corrosion of the steel. The rich concrete used in this building did not afford the required protection.

For the Fayoum building, it seems that leakage of water containing SO_4^{--} ions from the filtration pipes together with the heterogenity of grain size and the relatively high C content of the steel might have provided favorable conditions for corrosion.

In the case of the Cairo building, the high Cl^- ion in the concrete may be due to contamination of the aggregate or the water used for mixing was chlorinated. The high sulfide content, however, is to be expected, since portland blast furnace slag cement had been used instead of portland cement. Also, there are relatively high C & S contents of the reinforcing steel. It seems that all these factors plus the presence of tensile stress enhanced the susceptibility to SCC.

In our present status of knowledge, practical means to protect reinforcing steel are greatly needed, especially for prevailing conditions in Egypt, including environmental, diversity of types of cement, and economics of construction.

REFERENCES

1. P. E. Halstead, Chemy. Ind., 34, 1133 (1957).

2. R. J. Wig & L. R. Fergunson, Engng. News RCC, 79, 689 (1917).

3. R. F. Stratful, Corrosion, 13, 173 (1957).

4. R. F. Blanks, Proc. Am. Concr. Inst., 49, 601 (1953).

5. R. F. Stratful, Chem. Abstr., 59, 15 015 (1965).

6. F. M. Lea, The Chemistry of Cement and Concrete, Edward Arnold Publishers Ltd., London, 549 (1956).

7. J. C. Hudson & F. Wormoll, Chem. Ind., 32, 1078 (1957).

8. H. R. Touchin, Corros. Technol., 4, 417 (1957).

9. Concrete on Sea Water, Den Norske, Norwegian Engineering & Society Concrete Committee Monograph No. 3, (1936).

10. G. Zingone, Cemento, 59, 23 (1962).

11. K. S. Rajagopalan, N. S. Rengaswamy & T. M. Balasubramanian, J. Sci. Indust. R.S., 28, 382 (1969).

12. D. A. Lewis & W. J. Copenhagen, Corrosion, 15, 382 (1959).

13. M. G. Zahran, Ph.D. Thesis, Faculty of Engineering, Cairo University (1969).

14. A Rapid Method for Studying Corrosion Inhibition of Steel in Concrete, V. K. Gouda and G. S. Monfore, J. of the PCA Res. & Dev. Labs (U.S.A.), 7, 24 (1965).

15. Anodic Polarization Measurements of Corrosion and Corrosion Inhibition of Steel in Concrete, V. K. Gouda, Br. Corros. J., 1, B 8 (1966).

16. Corrosion and Corrosion Inhibition of Reinforcing Steel, V. K. Gouda, Br. Corros. J., 5, 193 (1970), 5, 204 (1970).

17. A Comparative Study of the Corrosion Behavior of Steel in Neutral and Alkaline Media, V. K. Gouda and S. M. Sayed, Proc. 2nd Cairo Solid State Conference 1973, Vol. 2, 353.

18. Protection of Reinforcing Steel, V. K. Gouda, Patent No. 270/13 21/6/1972, Egypt.

19. Additives to Cement Pastes: Simultaneous Effects on Pore Structures and Corrosion of Steel Reinforcement, V. K. Gouda, W. E. Mourad, and R. Sh. Mikhail, J. Colloid & Interface Sci., 43, 294 (1973).

20. Some Aspects of Steel Reinforcement Corrosion in Egyptian Structures, V. K. Gouda, A. A. Abdul-Azim, and H. A. El Sayed, Br. Corros. J., 9, 185 (1974).

21. Hardened Portland Blast Furnace Slag Cement Pastes: II-Corrosion Behavior of Steel Reinforcement, V. K. Gouda, M. A. Shater, and R. Sh. Mikhail, Cement & Concrete Res., 5, 1 (1972) and 5, 99 (1975).

22. Galvanic Cells Encountered in the Corrosion of Steel Reinforcement, V. K. Gouda and H. M. Mourad, Corros. Sci., 14, 681 (1974), 15,307 (1975), 15, 317 (1975) and 15, 329 (1975).

23. Corrosion Diagrams of Galvanic Cells Involved in the Corrosion of Steel in Practice, V. K. Gouda and H. M. Mourad, 6th International Congress on Metallic Corrosion, Sydney, (1975).

24. H. H. Steinour, Bulletin No. 168, Res. Dev. Labs. Portland Cement Association, (1964).

Table 1

Inhibition of Corrosion by Addition of Inhibitors in Presence of 2% of Sodium Chloride

Inhibitor	Critical Concentration for Inhibition, %	
	Portland Cement Concrete	Portland Blast Furnace Slag Cement Concrete
Sodium nitrite	0.75	1.5
Potassium chromate	3.00	3.5
Sodium benzoate	5.50	6.0
Disodium phosphate	5.50	6.0
Black lye	2.00	3.0

Table 2

Effect on Corrosion Inhibition of Coating Reinforcing Steel with Portland Cement Slurry and Inhibitors

Coating	Critical Concentration of Admixed Inhibitor	Maximum Concentration of Chloride Tolerated, %
Cement slurry	-	1.2
Cement slurry + 8% sodium nitrite	-	1.6
Cement slurry + 2% Sodium nitrite	1% Sodium nitrite	2.0
Cement slurry + 10% Potassium chromate	-	1.5
Cement slurry + 5% Potassium chromate	2% + 5% Potassium chromate	2.0

Table 3

Corrosion Parameters Obtained from Polarization Measurements

Solution	E_a^o (mV)	E_c^o (mV)	$(E_c^o - E_a^o)$ (mV)	E_M (mV)	$I^*_{corr.}$ (μA)	$\frac{dE_a^{**}}{di}$ $\frac{mV}{\mu A}$	$\frac{di^{***}}{dE_a}$ $\frac{\mu A}{mV}$	$\frac{dE_c^{**}}{di}$ $\frac{mV}{\mu A}$	$\frac{di^{***}}{dE_c}$ $\frac{\mu A}{mV}$	Percent Anodic	Control Cathodic
A. Differential pH cells (pH 8 : pH 12)											
0 Cl^-	-720	-215	505	-545	34	5.12	0.19	8.00	0.12	34.30	65.70
10^{-3}M Cl^-	-620	-140	480	-590	40	0.60	1.66	9.00	0.11	6.30	93.70
10^{-1}M Cl^-	-635	-250	385	-610	60	0.40	2.50	5.37	0.18	6.50	93.50
B. Differential salt concentration cells (10^{-3}M Cl^-:10^{-1}M Cl^-)											
NaOH of pH 6.5	-670	-290	380	-610	69	0.88	1.13	5.63	0.178	15.80	84.20
NaOH of pH 10	-712	-340	372	-665	72	0.61	1.64	3.50	0.286	12.65	87.35
NaOH of pH 12	-485	-165	320	-455	27	1.11	0.90	6.13	0.163	9.30	90.70
NaOH of pH 12.5	-520	-195	325	-485	32	1.05	0.95	5.50	0.183	10.70	89.30
C. Passive/active cells											
NaOH of pH 10	-745	-305	440	-695	66	0.80	1.25	5.8	0.17	11.3	88.7
NaOH of pH 10.5	-710	-290	420	-675	47	0.80	1.25	8.3	0.12	8.3	91.7
NaOH of pH 11	-660	-245	415	-635	32	0.80	1.25	10.0	0.10	6.0	94.0
(10^{-3}M Cl^-) pH 12	-585	-198	387	-525	22.5	2.77	0.36	8.1	0.12	15.5	84.5
(10^{-2}M Cl^-) pH 12	-610	-175	435	-565	26	1.72	0.58	7.0	0.14	10.3	89.5

Solution	E_a^o (mV)	E_c^o (mV)	$(E_c^o - E_a^o)$ (mV)	E_M (mV)	$I^*_{corr.}$ (μ [illegible])	$\frac{dE_a^{**}}{di}$ $\frac{mV}{\mu [illegible]}$	$\frac{di^{***}}{dE_a}$ $\frac{\mu [illegible]}{mV}$	$\frac{dE_c^{**}}{di}$ $\frac{mV}{\mu [illegible]}$	$\frac{di^{***}}{dE_c}$ $\frac{\mu [illegible]}{mV}$	Percent Annodic	Control Cathodic
D. Differential aeration cells											
NaOH of pH 10	-735	-255	480	-675	110	0.54	1.85	4.75	0.210	12.5	87.5
NaOH of pH 10.5	-690	-225	465	-635	105	0.54	1.85	5.25	0.190	11.8	88.2
NaOH of pH 11	-655	-210	445	-605	90	0.55	1.82	5.50	0.182	11.2	88.8
NaOH of pH 11.5	-565	-115	450	-520	85	0.57	1.75	6.75	0.148	10.0	90.0
(10^{-3}M Cl^-) pH 12	-535	-225	310	-465	32	2.25	0.44	4.40	0.230	22.0	78.0
(10^{-2}M Cl^-) pH 12	-565	-185	380	-475	62	1.50	0.67	3.75	0.266	24.0	76.0

* I_{corr} Measured galvanic current/electrode area (4.7 cm^2).

** $\frac{dE}{di}$ The true polarization of the electrode (anode or cathode).

*** $\frac{di}{dE}$ The actual electrode reaction rate (anodic or cathodic).

Table 4

Analysis of Fayoum and Alexandria Water

Substance	Concentration, mg/l	
	Fayoum	Alexandria
Total dissolved solids	180	25,550
Total alkalinity	136	1,200
Total hardness	116	4,800
Chloride	22	13,200
Sulfate	18	1,489
Fluoride	0.35	1.1
pH	7.2	8.1

Table 5

Disaggregation of Gravel and Mortar and Determination of Cement Percentage (500 g. Samples)

Sample	Components, Grams				% Cement as Dry Mix in Concrete
	Gravel	Mortar	Sum	Loss on Disagg.	
Cairo	216.3	280.0	496.3	3.7	17.8
Fayoum	359.5	138.5	498.0	2.0	16.1
Alex.	271.5	214.5	486.0	14.0	32.5
Tanta	298.5	193.5	492.0	8.0	19.8

Table 6

Chemical Aanlysis of 1 g. of Mortar

Sample Component	Cairo, %	Fayoum, %	Alex., %	Tanta, %
Loss on ignition	12.80	15.88	27.39	13.04
SiO_2	61.40	38.62	22.89	45.40
Fe_2O_3	1.28	1.48	1.56	1.92
Al_2O_3	2.98	3.66	2.74	2.88
CaO	18.57	35.74	42.00	34.38
MgO	0.85	1.18	1.25	0.29
SO_3	1.58	2.82	2.53	1.74
Sum	99.46	99.38	100.38	98.85
Cl^-	0.417	0.325	0.390	0.106
S^{--}	0.999	Zero	0.479	0.290
Free CaO	1.30	0.86	1.26	1.74
Na_2O	0.74	0.66	0.66	0.61
K_2O	0.35	0.31	0.20	0.32
Sum (alkalinity)	2.39	1.83	2.12	2.67

Table 7

Chemical Analyses of the Reinforcing Steel Samples

Samples	Element, %			
	C	S	P	Mn
Cairo	0.25	0.070	0.080	0.52
Fayoum	0.15	0.034	0.70	0.31
Alex.	0.08	0.025	0.052	0.50
Tanta	0.11	0.050	0.096	0.42

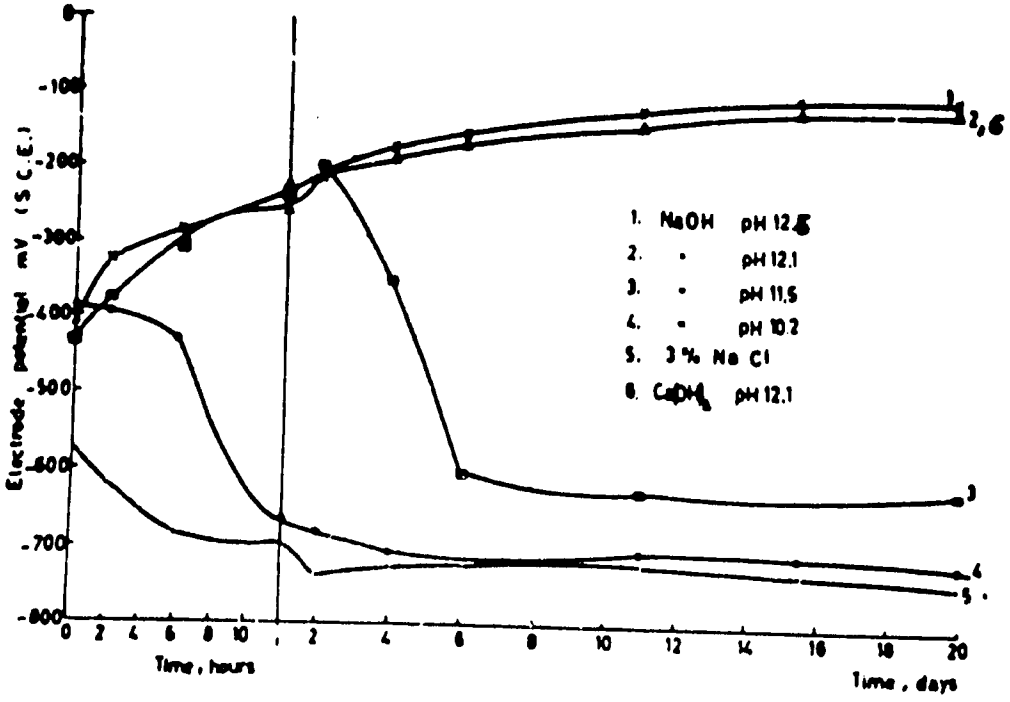

Figure 1

Potential /time curves of steel in different solutions

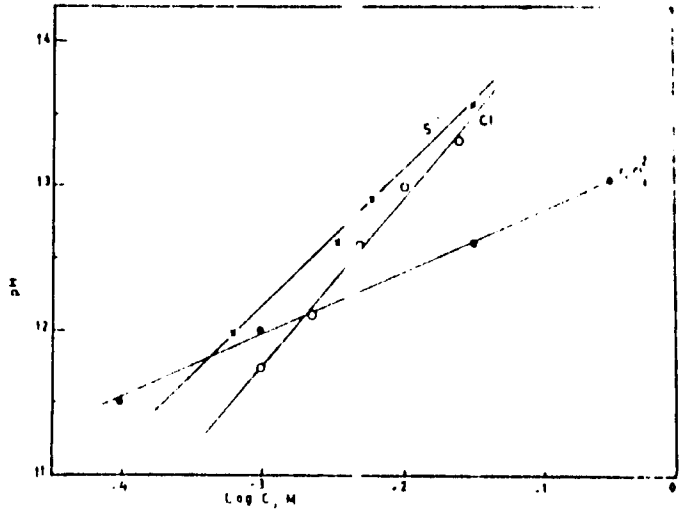

Figure 2

Effect of pH on the tolerable amounts of aggressive ions

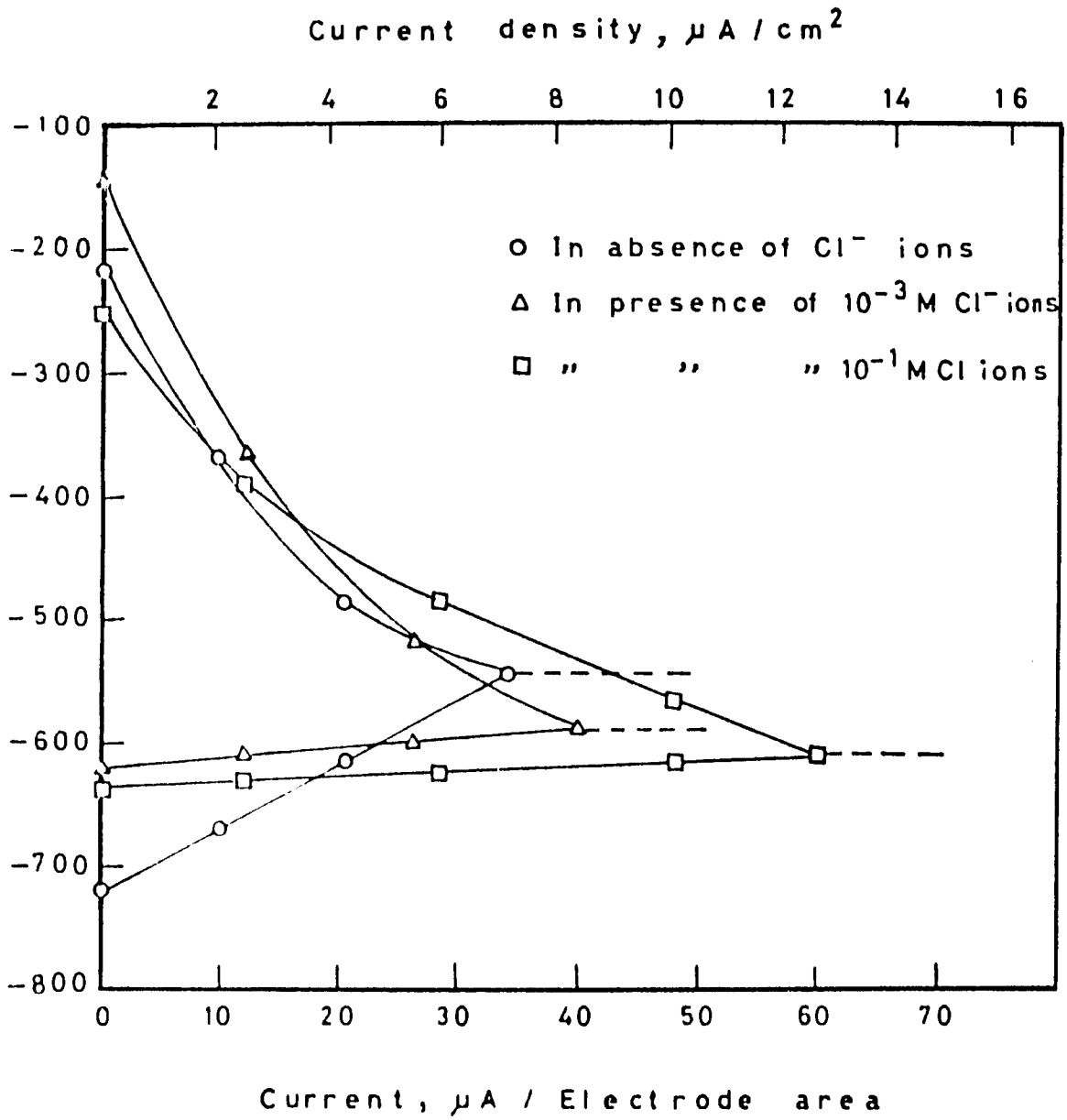

Figure 3

Evans diagrams of differential pH cells (pH 8 : pH 12)

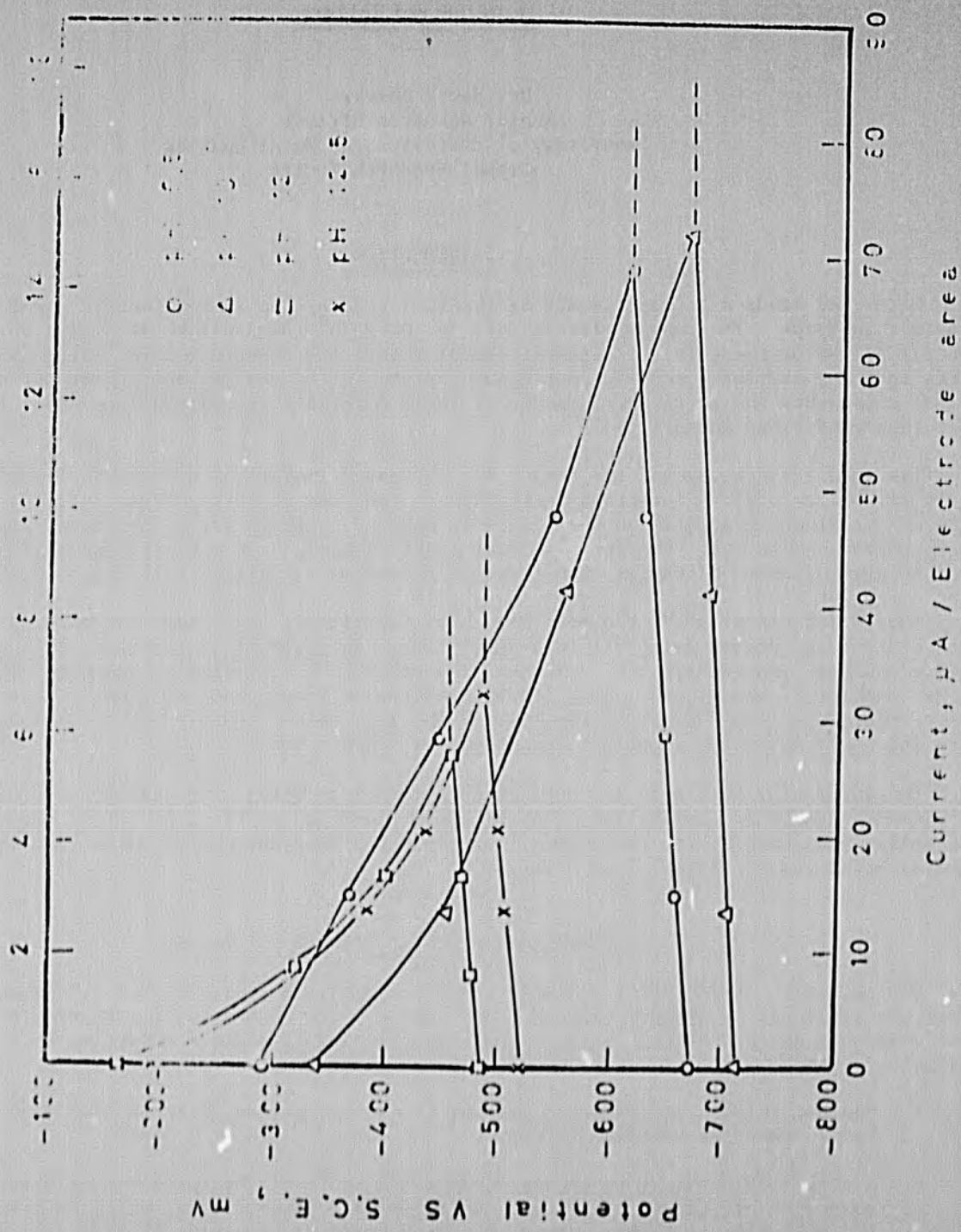

Figure 4

Evans disgrams of differential salt concentration cells (10^{-3}M Cl^- : 10^{-1}M Cl^-)

[Figures 5-9 showing microscopic examinations will be available during the lecture.]

Chemical Aspects of Fireside Corrosion in Oil-Fired Boilers

Dr. Saher Shawki
Senior Research Officer
Laboratory of Corrosion and Metal Coating
National Research Centre

INTRODUCTION

Mazot and crude oil comprise 92% of the fuel used by the thermoelectric power stations in Egypt. The consumption amounts to 105 x 10^4 tons/year by 16 plants to produce about 2,512 MW of electricity. Present trends toward the construction of large generating units in power stations requires continuous improvement in the reliability of various boiler components and in the performance of their materials of construction under the operation conditions encountered.

The need for economy and the demand for increased amounts of energy has forced large users of fuel to explore low-grade fuels for use in steam boilers and gas turbines. Fuels such as unrefined crude oil and residual oil, however, contain large amounts of impurities which corrode equipment. Failures in power stations because of corrosion of equipment lead to great losses and danger, and fireside corrosion is particularly troublesome.

Sodium and vanadium are the most corrosive impurities. They form low-melting slags that can destroy boiler materials in a short time. In spite of a great deal of theoretical evaluation and experimental evidence, the process of formation of vanadate compounds is not completely understood. Detailed information on V-compound reactions with sodium salts, therefore, could help clarify some of the less understood aspects of the constituents and could also have important technological applications.

The purpose of this work has been to investigate in detail the kinetics of formation of vanadate compounds and the relations to the composition of fly ashes. The effect of the sodium vanadates on the corrosion of boiler steel also has been studied to clarify the general mechanism of fireside corrosion.

FORMATION AND COMPOSITION OF FLY ASHES

The chemical, differential thermal, and X-ray analyses indicate that 71% of the fly ashes are compounds of sodium, vanadium, and sulfur. The mechanism of formation of vanadate compounds during the combustion process was assumed to proceed according to the following steps:

A. Sodium, sulfur, and vanadium present in the oil are oxidized to give Na_2O, SO_3, and a number of vanadium oxides.

B. A series of chemical reactions occur which start by the formation of different compounds of sodium (carbonates, sulfates, and thiosulfates) which in turn react with V_2O_5 to form a number of sodium vanadate compounds (Na_3VO_4, $Na_2V_{12}O_{31}$, NaV_3O_8, $Na_2V_4O_7$, $NaVO_3$).

C. Other elements present in mazot in small proportions such as Fe, Ni, and Al, are partly sulfatized and partly exist as oxides or mixed oxides.

CORROSION OF BOILER STEEL BY VANADATE COMPOUNDS

Comparative laboratory tests of corrosion caused by different vanadate compounds were conducted on a heat-resistant steel for boiler pipes in air in the temperature range of 500° to 800° C. It has been demonstrated that corrosion of boiler steel is accelerated in presence of vanadium bronzes ($Na_2V_{12}O_{31}$ and NaV_3O_8) compared to other V-compounds. The effect is not directly related to the temperature, and a sharp decrease in corrosion rate was observed at the melting point of the bronze compound followed by a linear increase of corrosion with temperature. There appears to be a strong indication that nacent oxygen liberated upon solidification of the vanadate bronzes is responsible for their unusually high corrosiveness below their melting points. The conclusion was supported with regard to the DTA cooling curves for these compounds.

The corrosion process caused by V-bronzes is characterized by two values for activation energy in the solid and molten phases, indicating a change in the nature and mechanism of the oxidation process. The change is attributed to the phenomenon of nacent oxygen evolution by these compounds; however, other vanadate compounds and V_2O_5 showed only one value for activation energy.

It was possible to calculate the value of initial corrosion rate and the blocking factor for corrosion caused by the vanadates in the fused state. The initial corrosion rate is indicative of the corrosivity of the molten compound to the naturally-formed oxide film, while the blocking factor can be an estimate for the protective character of the formed scale.

If the vanadate compounds are fused at frequent intervals, severe corrosion would continue and weight loss values would increase by the increasing number of fusions. This supports the conclusion of enhancement of corrosion because of liberated oxygen by vanadium bronzes every time the sample is cooled below the melting point of the compound. The results indicate also that the weight difference between repeated fusion numbers decreases as the exposure time increases, which may be due to the dilution of the V-bronzes by the oxide film dissolved in it upon fusion.

A series of periodic dipping experiments were carried out for the V-bronzes and $NaVO_3$, and the results showed a substantial increase in weight loss as the time interval between two droppings decreases. This is likely to be due to an increase of initial corrosion rate values with increasing number of dips, which can be safely predicted if we consider the fusion effect of molten salt on the formed layer of corrosion scales and the exposure of fresh metal surface to the vanadate compound and the atmosphere. The blocking factor calculated for these experiments decreases by increasing number of dipping because of excessive attack of the melt on the film of corrosion scale.

The effect of the intially formed oxide film on the corrosion rate by vanadate compounds was also investigated in order to examine the protective character of this film and its fusion characteristics with the vanadates. It was shown that the weight loss of the metal decreases as the thickness of the initially formed oxide film increases, which demonstrates the protective character of this film. The protection afforded by the oxide film decreases as the exposure temperature increases because of the greater ability of the film to fuse and react with the V-compound.

The affinity of bronze I ($Na_2V_{12}O_{31}$) to react with iron oxide, according to these experiments, was found to be greater than that for bronze II (NaV_3O_8). The explanation is based on the V_2O_5 contents in bronzes: $6V_2O_5$: $1Na_2O$ and $3V_2O_5$: $1Na_2O$.

The corrosion of boiler steel caused by V-compound/iron oxide mixtures of different concentrations was examined. The reaction between Fe_2O_3 and vanadium bronze II was studied by DTA to establish the equilibrium diagram of these mixtures. A new compound, $FeVO_3$ (m.p. 550° C.) was identified. With 5% Fe_2O_3, an exothermic peak appeared at 567° C., which is interpreted as caused by a flush of oxygen evolution prompted by the presence of iron oxide.

The mechanism of corrosion caused by vanadates has been proposed on the basis of:

A. The increase of the corrosion rate because of the delivery of atmospheric oxygen and liberated nacent oxygen of the V-bronzes to the metal skin through pores and fissures of the solid compounds formed on the metal.

B. The ability of the vanadate compounds to fuse with the protective oxide film on the metal skin.

C. The possibility of formation of iron vanadate compounds and its effect on the enhancement of corrosion.

RELATED RESEARCH ACTIVITIES

The corrosion group has carried out a number of research activities related to fire-side corrosion in collaboration with the General Egyptian Electricity Corporation:

A. Investigation of several failures of boiler pipes in power stations.

B. Laboratory evaluation of fuel additives to inhibit the corrosion of boiler steel by fly ashes.

C. Field corrosion tests using probes to be introduced in the combustion chamber.

FUTURE WORK

We suggest the following topics are among those that could be suitable for future research.

1. Evaluation of fuel additives using test rigs.

2. Elucidation of the equilibrium diagram between iron oxide and different vanadium compounds.

3. Development of a technique for rapid study of the interaction of corrosive slags with an alloy. An electrochemical method may be useful for this purpose.

Effect of Cations on the Corrosion of Stainless Alloys in Saline Water at Elevated Temperatures

S. M. El-Raghy**, S. M. Morsy*, A. A. Elsayed*, and A. E. El-Mehairy**

* Department of Metallurgy, Atomic Energy Establishment, Cairo

** Department of Metallurgy, Faculty of Engineering Cairo University, Cairo

INTRODUCTION

Extensive studies on the corrosion of steels and some other alloys in seawater have emphasized the destructive role of chloride ions (1-4). Desalination technology has led to an increasing interest in the effect of temperature (5-6). In most of these studies, synthetic seawater--that is, 3% NaCl solution--has been used. Among the other cations in actual seawater, only magnesium and calcium have been considered and have been shown to retard the corrosion of steels. The lower corrosion rate in actual seawater was attributed to the formation of a chalky film of calcium or magnesium carbonates (7).

A more recent study on the electrochemistry and corrosion of chromium steel (8) has shown a higher corrosion rate for 13% Cr steel in 0.33M $FeCl_3$ than in 1.0M HCl. Comparison (9) of the Tafel constants for the process of anodic dissolution of Pt in solutions of NaCl, HCl, and a mixture of both, showed that the corrosion process depends on the chloride ion activity and not on the pH of the solution. Bianchi, et al (10), chemically etched stainless steel in a series of chemical etchants and showed the role played by different cations (Li^+, Fe^{+++}, and Al^{+++}). The monovalent cations (Na^+, K^+, ..) are widely assumed to behave alike at the same chloride ion concentration, although no experimental evidence is available.

It appears, therefore, that cations exert an effect on the corrosion of steels in different solutions. The present work was designed to investigate the effect of KCl additions on the corrosion of stainless steel in aqueous solutions of NaCl at 80°C. and 90° C. Weight loss potentital-time and polarization techniques were utilized to investigate the effect of adding KCl to NaCl solutions.

EXPERIMENTAL

The chemical analysis of the austenitic steel used is as follows:

C	Mn	S	Si	Ni	Cr	Fe
0.12	0.62	0.014	0.38	10.58	17.8	Balance

For corrosion tests, coupons 15 x 15 mm. were cut from a rolled sheet 0.8 mm. thick. The specimens were annealed in vacuum (10^{-4} mm. Hg) at 1050° C. for 2 hr., followed by water quenching. The surface preparation consisted of grinding the specimen on emery paper (0-4/0), pickling in an aqueous solution of 15% HNO_3 and 20% HF, ultrasonic cleaning in water and ether, and finally drying. After weighing, the specimens were immersed in the corrosion test solution. Three specimens were tested at a time, and the average weight loss was taken.

The solutions of NaCl and KCl were prepared from Analar grade chemicals in distilled water.

The experimental set-up for weight loss measurement and for looking at the electrode behavior are reported in a separate publication (11).

RESULTS

Direct Corrosion Tests

Figure 1 shows the effect of NaCl concentration on the weight loss. The results indicate that the weight loss increases with increasing NaCl concentration. This finding is in agreement with previous investigations (5).

The effect of potassium chloride additions in the range of 0.1-0.7M to two base solutions -- namely 0.1M NaCl and 0.5M NaCl--was investigated. Figure 2 reports the corrosion of stainless steel in 0.5M NaCl with various additions of KCl at 90° C. It is clear that while KCl additions up to 0.4M have some retarding effect, i.e., cause a decrease in the weight loss, further additions of KCl result in a higher corrosion rate. The weight loss data after 10 hours of immersion in 0.5M NaCl with various additions of KCl are given in Table 1.

The effect of various KCl additions on the weight loss in 0.1M NaCl solution is shown in Figure 3. A minimum weight loss is displayed in a solution containing 0.08M KCl. Increasing KCl causes a rapid increase in the corrosion rate.

Table 2 summarizes the weight loss data as a function of the total chloride ion concentration in solutions of NaCl and NaCl-KCl mixtures. It is evident from this table that the weight loss is not directly related to the chloride ion concentration but is rather influenced by the NaCl to KCl ratio. For example, the weight loss in a solution 0.5M NaCl (112 ug./cm.^{2}) is almost three times that in a mixture solution having the same total chloride ion concentration (42 ug./cm.^{2}). This figure (112 ug./cm.^{2}) is also more than twice the weight loss resulting in a solution of NaCl and KCl of total molality 0.7.

Standing Electrode Potential

The stainless steel electrode potential measured against a calomel electrode was found to decrease with time for NaCl and NaCl-KCl solutions, as shown in Figure 4. The potential shift toward more base values is indicative of an active electrode, and this reactivity increases with the concentration of NaCl. The steady-state potential is attained after some time within 40 to 60 minutes. Adding KCl to the electrolyte (to a certain limit) minimized the decrease in the electrode potential.

In pure 0.5M NaCl, the stainless steel potential rested at 650 mV, whereas adding 0.4 KCl raised that potential to -570 mV (va. SCE). More potassium chloride additions shift the standing electrode potential to more basic values, as indicated in Figure 4.

A preliminary investigation of other types of stainless steels and copper nickel alloys has been carried out and has shown that the inhibiting effect of KCl is not limited to austenitic stainless steel. Figure 5 shows this phenomenon for martensitic stainless steel. The steady-state potentials after 60 minutes were -320 mV, -275 mV, and -150 mV for 0.5M NaCl, 0.5M NaCl + 0.2M KCl, and 0.5M NaCl + 0.4M KCl, respectively. On the other hand, adding 0.6M KCl to synthetic seawater at 80° C. showed more basic potentials (-350 mV). Figure 6 gives the results obtained for the standing electrode potentials of Cu-Ni alloy in 0.5M NaCl with different additions of KCl.

Anodic Polarization Measurements

Results of the anodic polarization measurements do not follow the same pattern of those given by direct corrosion and standing potential measurements. Increasing chloride ion concentration either by adding KCl to NaCl or just by increasing NaCl concentration did lower the Tafel's constant "a" at the same over potential. Figure 7 shows that the anodic current (assumed to be a measure of corrosion rate) increases by adding KCl to 0.5M NaCl.

DISCUSSION

Using autoradiographic techniques, Henriksen (12) has shown that Na^+ is located at the cathodic areas and Cl^- at the anodic sites on iron corroding in saline water. This study in parallel with other studies initiated by Evans (13) and others (14) may lead to the suggestion of a simple mechanism. According to that mechanism, the steps of free corrosion of steels in aqueous aerated solutions in the presence of chloride ions can be summarized as follows:

$$H_2O = H^+ + OH^- \quad (1)$$

$$M = M^+ + e^- \quad (2) \quad \text{--- anodic process}$$

$$H^+ + e^- = H \quad (3a)$$

$$\text{and/or} \quad H_2O + 1/2\ O_2 + 2e = 2OH^- \quad (3b) \quad \Big\} \text{ cathodic process}$$

$$NaCl = Na^+ + Cl^- \quad (4)$$

$$Na^+ + OH^- = (Na^+OH^-) \quad (5) \quad \text{near cathodic areas}$$

$$M^+ + Cl^- = (M^+Cl^-) \quad (6)$$

$$(M^+Cl^-) = MCl \quad (7) \quad \Big\} \text{ near anodic areas}$$

where (Na^+OH^-) and (M^+Cl^-) represent the associated form of ions in the electrolyte. The association may proceed to form a soluble compound as in the form shown by Equation 7 resulting in nonionized metal chloride. Solid products may form as a result of the following reaction:

$$M^+ + OH^- = MOH \quad (8)$$

In the present investigation, however, no solid products were detected, and the corrosion was of the general relatively uneven type at 90° C. The solubility of possible hydroxides or hydrated oxides of iron and chromium are quite high at these temperatures (15).

Simple application of the law of mass action to Equation 6 may explain the increase in the corrosion rate of steel in solutions of higher concentrations of sodium chloride (see Figure 2). The activity of Cl^- in $NaCl$-H_2O increases as the mole fraction of NaCl (16) increases. However, it seems that KCl additions upset the picture. According to early measurements (17) at 25° C., some complexation process between KCl and NaCl was suggested. This leads to lowering the activity of Cl^- in the solution. This may explain (Figure 3) which shows the inhibiting effect of some additions of KCl. Stable complex ion formation is rather difficult to visualize between alkali cations and halide anions. Petrucci (18) has reviewed and elaborated the modern concepts of statistical thermodynamics of ionic association and complexation in dilute solutions of electrolytes. He distinguished between ion pairs and complexes, though apparently they may have the same influence on the rate of reactions. The electrical conductivity method was utilized in the present study to investigate the possibilities of ionic association between NaCl and KCl in the aqueous electrolyte at 80° C. Figure 8 shows the analogy between electrolytic conductivity and the effect of KCl addition on the corrosion rate of stainless steel.

The interaction between NaCl and KCl is a maximum at a ratio of 5 to 4. It is interesting to note that this ratio is almost identical to the eutectic ratio of NaCl to KCl in the molten salt system which is the least corrosive salt mixture (19).

The standing electrode potential ennobling due to KCl addition is a maximum at the same mole ratio, namely, 5 to 4. Indeed, a comparison between Figures 2 and 4 emphasizes the analogy between direct corrosion rate and electrode potential. These two parameters are almost equal in both 0.5M NaCl and 0.5M NaCl + 0.6M KCl. The interaction between NaCl and KCl reduces the effective number of chloride ions needed for Reaction 6 to form iron and/or chromium chlorides.

Under applied external potential, the retarding effect of KCl addition is no longer evident. It may be a proof that the association is of the type named "outer sphere complex formation" (18) or ion-pair formation. The ion pairs formed from NaCl and KCl are so weak that they dissociate under applied potential. Dissociated ions under the applied potential (particularly Cl^-) are free to react with the anodic product on the metallic electrode. Optical spectroscopy may be the method to be followed to discriminate between ion pairs and complexes.

Preliminary investigations of other alloys confirms the inhibiting effect of KCl addition. However, the above mentioned model may not generally be applied, since other dissolved cations (e.g., Cr^{+++}, Cu^{++}, and Ni^{++}) may well play some role in the electrolyte. Thus, standing electrode potential does not follow the same route for different alloys as evident from Figure 2 (austenitic steel), Figure 5 (martensitic steel) and Figure 6 (copper-nickel alloy). More detailed measurements and investigations are still needed to understand the role of cations on the corrosion of metals.

CONCLUSIONS

1. The corrosion rate of stainless steels and copper-nickel alloy in pure NaCl aqueous solution is a function of the concentration between 0.1M and 0.5M NaCl.

2. Adding KCl to the base solution retards corrosion and ennobles the standing electrode potential. The maximum effect is at NaCl to KCl mole ratio of 5 to 4.

3. Ion-pair formation is suggested to explain the retarding effect of KCl. Conductivity measurements support this hypothesis.

REFERENCES

1. R. G. Hines, Corr. Sci. 1, 21 (1961).

2. H. P. Leckie, Corrosion, 21, 117 (1958).

3. W. D. France, Corrosion, 26, 189 (1970).

4. M. D. Peterson, T. D. Lenor, and R. E. Groover, Mater. Protec. 2, 23 (1970).

5. R. T. Foley, J. Electrochem. Soc., 122, 1493 (1975).

6. B. Todd, Desal., 3, 106 (1967).

7. U. R. Evans, Corrosion and Oxidation of Metals, 118, Arnold, London (1960).

8. E. A. Lizlovs and A. P. Bond, J. Electrochem. Soc., 122, 719 (1975).

9. J. A. Bittles and I. L. Littauer, Corr. Sci. 10, 24, (1970).

10. G. Bianchi, A. Cerquetti, F. Mazza and S. Torchio, Corr. Sci., 10, 19 (1970).

11. A. A. El-Sayed, S. M. Morsy and S. M. El-Raghy, A. R. E., AEE, Ext. Rept., in press.

12. J. F. Henriksen, Corr. Sci., 9, 573 (1969).

13. U. R. Evans, Corr. Sci. 9, 813 (1969).

14. B. T. Alexander and R. T. Foley, Corrosion, 13, 148 (1975).

15. R. J. Biernat and R. G. Robins, Electrochim. Acta, 17, 1261 (1972).

16. H. S. Harned and B. B. Owen, The Physical Chemistry of Electrolytic Solutions, 3rd ed., Reinhold, New York (1958).

17. F. H. Newman, Electrolytic Conductance, p. 136, Chapman & Hall, London (1930).

18. S. Petrucci, Ionic Interactions, 1, 117, Academic Press, New York (1971).

19. A. U. Seybolt, 4th International Congress on Metallic Corrosion, Amsterdam, 560 (1969).

Table 1

Effect of KCl Addition on Weight Loss of Stainless Steel in 0.5M NaCl

Molality of KCl	0.1	0.2	0.3	0.4	0.5	0.6	0.7
Weight loss, ug./cm.^{2}	78	66	60	48	92	100	120

Table 2

Corrosion of Stainless Steel at 90° C. after 10 Hours of Immersion in Different Solutions

Total Cl^-, (g ion)	Solution	Weight Loss (ug./cm.^{2})
0.1	0.1M NaCl	20
	0.1M KCl	23
0.2	0.2M NaCl	27
	0.1M NaCl + 0.1M KCl	29
0.3	0.3M NaCl	52
	0.1M NaCl + 0.2M KCl	36
0.4	0.4M NaCl	54
	0.1M NaCl + 0.2M KCl	40
0.5	0.5M NaCl	112
	0.1M NaCl + 0.4M KCl	42
0.6	0.5M NaCl + 0.1M KCl	78
	0.1M NaCl + 0.5M KCl	50
0.7	0.5M NaCl + 0.2M KCl	50
	0.1M NaCl + 0.6M KCl	53

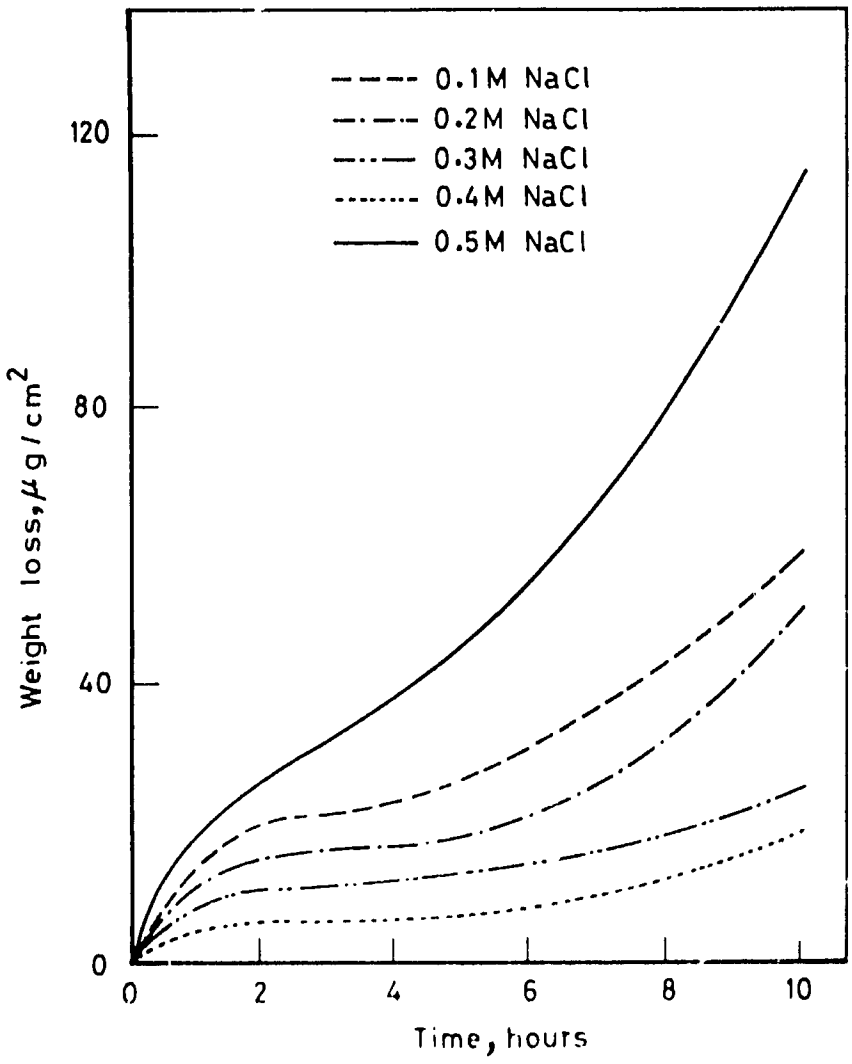

Figure 1

Effect of NaCl on direct corrosion of austenitic stainless steel at 90° C.

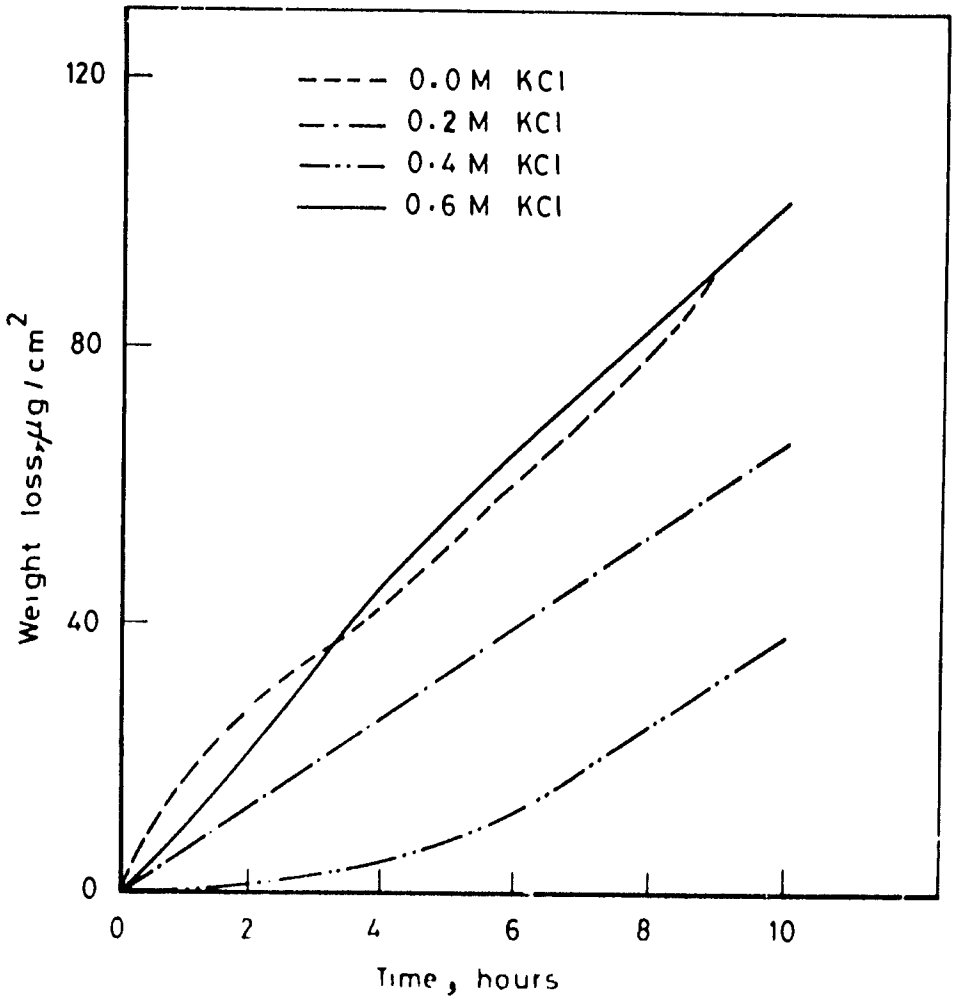

Figure 2

Effect of KCl additions on the corrosion of austenitic stainless steel in 0.5M NaCl.

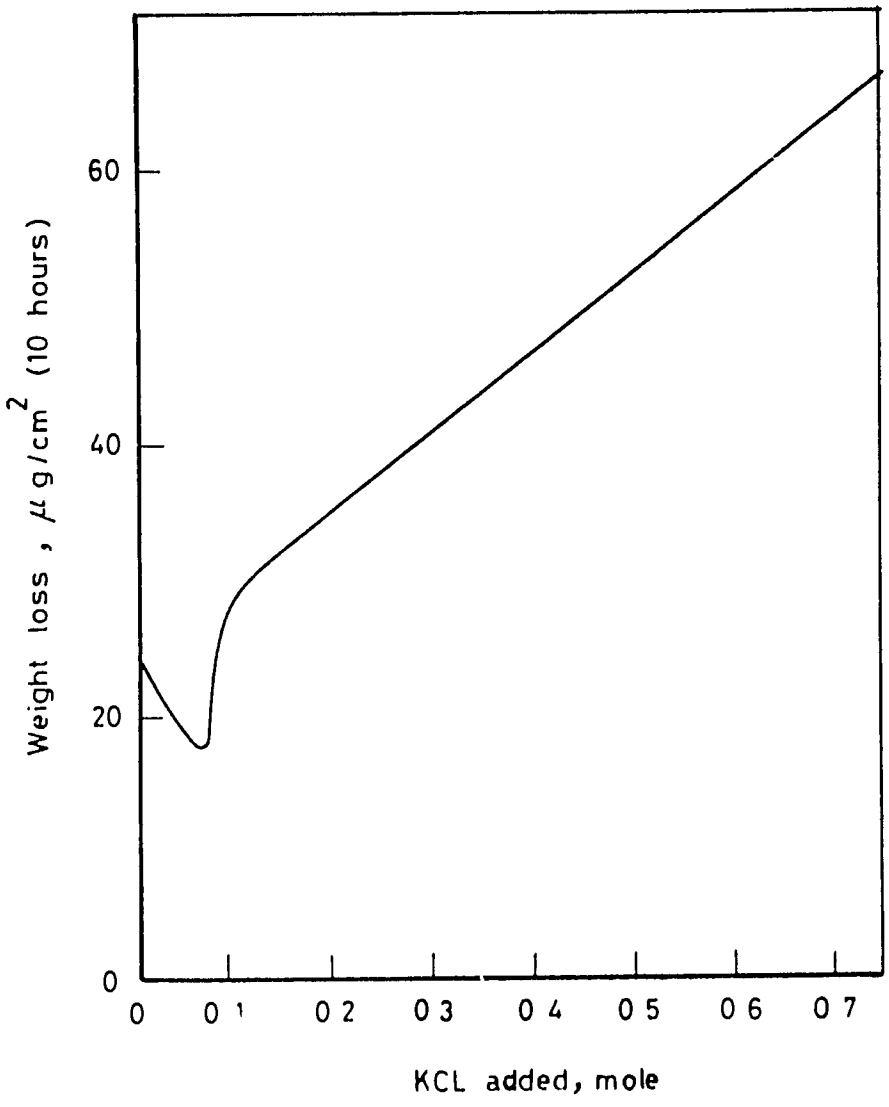

Figure 3

Direct corrosion of austenitic stainless steel

in 0.1M NaCl with additions of KCl.

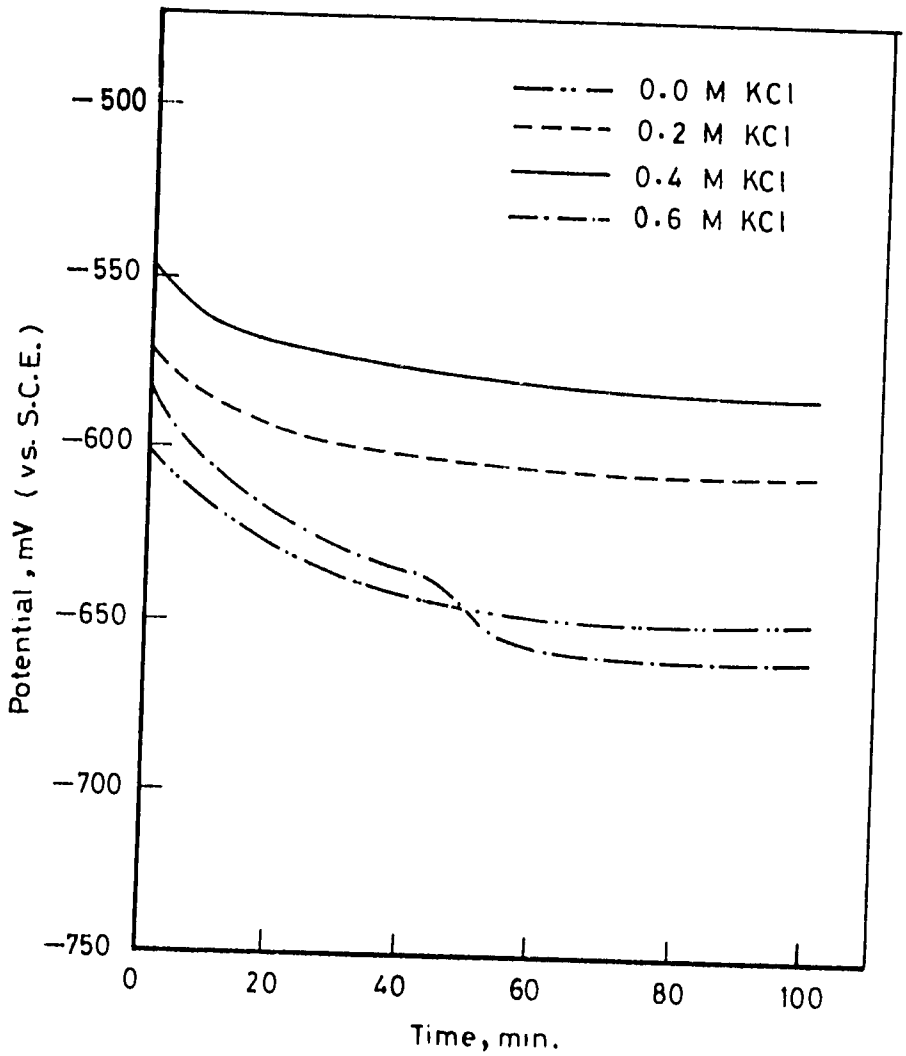

Figure 4

Standing electrode potential in 0.5M NaCl with additions of KCl.

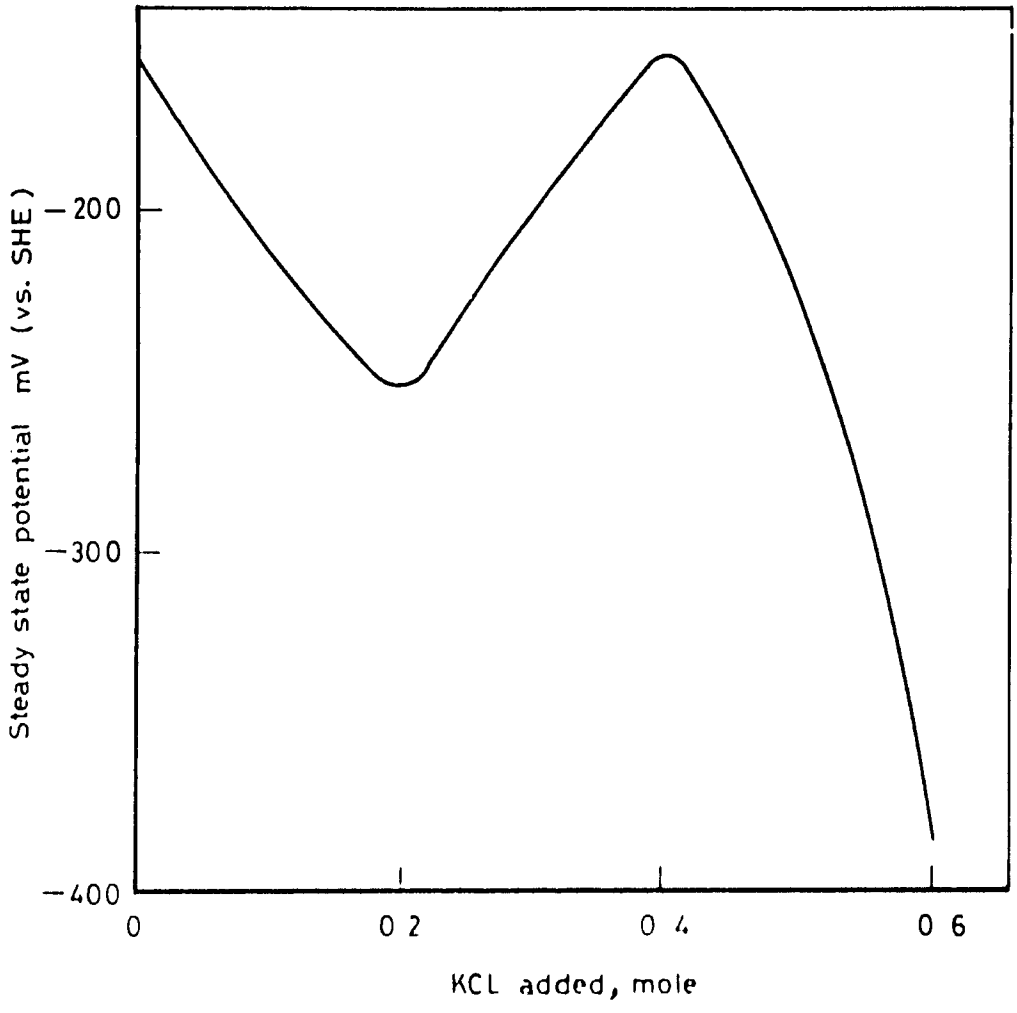

Figure 5

Steady state potentials of martensitic stainless steel electrode in 0.5M NaCl with additions of KCl.

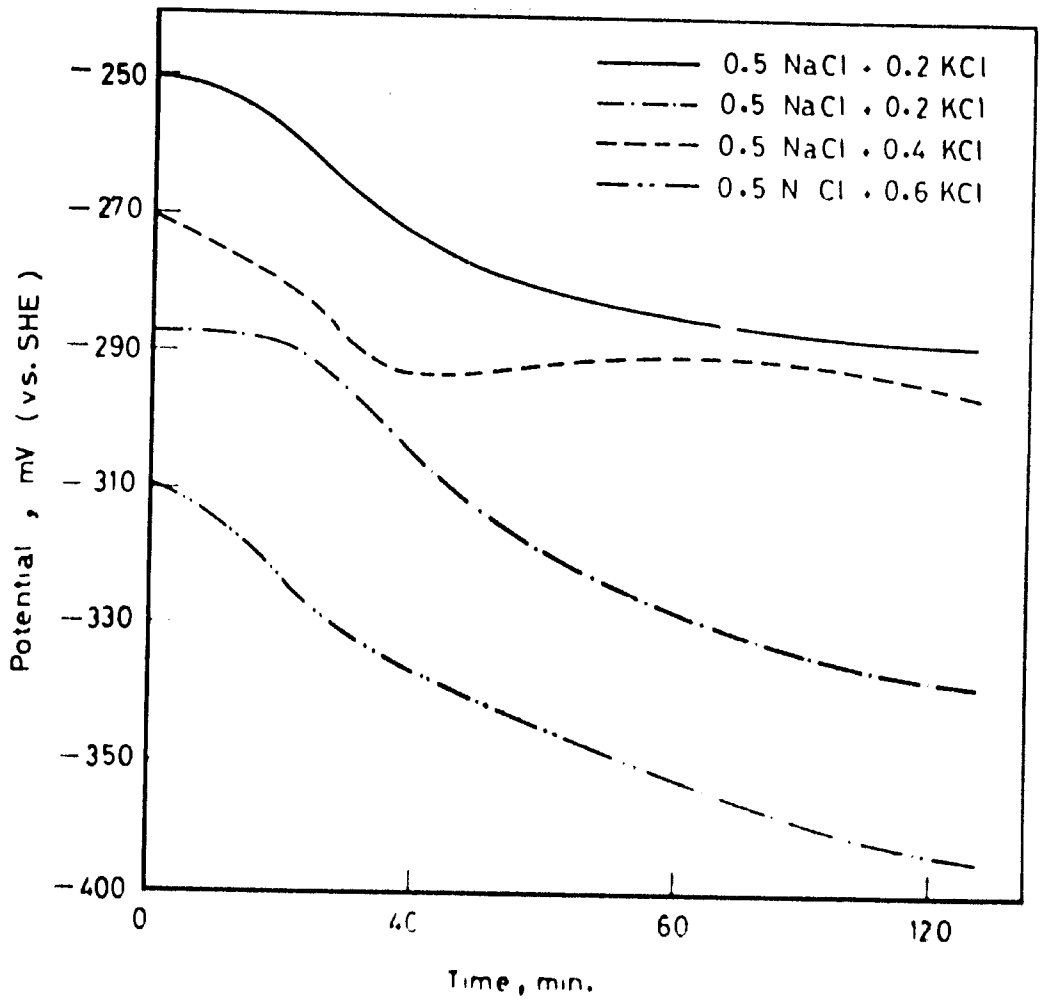

Figure 6

Standing electrode potential of 75-25 Cu-Ni alloy in saline water with additions of KCl at 80° C.

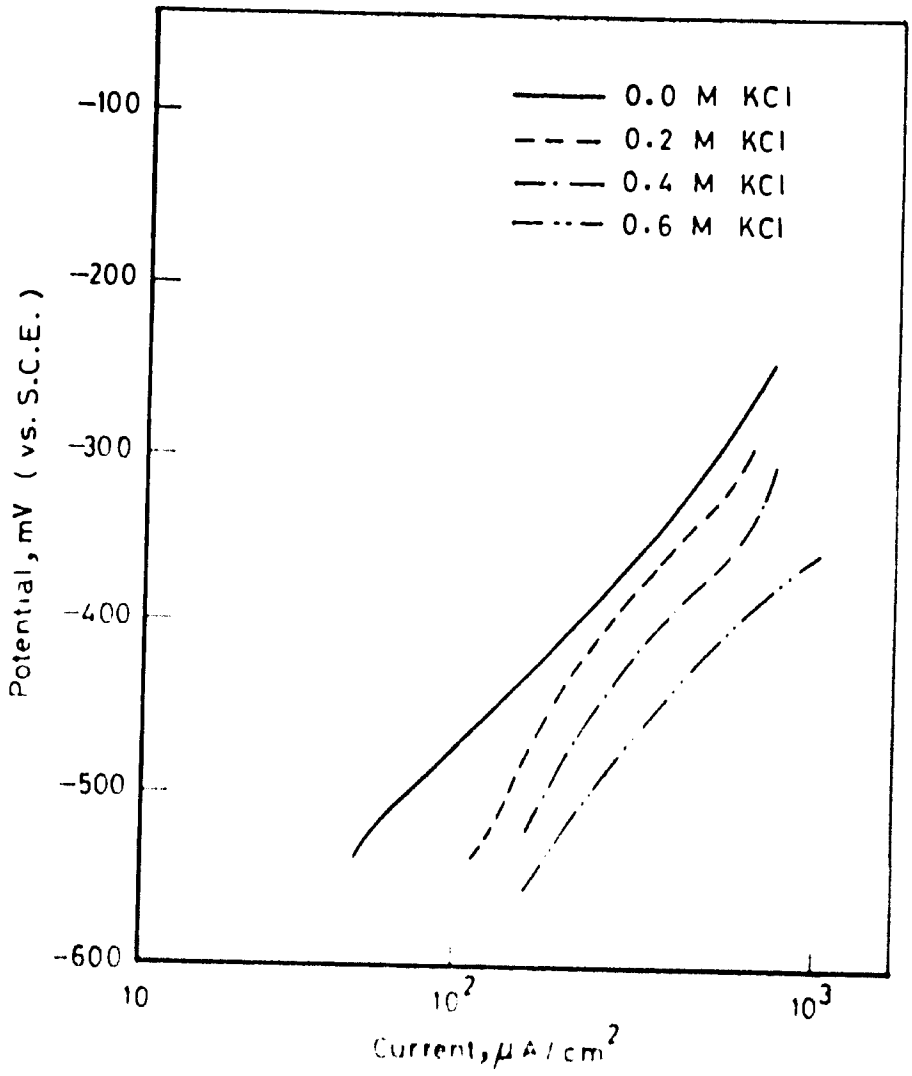

Figure

Anodic polarization of austenitic stainless steel in 0.5M NaCl with additions of KCl.

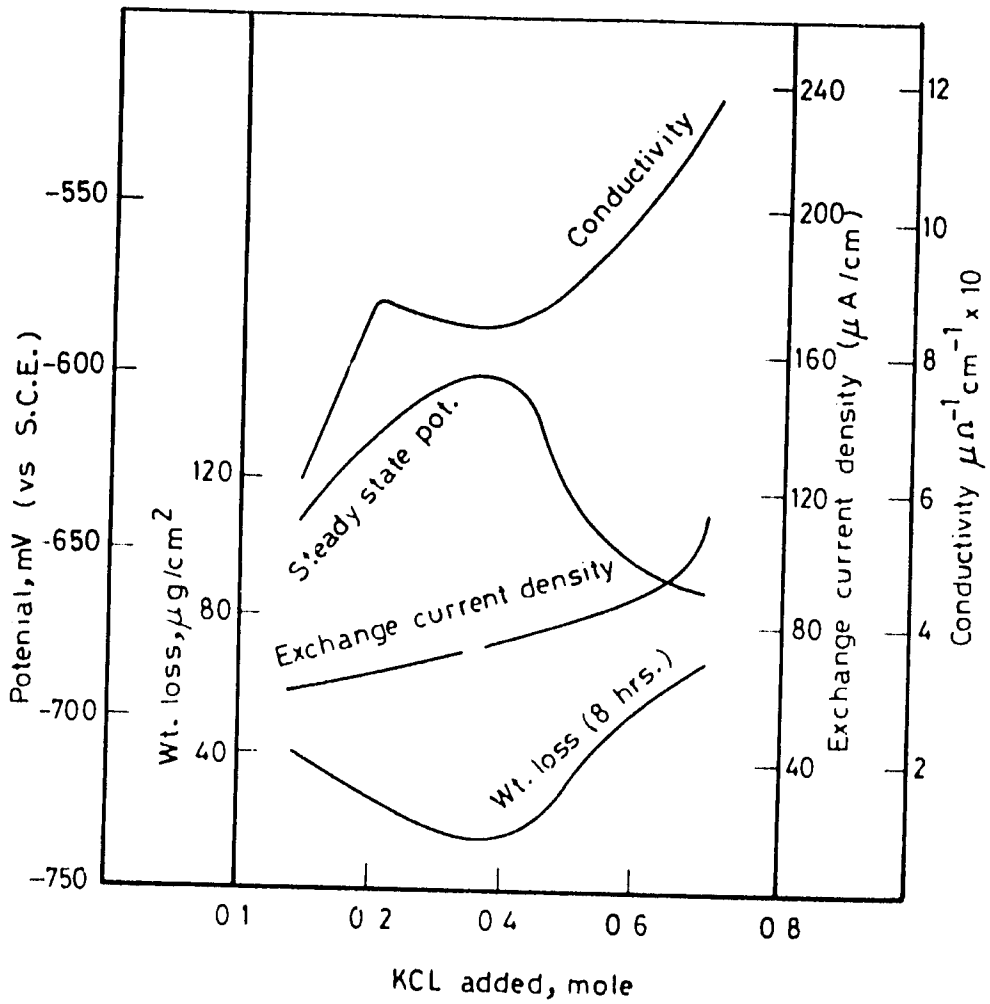

Figure 8

Effect of Cl additions on the electrode behavior and electrolyte conductivity.

A Review of the Thermometric Method of Corrosion Testing

Prof. Dr. A. M. Shams El Din, Head
and
Dr. J. M. Abd El Kader, Research Assistant Professor
Laboratory of Electrochemistry and Corrosion
National Research Centre

INTRODUCTION

The thermometric method of corrosion testing was developed by Mylius in 1922 to assess the dissolution of Al and its alloys in HCl solutions (1). In this test, a piece of the metal of known area is allowed to react with a definite volume of the corroding solution, and the variation of the temperature of the system is followed as a function of time. After an initial period of almost constant temperature, the temperature rises quickly to attain a maximum value. A reaction number, R.N., was defined by Mylius as:

$$R.N. = T_m - T_i/t = T/t \ ^\circ C./min. \quad (1)$$

where T_m and T_i are the maximum and initial temperatures, respectively, and t is the time in minutes from the start of the experiment to the attainment of T_m. Easily corroding materials are characterized by high R.N. values through an increase in T_m and/or diminution of t.

It is the object of the present review to reveal the potentialities of the thermometric method for studying phenomena of diverse nature. Although the technique was developed more than half a century ago, it is not included in reference books on the subject (2-4). A recent article described the application of the method in corrosion education (5).

EXPERIMENTAL

The reaction vessel (a shown diagramatically in Figure 1) is basically the same as described by Mylius (1). The total volume up to mark a amounts to about 30 cc. To minimize heat losses by radiation and to obtain reproducible results, we found it essential to keep the vessel immersed to level b in a Dewar flask of suitable dimensions (6).

When the corroding solution contains a cathodic depolarizer other than H^+, it might be necessary during the thermometric experiments to determine the distribution of the partial cathodic current between H_2 evolution and depolarizer reduction. For this purpose, vessel b (Figure 1) is employed (7) which allows the collection of H_2. The volume of the gas calculated at NTP plus the loss in weight of the metal specimen enable one to calculate the depolarizer equivalents reduced during dissolution (7). Vessel c (Figure 1), on the other hand, allows the metal potential during dissolution to be followed as a function of time, relative to a suitable reference half cell (8). In this case, the unwanted metal surface is covered by a thin layer of neutral wax.

Before use, the thermometric vessel is cleaned by a H_2CrO_4-H_2SO_4 mixture. It is advisable, particularly when studying the effect of surfactants on the rate of dissolution, to subject the vessel to a further washing by steam.

The metal test specimens can be of any convenient form. When the material is available in the form of thin sheets, strips measuring 1 x 10 cm. are used (6, 7, 9, 10). These are bent into a U form and are introduced into the test vessel with their edges downward. Cylindrical pieces cut from rods (11) or wires (8) can also be employed.

The cleaning of the metal surface is essential to obtain reproducible results. A variety of cleaning procedures is available, and the choice between one or the other is left to the worker. Strips of Al and Zn were degreased in a hot alkaline mixture, and this

was followed by washing with running distilled water and drying between filter paper (6). Degreasing in a Soxhlet apparatus with trichloroethylene gave equally clean surfaces (9, 10). Fe specimens were abraded with fine emery paper, degreased with methanol, and then etched in H_2SO_4-HNO_3 solution (11). The same procedure without the etching step was applied to Cu (8) and Cu-Zn alloys (12). A simple criterion for surface cleanness is its complete wetting when washed with water. It is recommended that a new test piece be used for each experiment.

The thermometer used should allow the measurement of the temperature to the nearest 0.5° C. Its Hg reservoir is to rest on the corroding specimen. When this is not feasible, as for example in vessel c, it should be brought as near to it as practical.

AVAILABLE INFORMATION

The thermometric technique was used to study the dissolution of Al in HCl (6) and NaOH (9) as well as of Zn in HCl (6), $HClO_4$, HNO_3, H_2SO_4, H_3PO_4, and H_2CrO_4 (13) and in mixtures of H_2CrO_4 with HCl, H_2SO_4, and H_3PO_4 (14). Sanyal and Srivastava (15) and Shams El Din and Fakhr (11) examined the reaction between Fe and HNO_3. Shams El Din and co-workers recently reported on the dissolution of Cu (8) and Cu-An alloys (12) in acid solutions. The thermometric technique was applied to study corrosion inhibition by surface active agents by a number of authors (6, 9, 10, 16-19). The results of corrosion assessment by the thermometric technique were confirmed by carrying out weight-loss (6, 12, 15), potential (7, 8, 13), and polarization (16) measurements and were complemented by collecting the evolved H_2 (14).

TYPES OF THERMOMETRIC CURVES

Three types of thermometric curves are commonly encountered, and these are represented diagramatically by the curves of Figure 2. The curves of Figure 2a are characteristic for the dissolution of Al in HCl solution (1, 6, 9). One recognizes at first an incubation period at the foot of the curves, along which the temperature remains constant. During this period, the Cl^- ion penetrates the preimmersion oxide film. When this film is fully undermined, the metal is exposed to the attacking action of the acid, and the temperature rises almost linearly with time to attain a maximum value. Note that the slope of the rising parts of the curves, which represents the actual dissolution of the metal, is practically independent of the concentration of the acid. This is taken to indicate that Al dissolution in acids is cathodically controlled.

The dissolution of Al in basic solutions, shown in Figure 2b, is characterized by an induction period (9), during which the temperature rises slowly with time. The preimmersion oxide film undergoes chemical dissolution, and the reaction is autocatalyzed by the heat evolved therefrom. The attack of the basic solutions on the bare metal is vigorous and is accompanied by the rapid rise of temperature. In contrast to the behavior in acid media, however, the slope of the rising parts of the curves increases hand in hand with the concentration of the aggressive solution. This signifies that metal dissolution under these conditions is anodically controlled.

Type c of the thermometric curves is obtained with base metals whose air-formed oxides offer no protection against acid attack, e.g., Zn in HCl, H_2SO_4, and $HClO_4$ (6, 7) or Fe in HNO_3 (11). The reaction with the acids starts from the instant the metal is introduced into the corroding solution.

FACTORS AFFECTING THE REACTION NUMBER

A number of variables effect the magnitude of the R.N. through influencing ΔT and/or t. These should be fully appreciated when dealing with the results of thermometric measurements. These are:

1. The initial temperature T_i.

2. Specimen area/solution volume ratio.

3. Strength of the corroding solution.

4. Presence of additives (surface active agents).

The effect of each of these parameters on the R.N. is outlined in the following discussion.

Effect of T_i on R.N.

With metals whose preimmersion oxide films offer an initial protection against attack (e.g., Al) the rise in T_i causes the shortening of the incubation or induction period. ΔT does not vary, however, in a systematic manner with the increase in T_i (20). This latter behavior (i.e., the nonlinear dependence of ΔT on T_i) is also noted with metals which do not exhibit an induction period such as Zn (12) and Fe (15). Accordingly, the R.N. of these metals depends greatly on the chosen initial temperature. For comparative work, this should be kept the same to $\pm$ 0.5° C.

For reasons to be disclosed in the following section, it is essential to establish the effect of T_i on the shape of the thermometric curves when studying the dissolution of binary alloys.

Effect of Specimen Area/Solution Volume Ratio on R.N.

Since the heat evolved from the interaction between the metal and the corroding solution warms the whole system, it is expected that variations in the area/volume ratio will influence the value of ΔT, and correspondingly R.N. This has been proved in a number of cases (12, 15). Within certain limits, the decrease in the ratio produces a linear lowering in R.N. (12). The volume of the solution should not, however, be too large so as to dissipate the heat evolved, nor should the specimen area be too small so as to undergo complete dissolution.

The area/volume parameter should be examined in detail when dealing with binary alloys. In the dissolution of a 70-30% Cu-Zn alloy in 4N HNO_3, a slight break in the thermometric curves was noted (12). This represents the preferential attack on the Zn component of the alloy. By increasing the volume of the corroding solution, the reaction was slowed down, and a clear step for Zn dissolution was recorded (Figure 3a). A similar effect as that produced by changing the area/volume ratio was obtained by lowering the initial temperature T_i, while keeping the other experimental conditions the same. As is seen from the curves of Figure 3b, the break in the thermometric curves which was well developed at low T_i, diffused into the main rising segment as T_i was raised (12).

Effect of Strength of the Corroding Solution on R.N.

When no other side reactions take place, the increase in the concentration of the corroding solution is accompanied by a corresponding increase in both ΔT and R.N. Usually, ΔT varies with the normality N of the solution as (6, 9, 12):

$$\Delta T = A_1 N \quad (2)$$

or

$$\Delta T = A_1 (N - N^\circ) \quad (3)$$

where N° is the concentration of the corroding medium which would not yield a measurable rise in temperature. A_1 is the rate of temperature rise per unit concentration, ° C./mole. l^{-1}, and is a measure of the tendency of the metal to be attacked. The dissolution of Fe in HNO_3 follows reaction 2 relation up to about 4N. In solutions $4 < N < 10.8$, ΔT is independent of N, as T_m approaches the boiling point of the solution (11, 15).

The variation of the thermometric corrosion rate, R.N., follows a power law of the form:

$$R.N. = A_2 N^n \quad (4)$$

where A_2 and n are constants. A_2 represents the R.N. measured in 1N solutions of the aggressor. Representative values are 6.3×10^{-2}, [Al in HCl] (9), 4.6×10^{-1} [Al in NaOH] (9), 7.8×10^{-3} [Cu in HNO_3] (8) and 2.69 [Zn in HNO_3] (12). These values parallel the rate of attack by the various solutions, as established by other techniques. The n values for the same systems are, successively, 2.9, 1.5, 2.8, and 1.7.

It is of interest to remark that the corrosion rates, as determined by the weight-loss method, are commonly expressed by a relation similar to 4, where n is equal to, or very near to, 0.5 (21-24). The disparity between this value and those determined by the thermometric method is apparently related to the experimental conditions. Thus, while weight-loss measurements are usually carried out in well-thermostated solutions, the continuous increase in temperature in a thermometric experiment leads to the augmentation of the dissolution rate and to its complex dependence on the concentration of the attacking solution.

Effect of Additives on R.N.

Substances added to the reaction medium can influence the R.N. in a number of ways. Surface active substances adsorb on the metal surface and interfere to various extents with the partial anodic and/or cathodic reactions. Additives might also offer an alternative path for the cathodic reaction other than the H_2-evolution reaction. The thermometric technique presents a simple and rapid method for establishing the effect of additives and allows, in the meantime, conclusions to be drawn regarding the type and mode of adsorption. To obtain a clear picture about the role of a certain substance, it is recommended that a series of experiments be performed with increasing additive concentrations. Sanyal (15) proposed, however, the progressive introduction of the additive in increments during the course of a single thermometric experiment.

Organic Additives. The effect of urea, thiourea, gelatin, egg albumin, glycogen, starch, 8-hydroxyquinoline, p-toluene sulfonic acid, carboxycellulose, methyl cellulose, sulfosalicilic acid, and hydrazine on the dissolution of Al in 2N HCl and Zn in 3N HCl was studied by Shams El Din and Aziz (6). Abd El Kader and Shams El Din (9) compared the effect of alkylammonium ions and alkylamines for retarding the dissolution of Al in acid and basic solutions, respectively. Saleh and Shams El Din (10) carried out a similar study on organic acids and their anions. Homologues of aliphatic, aromatic, and amino acids were tested. The thermometric technique was also employed to study corrosion inhibition by extracts of naturally occurring substances. The effect of extracts of karkade leaves (Hibiscus subdarifa) (16), of the fruit-juice and fruit-shell extracts of pomegranate (Punica granatum), of extracts of the fruits of tamarind (Tamarindus indica) and of the leaves of Ceylon tea on the dissolution of both Al and Zn in acid and basic solutions was similarly established (17). Issa and coworkers examined the inihibition of the dissolution of Al in acid solutions by cystine, cystein, semicarbazide, and thiosemicarbazide (18) as well as by methylethylketone, chloral hydrate, pinacolone, and mesityl oxide (19). These last authors, however, overlooked the fact that in most cases the effect noted was that of the reduction products rather than of the additives themselves. Shams El Din and Fakhr (11) compared the inhibition of the attack on Fe by HNO_3 by urea and gelatin, whereas Sanyal (15) studied the effect of thiourea on the same reaction.

From the bulk of this information, additives were found to:

1. Reduce the R.N. (inhibitors).
2. Raise the R.N. (accelerators).
3. Have no effect on the R.N. (inactive additives).

Inhibitors cause the decrease in R.N. in two main ways. In the first, the time t taken to attain T_m progressively increases with the increase of the additive concentration without noticeably affecting T_m. This denotes weak adsorption, since the inhibitor can be displaced by the attacking solutions when given ample time (6). In the case of Al dissolving in acid solutions, weakly adsorbed additives act as cathodic inhibitors. This is readily gleaned from the facts that the incubation period increases while the slope of the rising parts of the curves, which represents the actual dissolution of the metal, remains the same as in additive-free solutions. This behavior is represented schematically by curves a of Figure 4.

Besides increasing the time t, strongly adsorbed additives, on the other hand, lower the maximum temperature. This can occur while the slope of the rising parts of the curves remain the same (cathodic inhibitors), as in Figure 4b, or with the slope declining as the concentration of the additive is increased (mixed inhibitor), as in Figure 4c. A case where the additive adsorbs only on the anodic sites, causing a diminution of the slope of the rising parts of the curves without affecting the length of the induction period, shown in Figure 4d, has not hitherto been encountered.

Only a single example has been noted thus far where the R.N. decreases as a result of reduction in T_m while t remains the same (Figure 4e). This concerns the effect of urea on the thermometric curves of Fe in HNO_3 (11). Urea destroys HNO_2, which is the key product in the autocatalytic cycle involved in metal dissolution in HNO_3. The effect of the same additive on the dissolution of Cu differs from that on Fe in that it acts both as a destroyer for HNO_2 as well as an adsorption inhibitor (9).

Plots of the R.N. (6) or the percentage reduction in R.N. (9, 11, 16, 17) as a function of the logarithm of additive concentration are essential for comparing the action of various substances. These plots are sigmoid in nature, corresponding to monolayer and multilayer formation on the metal surface, before and after the inflexion, respectively. The form of the R.N./log C curves was derived theoretically on the basis of known adsorption isotherms (6). Issa's model of stepwise adsorption (19) is qualitatively the same as given above. The presentation of the data in terms of the time delay Δt (or log Δt) as a function of C (or log C) is, however, meaningless, since these are mere reflections of the original R.N./log C curves.

As expected, both the inflection in the R.N./log C curves and the extent of reduction in the R.N. depend on the nature of the additive used. These differences are the result of disparities in the energies of adsorption, cross-sectional areas, and probable interactions between the adsorbate and the metal surface. Comparison of the R.N./log C curves of inhibitors belonging to the same homologous series allows some definite conclusions to be drawn regarding the mode of adsorption. In the case of monoalkylamines in acid solutions (monoalkylammonium ions), inhibition increases with the increase of the chain length (9). This indicates that the additive molecules either lie flat on the surface or are inclined to the vertical. Inhibition increases also as one goes from the mono- to the di- and trisubstituted amines. A linear corrolation was established between the logarithm of concentration of the various amines necessary to inhibit attack to one end and the same extent and the cross-sectional area of the inhibitor used, indicating that the additives act by way of blocking (9). The inflections in the R.N./log C curves of aliphatic acids were independent of their chain length, a fact which was taken to support the conclusion that adsorption occurs through their carboxylic groups, while their tails protrude, brush-like, into the solution (10). In the case of aromatic acids, however, inhibition increases with the increase of the side-chain length, signifying the attachment to the metal surface through the benzene nucleus as well as through the carboxylic groups. The same is also true for amino acids, where both functional groups are involved in inhibition (10).

Acceleration of the dissolution of metals in acid media is brought about by those organic additives which catalyze the evolution of H_2 from solution. These are nitrogen-containing compounds having the ability to bind a free proton to the lone pair of electrons of their N atoms (25). The participation of the cation BH^+ (B is the additive molecule) in the H_2-evolution reaction, either as a proton carrier (26) or as recipient for electrons (27, 28), accelerates the rate-determining step and brings about a decrease in overpotential (29). Since an increase in the rate of the cathodic reaction is accompanied by a

corresponding increase in that of the anodic process, augmentation of the R.N. is recorded through a rise in T_m and/or decrease in $\bar{t}$. This state of affairs explains the acceleration of dissolution of Zn in acid solutions in the presence of hydrazine (6).

Inorganic Additives. The number of inorganic additives that can be tested by the thermometric technique is much smaller than that of organic compounds and is generally limited to the anions of the common acids. Shams El Din and co-workers (13) studied the dissolution of Zn in different acids of varying concentrations. Based on the ΔT-normality curves, distinction could be made between corroding (HNO_3, HCl, $HClO_4$, H_2SO_4), inhibiting (H_3PO_4), and passivating (H_2CrO_4) acids. For corroding acids, ΔT varied linearly with N at a rate depending on the nature of the acid anion. Dissolution was highest in HNO_3 and decreased in the succession HNO_3 > HCl > H_2SO_4 > $HClO_4$. With the passivating acid H_2CrO_4, no rise in temperature was recorded in solutions up to 4N. The ΔT-normality curve of H_3PO_4 was not linear and lay between those of corroding acids and that of H_2CrO_4 (13). The sequence of inhibition by the various anions, as established from thermometric experiments, was confirmed by measuring the potential of the Zn electrode in aerated solutions of the same anion (13). In the meantime, anions which enhance dissolution were found to accelerate the electroreduction of O_2 (30). On the other hand, inhibition of dissolution by CrO_4^{--} was due to the formation of mixed $ZnO.Cr_2O_3$ on the surface of the metal (31).

The dissolution of Fe in HNO_3 was inhibited by additions of Cl^- and I^- (11-15), which displaced one of the products of the autocatalytic cycle of the HNO_3 reactions (11). A similar effect was noted with HSO_4^- (11). Dissolution was promoted, however, by NO_2^- and to a lesser extent by NO_3^- (11). The attack of HNO_3 on Cu was also retarded by Cl^-, HSO_4^-, $H_2PO_4^-$, and, in contrast to the case of Fe, by NO_3^- (8). The same was also true for Cu-Zn alloys of various compositions (12).

As is the case with organic compounds, the dissolution of metals in acid solutions can be enhanced through inorganic additives which can depolarize the complementary cathodic reaction. This latter can be the same as in additive-free media (i.e., the H_2-evolution reaction) but kinetically favored. This state of affairs is noted when the reduction of the additive leads to the formation of a metallic deposit on which the H_2 overpotential is lower than that on the dissolving metal (6). Impurities of metals with low H_2 overpotential (e.g., Cu) are more harmful than those with high overpotential (e.g., Hg), even when the reduction of the latter is accompanied by a larger decrease in free energy (6).

Depolarization of the cathodic reaction, leading to augmentation of the corrosion rate, can also occur when the additive offers a reduction path which is thermodynamically more feasible than the evolution of H_2. Thus, the dissolution of Al in HCl was considerably accelerated through additions of $K_2Cr_2O_7$ (6) or $FeCl_3$ (20). Similarly, H_2CrO_4, which alone acts as a strong passivator for Zn, reversed its action and became a corrosion stimulant when mixed with other acids (14). Under these conditions, the overall cathodic current, accounting for the dissolution reaction, was divided between that taken in the evolution of H_2 and that consumed in the reduction of the oxidizing agent. The ratio of the two partial currents depended on the relative concentrations of the two acids, as well as on the nature of the attacking one (14).

STUDY OF LOCALIZED ATTACK BY THE THERMOMETRIC TECHNIQUE

Although the thermometric technique is commonly applied to study the general dissolution of metals in corroding media (general corrosion), it can be used to investigate localized (pitting) attack. For this type of attack to occur, two requirements should be satisfied; namely, the development of a large passive or inhibited area, upon which the cathodic reaction occurs, and the presence of an anion capable of stimulating attack. In concentrated HNO_3 (c $\geqslant$ 10.8N), Fe is present in the passive state as a result of formation of a γ-Fe_2O_3 film on its surface (11). When a pitting corrosion agent such as Cl^- is introduced into the solution, it initiates attack, and the temperature rises to almost the boiling point of the solution. Practically all features of pitting corrosion, as established from other, more sophisticated techniques, are noted by the thermometric procedure. Thus, the reaction starts after only a certain lapse of time, the so-called induction period (32-34). In the same passivating solution, this time decreases as the Cl^-

ion concentration is raised (35). Not all the added Cl^- ion initiates attack, and the solution can tolerate the action of a certain concentration of the aggressor without corrosion taking place (36, 37). In accordance with known information about pitting corrosion (33, 35, 38-40), the thermometric results reveal that the tolerable concentration of the attacking agent increases with that of the passivator following a double logarithmic relationship:

$$\log C_{agg.} = a + b \log C_{pass.} \quad (5)$$

where a and b are constants. The practical applicability of these results is quite apparent. Concentrated solutions of HNO_3 are transported and stored in iron containers. Extreme care should be taken to avoid contamination with any pitting corrosion agent. The thermometric technique offers a rapid and easy way for determining the purity and safety of the acid before being introduced into the container.

A somewhat different case of pitting corrosion was noted in the case of Cu (8) and Cu-Zn alloys (12). These materials are immune to attack by cold, concentrated solutions of HCl. The addition of KNO_3 to the medium initiates attack, and a special type of thermometric curves is recorded. These exhibit an induction period, a sudden rise in temperature ending in a sharp maximum, and a rapid decrease in temperature thereafter. For the same HCl concentration, the length of the induction period varied inversely with the KNO_3 content when plotted on a double logarithmic scale (8). Similarly, the R.N. varied with the concentration C of NO_3^- according to:

$$R.N. = A\,(C - C^\circ)_{NO_3^-} \quad (6)$$

where C° is the concentration of the anion that can be tolerated by the particular concentration of HCl. Both A and C° in Equation 6 changed with the concentration of HCl in a manner which suggested that the conditions prevailing during attack propagation were practically the same as those governing pitting initiation (8). It is of interest to remark here that the Cl^- ion, which normally acts as a pitting corrosion agent, acts in the case of Cu and Cu-Zn alloys as corrosion inhibitor. On the other hand, the NO_3^- ion reverses its function and behaves as a corroding agent.

CONCLUSION

The thermometric method of corrosion testing is a simple and rapid procedure that can be applied for the assessment of a variety of corrosion phenomena. The results obtained therefrom conform with those of other more elaborate and sophisticated techniques. The first direct use of the method is to compare the ability of a number of materials to withstand the attacking action of the same aggressive electrolyte or the corrodability of the same material in different media. Based on the dependence of the thermometric curves and the R.N. values on the concentration of the aggressive solution, one can conclude whether attack is under cathodic or anodic control.

One of the prime advantages of the thermometric method lies in the study of the effect of surface active agents on the dissolution of metals in corroding solutions. The method allows the rapid establishment of the inhibition efficiency of surfactants and assists in the choice of the most suitable retardant from among a group of possible ones. Distinction can be easily made between weakly and strongly adsorbed substances as well as between cathodic, anodic, and/or mixed inhibitors. In some instances, information can be gained regarding the mode and orientation of the adsorbate on the surface of the metal.

The feasibility of the thermometric method for studying the dissolution of binary alloys has been recently established. The full merits of the technique in this domain, however, must await the gathering of more information. Work is also needed to establish the variety of conditions under which the method can be applied to the understanding of pitting corrosion. The results now at hand indicate that all characteristics of this type of localized attack, as obtained from other techniques, are revealed from the thermometric curves.

The method might find useful applications in the fields of surface finishing, pickling, and chemical polishing.

REFERENCES

1. F. Mylius, Z. Metallk., 14, 233 (1922).
2. H. N. Uhlig, Corrosion Handbook, John Wiley (1948).
3. F. Todt, Korrosion, Verlag Chemie (1954).
4. U. R. Evans, The Corrosion and Oxidation of Metals, Arnold (1960).
5. A. M. Shams El Din, Proc. 5th Int. Corr. Cong., Tokyo (1972).
6. K. Aziz and A. M. Shams El Din, Corr. Sci., 5, 489 (1965).
7. M. G. A. Khedr, M. Sc. Thesis, University of Cairo, (1968).
8. R. M. Saleh, J. M. Abd El Kader, A. A. El Hosary and A. M. Shams El Din, J. Electroanalyt. Chem., in press.
9. J. M. Abd El Kader and A. M. Shams El Din, Corr. Sci., 10, 551 (1970).
10. R. M. Saleh and A. M. Shams El Din, Corr. Sci., 12, 689 (1972).
11. A. M. Shams El Din and M. Y. Fakima, Corr. Sci., 14, 635 (1974).
12. A. M. Shams El Din, A. A. El Hosary and M. M. Gawish, Corr. Sci., submitted for publication.
13. V. K. Gouda, M. G. A. Khedr and A. M. Shams El Din, Corr. Sci., 7, 221 (1967).
14. A. M. Shams El Din and M. G. A. Khedr, Metalloberfl., 25, 200 (1972).
15. B. Sanyal and K. Srivastava, Br. Corr. J., 8, 28 (1973).
16. A. A. El Hosary, R. M. Saleh and A. M. Shams El Din, Corr. Sci., 12, 897 (1972).
17. R. M. Saleh and A. A. El Hosary, Proc. 13th Sem. Electrochem., Karaikudi (India) (1972).
18. I. M. Issa, A. A. El Hosary and Y. M. Temerk, U. A. R. J. Chem., 13, 121 (1970
19. I. M. Issa, M. N. H. Moussa and M. A. A. Ghandour, Corr. Sci., 13, 791 (1973).
20. Unpublished results.
21. V. K. V. Unni and T. L. Rama Char, Corr. Technol., 11, 35 (1964).
22. M. A. Streicher, Trans. Electrochem. Soc., 93, 285 (1948).
23. S. D. Dionisev and L. I. Antropov, Diagrammy Plavkosti Nekotorykh Solevykh Sistem, 60, (1964); C. A., 63, 17629 (1965).
24. A. C. Mackrides, N. M. Komodromos and N. Hackerman, J. Electrochem. Soc., 102, 363 (1955).
25. J. Heyrovsky and J. Kuta, Principles of Polarography, Czeck Akad. Sci. Pub. Hoause, 426 (1965).

26. J. Heyrovsky, Chem. Listy, 31, 440 (1937); Coll. Czech. Chem. Commun., 9, 273 (1937).

27. A. N. Frumkin and E. P. Andreyeva, Dokl. Akad. Nauk SSSR, 40, 417 (1953).

28. M. V. Stackelberg, W. Hans and W. Jensch, Z. Elektrochem., 62, 839 (1958).

29. A. M. Shams El Din and T. M. H. Saber, Electrochim Acta., 15, 711 (1970).

30. A. M. Shams El Din and L. Holleck, Z. Elektrochem., 71, 739 (1967).

31. R. H. Abu Zahra and A. M. Shams El Din, Corr. Sci., 5, 517 (1965).

32. U. R. Evans, J. Chem. Soc., 1020 (1927); S. C. Britton and U. R. Evans, ibid, 1773 (1930).

33. S. Matsuda and H. H. Uhlig, J. Electrochem. Soc., 111, 156 (1958); H. H. Uhlig, Z. Elektrochem., 62, 626 (1958).

34. I. Rosenfeld and H. Maximtochuk, Z. Phys. Chem., 215, 25 (1960).

35. A. M. Shams El Din and S. M. Abd El Haleem, Werkst. Korros., 24, 389 (1973).

36. F. N. Speller, Corrosion, 11, 303 t (1955).

37. H. H. Uhlig and J. R. Gilman, Corrosion, 20, 289 t (1964).

38. D. M. Brasher and A. D. Mercer, Br. Corr. J., 3, 120 (1968); A. D. Mercer and I. R. Jenkins, ibid, 3, 130 (1968); A. D. Mercer, I. R. Jenkins and J. E. R. Brown, ibid, 3, 136 (1968); D. M. Brasher, D. Rachenberg and A. D. Mercer, ibid, 3, 144 (1968).

39. E. V. Bogatyreva and S. A. Balezin, Zh. Prik. Khim., 32, 1071 (1957).

40. P. J. Anderson and M. E. Hocking, J. Appl. Chem., 8, 352 (1958).

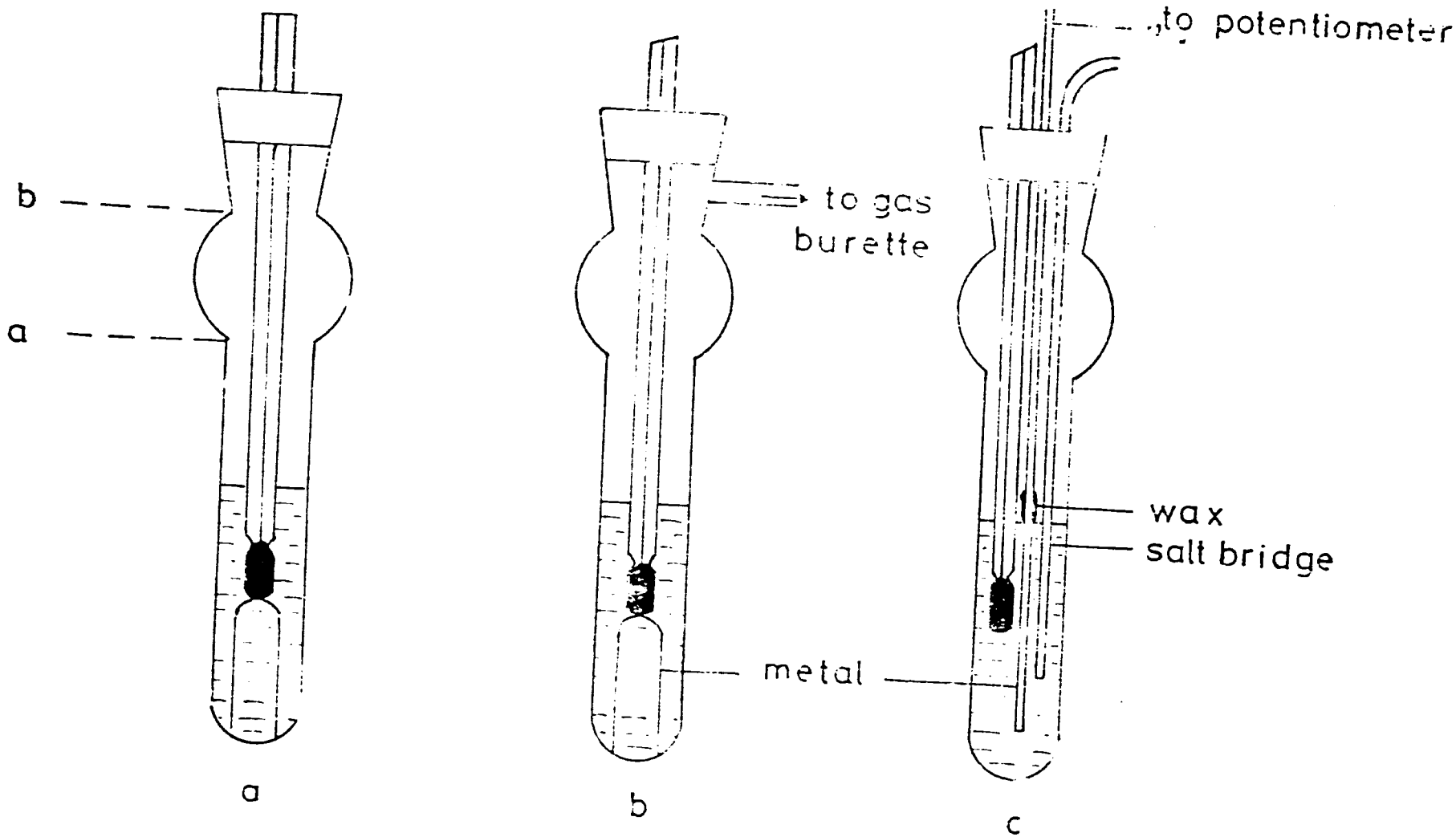

Figure 1. Various vessels for carrying out thermometric corrosion experiments (1, 7).

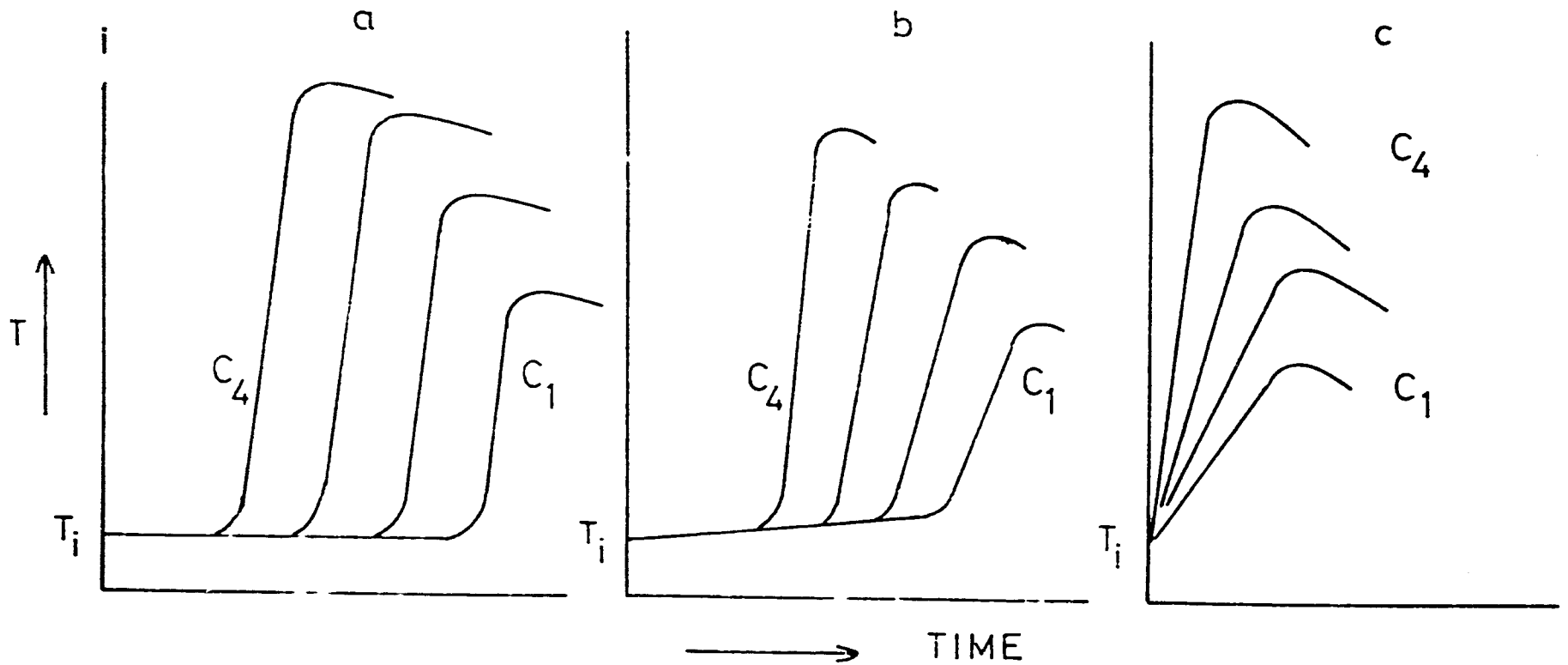

Figure 2. Different types of thermometric curves.
a. Al in HCl (6).
b. Al in NaOH (9).
c. Zn in HCl (13).
$C_1 < C_4$

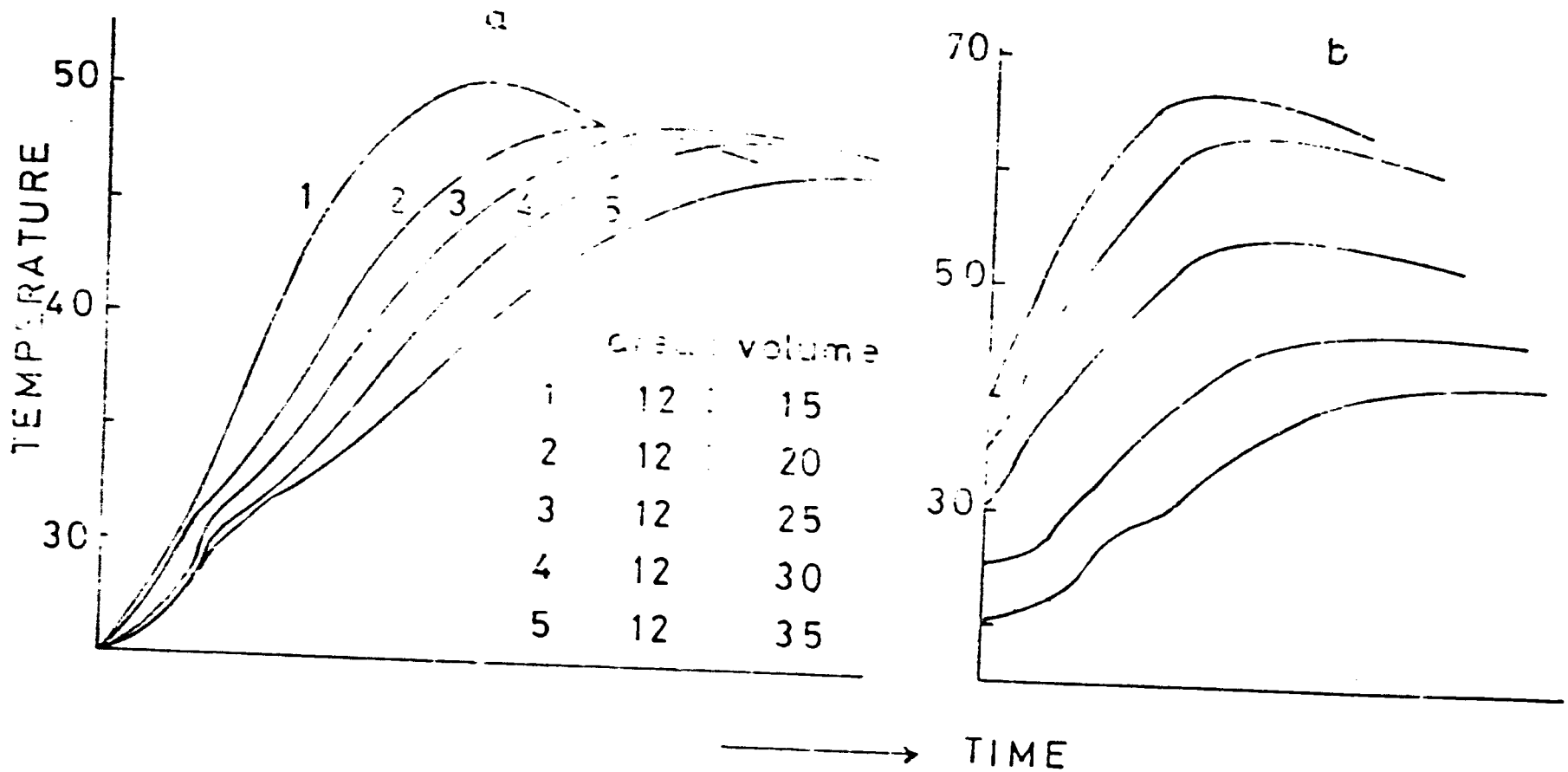

Figure 3

Effect of specimen area/solution volume (a) and of initial temperature (b) on the thermometric curves of 70-30% Cu-Zn allow in 4N HNO_3 (12).

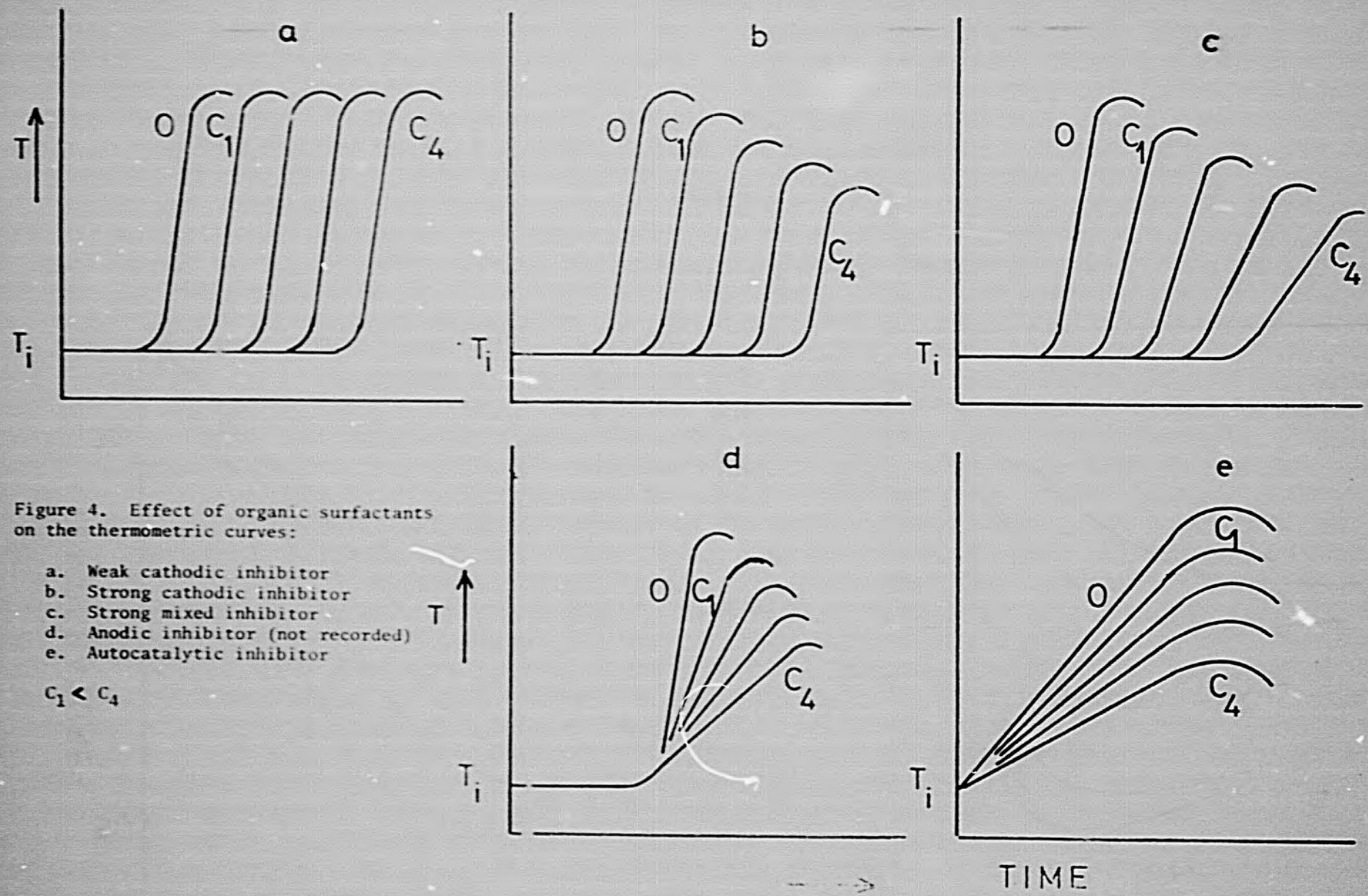

Figure 4. Effect of organic surfactants on the thermometric curves:

a. Weak cathodic inhibitor
b. Strong cathodic inhibitor
c. Strong mixed inhibitor
d. Anodic inhibitor (not recorded)
e. Autocatalytic inhibitor

$C_1 < C_4$

Hot Corrosion of the Sinter Grates by A Chloride-Containing Iron Ore

Prof. Dr. A. A. Abdul Azim
Head, Department of Physical Metallurgy
Co-Project Manager, Central Metallurgical Research
and Development Institute
National Research Centre

THE NATURE OF THE PROBLEM

Baharia iron ore, unlike any other iron ore in the world, is contaminated with alkali halites. These contaminants vary from 0.35 to 1.35% depending on the location and the depth of bed. The use of such ores in the sinter stand is likely to cause trouble by corroding the cast iron grate and suction chamber. A research project has been initiated in the Corrosion Section of the Central Metallurgical Research and Development Institute to study hot corrosion of cast iron under conditions which do not differ greatly from those prevailing in the sintering plant. The threshold amount of sodium chloride, below which attack is not encountered, will be determined. Other types of cast iron, expected to be more corrosion resistant than the type used in the sinter plant, will be tested under the same conditions.

THE ENVIRONMENT AND SINTERING CYCLE

The change consists of 50% iron ore ($Fe_2O_3 \cdot H_2O$), dolomite and limestone furnishing a basicity of 1.2%, and 5% coke breeze. The moisture amounts to 10-12% and sodium chloride to 1.6%. The charge moves through a distance of 30 m. at a rate of 2-5 m./min. It starts at room temperature and reaches a maximum of 1000° C.

MECHANISM OF HOT CORROSION OF CAST IRON

Cast irons are useful in elevated temperature service because the oxide film commonly produced adheres quite well to the base metal. The rate of attack decreases with time as the oxide film forms. The thickness of the scale naturally depends on temperature and duration. Ideally, the thickness of the scale should increase as $t^{1/2}$, but in practice cracks develop in the scale and allow the gases to reach the metal surface somewhat more readily than is postulated by this relationship. Cracking will always tend to occur as the film thickness increases, but if the iron is subjected to cycle variations in temperature, the extent of cracking will increase. With flake graphite cast irons, since there is a tendency for oxide penetration to occur along the graphite, the scale adheres to the metal surface more securely than is the case with steels and therefore becomes detached less readily.

The scale on cast iron is usually continuous and adherent at least up to 800° C. Oxidation of the metallic matrix around the graphite flakes may occur preferentially to graphite oxidation at temperatures above 400° C. and below 650°-700° C. Above 650°-700° C., carbon and iron oxide will not exist together in equilibrium, and oxide so formed at a lower temperature may be reduced by graphite if the temperature rises above 650°-700° C., yielding a layer of ferrite around graphite flakes. Breakdown by scaling does not normally become important until temperatures in excess of 600°-700° C. are reached. Above 750° C., unalloyed irons are attacked with rapidly increasing speed as the temperature increases.

It is usual to assess the heat resistance of cast irons in terms of their resistance when exposed to air at a given temperature for a given period of time. However, very few service conditions actually conform to these experimental conditions, and the results may be markedly modified by, for example, the presence of reducing gases, the conditions

occuring during heating up, cooling, or standby, such as moisture condonsation, the presence of ash, clinker, fluxes, etc. The presence of trace gases such as steam, CO_2, and SO_2 in air can appreciably increase the scaling rate. No final explanation of this effect has been produced, but it is possible that it is connected with the development of a more porous scale. Such a scale might be expected to result if the first product of the reaction were a compound, such as a hydroxide or carbonate, which subsequently decomposes to give the oxide. Scaling can be minimized by the use of an atmosphere containing hydrogen or carbon monoxide, but above 800° C. scaling can be only prevented where the reducing gas appreciably exceeds the amount of water vapor or CO_2. Carbon deposition can occur where free CO (13%) is present, and deposition on graphite flakes can cause severe growth and distortion at temperatures of 350°-530° C. and probably above.

At temperatures of 400° C. or more, the combined carbon in most cast irons changes to graphite. When most cast irons are heated within the temperature range of 700° to 780° C., an allotropic transformation occurs which is accompanied by an increase in volume. Heating and cooling through the temperatures, therefore, can also cause an incipient cracking.

AFFECT OF ALLOY CHEMISTRY

The three principal alloy elements employed to improve oxidation resistance above 750° C. are Si, Cr, and Al. Some resistance to oxidation above 750° C. is conferred by Si contents above 3%, Cr contents above 1%, and Al contents above 0.9%. Solely from the point of view of scaling, low contents of Cr (below 1.5%) are of limited value.

Alloy cast irons containing carbide-stabilizing elements, such as Cr, Mo, or V or these elements in combination with Ni or Cu, are employed successfully in commercial applications up to 400° C. These same irons can be used at or slightly above 500° C. with some reduction in service life. Good oxidation and growth resistance up to 800° C. is obtained by the use of high-alloy cast irons such as austenitic, high silicon (5-8% Si), or high Cr cast irons. Cast irons containing 15% or more Cr show practically complete resistance to scaling and growth up to 900° C.; with 35% Cr, they show resistance up to 1000° C.

The rate of oxidation is also influenced by the size of the graphite flakes. If they are fine, the diffusion of oxygen along the graphite into the metal will be suppressed. The form of the graphite greatly affects growth and oxidation resistance. For example, spheroidal graphite in ductile iron improves the resistance to high-temperature oxidation and growth.

TEST METHOD

The selection of a test method is extremely important. It is important to have a preliminary sorting test which is nevertheless realistic and correlates with the actual operating conditions. A number of laboratory tests have been employed. These include the crucible test and the salt-coated oxidation test. This last method in which a specimen is coated with a layer of salt and then oxidized in a thermobalance has been used by a Bornstein, et al (1), Petit, et al (2), and Stringer, et al (3), to elucidate the mechanism of the reaction. The crucible test was used until quite recently in the evaluation of alloys, but it certainly represents untypical conditions and the correlation with experience seems poor.

THE RESULTS OF SOME PRELIMINARY EXPERIMENTS

Experimental

Table 1 shows the chemical composition of the irons used in the manufacture of the grate bars.

Table 1

Chemical Analyses of Bars

	C	Si	M	P	S	Cr
524	3.25	1.96	0.58	0.19	0.066	0.78
537	3.25	2.10	0.88	0.31	0.040	0.58
434	3.35	1.86	0.66	0.19	0.064	0.76

The specimens, which were machined from bars provided by Iron & Steel Co., had the dimensions 20 x 30 x 2 mm. A thermobalance was used, and coating with sodium chloride was effected by a spraying technique.

Results

Metallographic examination of the corroded samples revealed that they are pearlitic grey cast irons. Signs of attack on the graphite flakes to a depth of about 25 μ. were noticed.

Uncoated Samples. The weight gain-time curves obtained at 700°, 800°, 900°, and 1000° C. in air display a minimum which appears earlier the higher the temperature. The minimum is followed by weight increase along one or more linear sections. The number of these sections and the corrosion rates characterizing each of them increases with increasing temperature. The corresponding curves obtained for a mild steel conform with a parabolic law.

Coated Samples. The corresponding curves obtained for samples which had been coated with a layer of sodium chloride reveal the minimum mentioned above. The appearance of the minimum is delayed by coating. However, the corrosion rates are higher in presence than in absence of the salt film.

Metallographic Examination of Heated Samples. Heating for 3 hrs. at 900° C. in air results in decarburization across a 20 μ-thick layer. Visual examination of the samples coated with films of NaCl and heated for 5 hrs. within the temperature range 700°-1000° C. shows that the corrosion scales are not adherent to the base metal. There are signs of deep attack on the metal especially along the graphite flakes. Decarburization occurs at 800° C. and above. However, the thickness of the decarburized layer is smaller than the corresponding one for uncoated samples.

The preliminary results obtained hitherto are not sufficient to allow any sound conclusions to be drawn. However, the minimum can be clearly ascribed to the escape of graphite from the uppermost layers. The linear gain in weight both in absence and presence of NaCl shows that in the initial stages of oxidation (first 8 hrs.) the oxide film formed is not protective. Continuous cracking results in exposure of the metal to further oxidation. It may be anticipated that NaCl vapor reacts with steam to give NaOH and HCl. The latter attacks the oxide film formed. It may be proposed that the salt coating delays the escape of carbon oxides as well as HCl.

PLAN FOR FUTURE WORK

It is planned to modify the composition of the coating in order to simulate the conditions prevailing in practice. The weight-gain experiments will be extended to longer periods, and other alloy cast irons will be tested.

SUMMARY

The sinter grates in a sintering plant have been severely corroded presumably because the iron ore is contaminated with alkali halites. Trials are made to understand the mechanism of the corrosion process and to consider the possibility of using other types of cast iron.

REFERENCES

1. N. S. Bornstein and M. A. Decrescente, Corrosion 24, 127 (1968).

2. F. S. Petit, J. A. Goebel, and F. W. Goward, Corro. Sci., 10, 903 (1969).

3. D. M. Johnson, D. P. Whittle, and J. Stringer, Corro. Sci., 15, 649 (1975).

4. H. T. AnGus, Cast Iron, Butterworths (1976).

5. L. L. Shreir, Corrosion, Butterworths (1976).

6. La Que and Copson, Corrosion Resistance of Metals and Alloys, Reinhold (1963).